

The role of initiators in epoxide-based thin-film composite membranes

De rol van initiatoren in epoxide-gebaseerde dunne film composiet membranen

Promotor:

Prof. Ivo F. J. Vankelecom
Departement Microbiële en
Moleculaire Systemen (M2S)

Afdeling Membraanscheidingen, Adsorptie,
Katalyse en Spectroscopie voor Duurzame
Oplossingen (cMACS)

Masterproef voorgedragen
tot het behalen van het diploma van
Master of Science in de bio-ingenieurswetenschappen:
Milieutechnologie

Irian BAERT

Januari 2023

Dit proefschrift is een examendocument dat na de verdediging niet meer werd gecorrigeerd voor eventueel vastgestelde fouten. In publicaties mag naar dit proefwerk verwezen worden mits schriftelijke toelating van de promotor, vermeld op de titelpagina.

Acknowledgments

By starting my thesis in February, choosing a topic was quite difficult. I knew I wanted to work on epoxide membranes, but at the time, there was no topic available. Prof. Ivo Vankelecom made sure I was going to be able to do my thesis around this by saving me a spot as a thesis student, and by looking at available subjects later in the year, and this is how I got this topic. I would like to thank him for doing all this effort to offer me a subject and also for giving me a chance as a PhD researcher in the future.

Next, I would like to express my gratitude towards the people who helped me so much during the last year, Dr. Rhea Verbeke and Daan Van Havere. Thank you for signing up so last-minute to supervise me in my thesis, as I cannot imagine having two better people to guide and encourage me in this process of ups and downs, frustrations and excitement, determination and hard work. You taught me so many things, both practical (planning, academically writing down what is in my head, data analysis) as personal (I am not defined by my studies or grades, “work hard play hard”...). I look up to both of your excitement and passion about what you invest your time in, your unbelievable knowledge, and open mindset. I am grateful to have worked with you as I am convinced both of you will accomplish great things in the future.

When thanking my supervisors, I should thank Nathalie Lenaerts, *aka* my third supervisor, for all the things she did for me like finishing a synthesis when I had to go to class, all the porometry measurements, answering my 1000 membrane texts, giving feedback on my thesis, and always being up to discuss my latest results or questions. So, thank you for being there and making the lab life better!

I am lucky to have ended up in such a nice research group. Thank you Laurens for doing the zeta potential measurements on such short notice, Simon for all the spider related questions and interesting membrane conversations, Scallebout for being there in any way, related or unrelated to the thesis, I needed, Sutapa for all the fun conversations we had in the lab, the epoxide group for all your input and tips, and the rest of the group for being so helpful. I would also like to thank Samuel Eyley for the XPS measurements and interpretation.

Of course, I am grateful to have had the opportunity to meet two “batches” of thesis students, which all made the days better by having fun, working hard together and

supporting each other. Beau, it has been a great experience to have done this Bio-science engineering program alongside you, as we continue to push each other to grow.

Lastly, I need to express my gratitude towards my parents to push me to play some board games once in a while, all the encouragement during this year, and for while providing me with an environment where I could focus on my work, and Lara, thank you for being such a considerate, kind person and help me make my day no matter what.

CONTENTS

Summary	V
Samenvatting	VII
Vulgariserende samenvatting	IX
List of abbreviations	X
List of symbols	XII
List of Figures	XIV
List of Tables.....	XVIII
Context and thesis goals.....	1
.....	Part 1: Literature review
.....	2
1.1 Membrane technology	2
1.1.1 Principle.....	2
1.1.2 Membrane performance characterization	3
1.1.3 Classification	5
1.1.4 Transport through membranes	6
1.1.5 Membrane Processes.....	8
1.1.6 Membrane fouling and concentration polarization.....	11
1.2 Thin film composite membranes.....	12
1.2.1 Phase inversion	13
1.2.2 Interfacial polymerization	15
1.2.3 Interfacial initiation of polymerization (IIP)	17
1.3 Poly(epoxyether) membranes.....	18
1.3.1 Ether Characteristics	18
1.3.2 Epoxides.....	19
1.3.3 Polymerization	20
1.3.4 Advantages of PEE membranes.....	26
.....	Part 2: Materials and Methods
.....	28
2.1 Materials.....	28
2.1.1 Support layer	28
2.1.2 Selective layer	28
2.1.3 Spin coating.....	29
2.1.4 Feed solutions for filtration experiments	29
2.1.5 Gas separation experiments	30

2.1.6	Zeta potential measurements	30
2.1.7	Porometry	30
2.2	Methods	30
2.2.1	Commercial PAN support pretreatment	30
2.2.2	In-house PAN support synthesis.....	30
2.2.3	Initiator concentration calculation.....	31
2.2.4	Support-free interfacial polymerization.....	31
2.2.5	Selective layer synthesis	32
2.2.6	Solvent annealing of supports.....	33
2.2.7	Spin coating.....	33
2.2.8	Adsorption tests.....	33
2.2.9	Membrane characterization	34
..... Part 3: Results and discussion		
.....		38
3.1	RO system.....	38
3.1.1	Support-free interfacial polymerization tests	38
3.1.2	Defining the reference system: TMHD	39
3.1.3	Changing the reaction time during TMHD 2S synthesis.....	47
3.1.4	Initiator properties	52
3.1.5	Imidazole (IM).....	53
3.1.6	1-Methylimidazole (1-MIM)	59
3.1.7	2-Methylimidazole (2-MIM)	64
3.1.8	1,4-diazabicyclo[2.2.2] octane (DABCO) and Tris(2- dimethylaminoethyl)amine (Me6Tren)	67
3.1.9	Selecting important initiator characteristics for selective layer formation ...	70
3.2	GS system.....	71
3.2.1	Introduction.....	71
3.2.2	Support-free interfacial polymerization tests	72
3.2.3	TMHD – TMPD – 1-MIM comparison.....	72
3.2.4	MBDA and 1-MBI.....	75
..... Part 4: General conclusions and perspectives		
.....		77
..... References		
.....		81
..... Appendix		
.....		97

Summary

The increasing prevalence of water scarcity has presented a significant challenge for humanity, and membrane technology has been utilized as an energy-efficient way to treat water. As current state-of-the-art polyamide-based desalination (via reverse osmosis, RO) membranes are insufficiently chemically stable, epoxide-based thin-film composite (TFC) membranes have been introduced as a more durable and chemically robust alternative. A poly(epoxyether) film is synthesized through interfacial initiation of polymerization (IIP), in which the ring-opening polymerization (ROP) of the epoxide monomer is initiated by a tertiary amine initiator. This happens in two key steps, the first of which yields an ether-linked network (1S membrane) and the second step a densified, crosslinked film (2S membrane). The synthesis procedure however remains time-consuming and a black-box process. In order to move away from the trial-and-error approach to optimize these membranes, fundamental research was conducted in this work about the influence of the initiator on the synthesis-structure-performance relationship of these chemically robust TFC epoxide-based membranes.

By measuring the performance and physicochemical characteristics of membranes synthesized under different conditions (reaction time, initiator concentration, 1S or 2S) with a strategically chosen set of initiators, fundamental insights were gained regarding the mechanism behind the ROP of the epoxide monomer, and important initiator properties were derived related to obtaining salt selective membranes. In the synthesis system where the initiator (TMHD, IM, 1-MIM, 2-MIM, DABCO, Me6Tren) is dissolved in the aqueous phase and epoxide monomer (EPON) in the organic phase in order to synthesize RO membranes, ROP of EPON is confirmed for the membranes initiated by the IM, 1-MIM and 2-MIM by SEM pictures, XPS- and FTIR measurements. Filtration results suggest low polymerization for Me6Tren-initiated membranes, and do not indicate polymerization for DABCO-initiated membranes. Only when TMHD is used as an initiator, salt selective membranes are obtained. Hence, it can be concluded that this synthesis system prefers highly nucleophilic, bifunctional tertiary amine initiators (*e.g.*, TMHD) with a total length similar to TMHD (~octane), as they both act as initiators and crosslinkers. Due to these properties, charges are incorporated and the toplayer is densified. Further information is gathered about the initiation and densification mechanism of TMHD by varying the reaction times. Filtrations and characterization of the membranes suggests that the re-initiation and densification is the most important step to achieve salt selectivity.

As ether oxygens have strong interactions with CO₂, the application of epoxide-based TFC membranes can be extended to gas separation (GS) processes. For the synthesis of GS membranes, the initiator and epoxide monomer are dissolved in their preferred phase (organic and aqueous, respectively) to create a more defined interfacial reaction and hence a thinner film. However, low permeability due to a pore plugging issue is experienced, which is not alleviated by the use of initiators with different properties (TMHD, TMPD, 1-MIM, 1-MBI, MBDA).

Samenvatting

De toenemende waterschaarste is een belangrijke uitdaging voor de mensheid, en membraantechnologie wordt gebruikt als een energie-efficiënte manier om water te behandelen. Aangezien de huidige *state-of-the-art* ontziltingsmembranen (via *reverse osmosis*, RO) op basis van polyamide chemisch onvoldoende stabiel zijn, werden epoxide-gebaseerde dunne-film composiet (TFC) membranen geïntroduceerd als een duurzamer en chemisch robuuster alternatief. Een poly(epoxyether) film wordt gesynthetiseerd door interfaciale initiatie van polymerisatie (IIP), waarbij de *ring-opening polymerization* (ROP) van het epoxide monomeer wordt geïnitieerd door een tertiaire amine initiator. Dit gebeurt in twee stappen, waarvan de eerste een ether gebonden netwerk oplevert (1S membraan), en de tweede stap een dense, vernette film (2S membraan). De syntheseprocedure blijft echter tijdrovend en een black-box proces. Om af te stappen van de *trial-and-error* aanpak om deze membranen te optimaliseren, werd in dit werk fundamenteel onderzoek verricht naar de invloed van de initiator op de synthese-structuur-prestatie relatie van deze chemisch robuuste TFC epoxide-gebaseerde membranen.

Door het meten van de prestaties en fysicochemische eigenschappen van membranen gesynthetiseerd onder verschillende condities (reactietijd, initiator concentratie, 1S of 2S) met een strategisch gekozen set initiatoren, werden fundamentele inzichten verkregen over het mechanisme achter de ROP van het epoxide monomeer, en werden belangrijke eigenschappen van de initiator afgeleid met betrekking tot het behalen van zout selectieve membranen. In het synthesesysteem waarbij de initiator (TMHD, IM, 1-MIM, 2-MIM, DABCO, Me6Tren) is opgelost in de waterige fase en het epoxidemonomeer (EPON) in de organische fase om RO-membranen te synthetiseren, is de ROP van EPON bevestigd voor de membranen geïnitieerd door het IM, 1-MIM en 2-MIM door SEM-beelden, XPS- en FTIR-metingen. Filtratie resultaten wijzen op een lage graad van polymerisatie voor door Me6Tren geïnitieerde membranen, en wijzen niet op polymerisatie voor door DABCO-geïnitieerde membranen. Alleen wanneer TMHD als initiator wordt gebruikt, worden zout selectieve membranen verkregen. Hieruit kan worden geconcludeerd dat dit synthesesysteem de voorkeur geeft aan zeer nucleofiele, bifunctionele tertiaire amine-initiatoren (bv. TMHD) met een totale lengte die vergelijkbaar is met die van octaan, aangezien zij zowel als initiator en als *crosslinker* fungeren. Dankzij deze eigenschappen worden ladingen ingebouwd en wordt de toplaag dener. Verder werd meer informatie verzameld over het initiatie- en verdichtingsmechanisme van TMHD door de reactietijden

te variëren. Filtraties en karakterisering van de membranen suggereren dat de herinitiatie en verdichting de belangrijkste stap is om zoutselectiviteit te bereiken.

Aangezien ether zuurstofatomen sterke interacties hebben met CO₂, kan het toepassingsgebied van de epoxide gebaseerde TFC-membranen worden uitgebreid tot gas scheidingen (GS). Voor de synthese van GS-membranen worden de initiator (TMHD, TMPD, 1-MIM, 1-MBI, MBDA) en het epoxidemonomeer (PEGDE) opgelost in hun voorkeursfase (respectievelijk organisch en waterig) om een meer gedefinieerde interfaciale reactie en dus een dunnere film te creëren. De membranen hebben echter een lage permeabiliteit als gevolg van de verstopping van de poriën, die niet werd verminderd door het gebruik van initiatoren met verschillende eigenschappen.

Vulgariserende samenvatting

De toenemende waterschaarste is een belangrijke uitdaging voor de mensheid, en membraantechnologie wordt gebruikt als een energie-efficiënte manier om water te behandelen. Een membraan kan gezien worden als een koffiefilter: het houdt bepaalde componenten van een voedingsstroom tegen en laat anderen door. Door de poriën van zo een membraan heel klein te maken kan zelfs zout uit zeewater worden afgescheiden (ontzilting), of kunnen gassen worden gescheiden. De ontziltingsmembranen die vandaag de dag worden gebruikt zijn echter onvoldoende stabiel. Daarom is recent een nieuw type membraan ontwikkeld op basis van een nieuwe chemie, die een duurzamer en chemisch robuuster alternatief is. Deze membranen worden gemaakt door middel van 2 reactiestappen: eerst wordt een eerder losse polymeerstructuur gevormd, die daarna verdicht wordt en er ladingen worden ingebouwd die de capaciteit om zouten tegen te houden vergroot. Het maken van dit type membranen duurt echter lang, en er wordt vaak via *trial-and-error* gewerkt om ze te optimaliseren. Daarom werd er in dit werk fundamenteel onderzoek gedaan naar het reactieproces, meer specifiek werd de invloed van de initiator, de molecule die de reactie start, bekeken. Door membranen te maken met initiatoren met verschillende eigenschappen kon meer kennis vergaard worden over hoe de reactie verloopt, welke stappen belangrijker zijn dan anderen en ook de manier hoe de initiator wordt ingebouwd in het vernetete netwerk in functie van de reactietijd. Daarnaast werd er ontdekt dat het systeem nood heeft aan een voldoende reactieve en voldoende lange initiator die langs twee kanten kan reageren. Dankzij deze nieuwe inzichten kunnen nieuwe methodes ontwikkeld worden om de membranen op een minder tijdsintensieve manier te maken, en de opschaling van de membranen te vergemakkelijken. Er werd verder ook gekeken naar de mogelijkheid om gasscheidingsmembranen te maken via een gelijkaardig proces, maar daar werden de poriën verstopt wat resulteerde in een lage doorlaatbaarheid. Dit probleem kon niet verholpen worden door initiatoren met verschillende eigenschappen te gebruiken.

List of abbreviations

1-MIM	1-Methylimidazole
2-MIM	2-Methylimidazole
AROP	Anionic ring-opening polymerization
CDMP	Concentration-driven membrane processes
CROP	Cationic ring-opening polymerization
D	Diffusivity
Da	Dalton
DABCO	1,4-Diazabicyclo[2.2.2]octane
DI	Deionized
DMAc	<i>N,N</i> -Dimethylacetamide
DMAc12	Support of which the dope solution consisted of 12 wt% PAN in DMAc
DMAc15	Support of which the dope solution consisted of 15 wt% PAN in DMAc
DMF	Dimethylformamide
DMSO	Dimethyl sulfoxide
EPON	Tetraphenoethane tetraglycidyl ether
GS	Gas separation
HSP	Hansen solubility parameters
IP	Interfacial polymerization
IIP	Interfacial initiation of polymerization
IM	Imidazole
IPA	2-Propanol
LMH/bar	$\text{L m}^{-2} \text{h}^{-1} \text{bar}^{-1}$
MB	Methylene blue
MBDA	4,4'-Methylenebis(<i>N,N</i> -dimethylaniline)
MBI	1-Methylbenzimidazole
Me6Tren	Tris(2-dimethylaminoethyl)amine
MF	Microfiltration
MW	Molecular weight
MWCO	Molecular weight cut-off
MQ	Milli-Q
NF	Nanofiltration
NI	No initiator
NIPS	Nonsolvent-induced phase separation

NMP	1-methyl-2-pyrrolidone
NROP	Nucleophilic ring-opening polymerization
P	Permeance
PAN	Polyacrylonitrile
PAN PX	PX (MWCO 400 000 Da) UF PAN-based support
PDMP	Pressure-driven membrane processes
PDMS	Polydimethylsiloxane
PEE	Poly(epoxyether)
PEGDE	Poly(ethylene glycol) diglycidyl ether
PV	Pervaporation
PVAc	Polyvinylacetate
R	Rejection
R&V	Ridge-and-valley
RO	Reverse osmosis
ROP	Ring-opening polymerization
RT	Room temperature
S	Solubility
SD	Solution-diffusion
TMHD	<i>N,N,N',N'</i> -Tetramethyl-1,6-hexanediamine
TMPD	<i>N,N,N',N'</i> -Tetramethyl-1,6-propanediamine
UF	Ultrafiltration

List of symbols

A	Membrane surface, water permeation coefficient
α	Separation factor (mixed-gas selectivity)
α_{ab}	Ideal selectivity
B	Solute permeability coefficient
C_p	Concentration of the permeate
C_r	Concentration of the retentate
D	Diffusivity
ΔC_s	Difference in solute concentration over the membrane
ΔP	Pressure gradient over the membrane
$\Delta \pi_m$	Osmotic pressure gradient across the membrane active layer
ΔX	Potential difference over the membrane
E	Electrical potential
F	Driving force
i	Number of osmotically active solute particles
l	Membrane thickness
J	Flux
J_A	Solvent flux
J_B	Solute flux
m	Mass
μ	Chemical potential
P	Permeability
P_f	Pressure at feed side of the membrane
P_i	Intrinsic permeability
P_p	Pressure at permeate side of the membrane
q	adsorption capacity
Q	Permeate volume
R	Rejection, universal gas constant
S	Solubility
σ	Correction factor
t	Time
T	Absolute temperature
V	Volume

x_i Mole fraction of component i in the feed
 y_i Mole fraction of component i in the permeate

List of Figures

Figure 1: A schematical representation of the principles of membrane separation. Adapted from9.	2
Figure 2: Cut-off curve of a membrane to determine the MWCO.	5
Figure 3: Representation of different membrane morphologies. Adapted from21.	6
Figure 4: The two main membrane transport mechanisms: pore flow vs solution-diffusion. Adapted from21.	7
Figure 5: Graphical illustration of osmotic phenomena. From32.	10
Figure 6: Concentration profile with concentration polarization. Adapted from50.	12
Figure 7: Schematic representation of the PA TFC membrane structure. From55.	13
Figure 8: Ternary phase diagram. Adapted from62.	14
Figure 9: Sponge-like (A) ⁶³ and finger-like (B) ⁶⁴ membrane morphology.	14
Figure 10: Selective PA layer growth. A) hydrophobic PTFE membrane, first immersed in organic phase, then aqueous phase. B) hydrophilic PTFE membrane, first immersed in aqueous phase, then organic phase. From72.	16
Figure 11: Left) Surface ridge-and-valley structure of PA layer, typical for MPD-TMC membranes. From73. Right) surface globular structure, typical for PIP-TMC membranes. From	17
Figure 12: Schematic representation of A) IIP B) conventional IP.	18
Figure 13: Chemical reactions occurring in the chlorohydrin process. From	19
Figure 14: Reaction mechanism for step-growth polymerization in presence of (a) primary amines and (b) secondary amines. From98.	20
Figure 15: Polymer network formation via step growth polymerization. Adapted from103.	21
Figure 16: Polymer network formation via chain growth polymerization.	21
Figure 17: Possible reaction mechanisms for anionic ring-opening polymerization of epoxides initiated by a tertiary amines, including donor-acceptor complex formation by a proton donor to form the propagating species. Adapted from 100, 79.	23
Figure 18: Propagation step in the AROP of epoxides with a tertiary amine as initiator.	23
Figure 19: Termination step in the AROP of epoxides with a tertiary amine as initiator.	24
Figure 20: Transfer reaction of the propagating alkoxide and epoxide monomer. Adapted from94.	24
Figure 21: Generally accepted reaction mechanisms of imidazoles with an epoxy resin. Adapted from157.	25
Figure 22: A: EPON structure, B: PEGDE structure.	29
Figure 23: Overview of the vial tests with different initiators for the RO membranes. Upper phase: 1.5 w/v% EPON in toluene, lower phase: 1N initiator in MQ water. Most left picture: reference experiment: no initiator added in the water phase. Pictures are taken after one week of reaction. At the bottom, the time after which film formation is first visually observed has been provided.	39
Figure 24: Performance of 1S and 2S membranes synthesized with TMHD as the initiator at a concentration of 1N, with reaction steps of 1 h. Literature performance of the 1S and 2S membranes are depicted as “1S lit” and “2S lit” ¹¹⁹ . Filtration conditions: 10 bar, 5 mM NaCl aqueous solution.	40

Figure 25: Performance of the PAN PX support. Pristine refers to a washed PAN PX membrane, Solvent annealed to a synthesis procedure of a 2S membrane but without EPON or initiator present in the toluene and water phase. Filtration conditions: 10 bar, 5 mM NaCl aqueous solution.	41
Figure 26: Performance of support membranes and membranes synthesized with TMHD as the initiator at a concentration of 1N, with reaction steps of 1 h. SA is short for solvent annealed. White background: membranes with DMAc12 support, blue background: membranes with a DMAc15 support. Filtration conditions solvent annealed and NI membrane: 10 bar, 5 mM NaCl aqueous solution. Pristine: 1 bar, pure water.	43
Figure 27: ATR-FTIR spectra of PAN PX and a cast PAN support from a dope solution of PAN in DMAc. PVAc absorption bands are highlighted in blue, DMAc absorption bands highlighted in orange.	43
Figure 28: ATR-FTIR spectrum of the supports, pure EPON monomer, NI membrane, TMHD 1N 1&2S 1h membranes. Black lines are used are for membranes containing a PAN PX support, green lines for membranes with a DMAc12 support. The cast PAN spectrum is equal for DMAc12 and DMAc15. Epoxide signal highlighted in blue. Signals around 1508 cm ⁻¹ and 1450 cm ⁻¹ highlighted in red. The membrane spectra are scaled towards the PAN nitrile signal at 2245 cm ⁻¹	44
Figure 29: Top-view SEM images of membranes synthesized with a 1N concentration of TMHD. Top four images: on PAN PX. NI WTOL relates to a 2S NI membrane washed in toluene for 18 h. Bottom 6 images on in-house cast supports: white background: on DMAc12, blue background: on DMAc15.	46
Figure 30: Performance of 1S and 2S membranes synthesized with TMHD at a concentration of 1N, with varying reaction times (20, 40 mins and 1 h) White background: membranes with DMAc12 support, blue background: membranes with a DMAc15 support. Filtration conditions: 10 bar, 5mM NaCl aqueous solution.	47
Figure 31: Performance of 1S and 2S membranes synthesized on DMAc12 with TMHD as the initiator at a concentration of 1N, with varying reaction times (20, 40 mins and 1 h). Filtration conditions: 10 bar, 5 mM NaCl aqueous solution.	48
Figure 32: XPS measurements on membranes synthesized with TMHD as an initiator. Two membranes on the left: on DMAc15, membrane on the right: on PAN PX. Y axis: atom percentage of a certain bond.	49
Figure 33: top-view SEM images of the DMAc12 support and 2S membranes synthesized on DMAc12 with TMHD as the initiator at a concentration of 1N, with varying reaction times (20, 40 mins and 1 hour).	51
Figure 34: Performance of the IM membranes synthesized using different conditions: concentrations of 1N, 4N, type 1S and 2S, reaction times of 1 h and 3 h. Filtration conditions: 10 bar, 5 mM NaCl aqueous solution.	55
Figure 35: Performance of IM membranes synthesized under different conditions. White background: membranes with DMAc12 support, blue background: membranes with a DMAc15 support. Filtration conditions: 10 bar, 5mM NaCl aqueous solution.	56
Figure 36: ATR-FTIR spectra of IM membranes on top of a PAN PX support (black lines), or on DMAc12 (blue lines) Epoxide signal at 910 cm ⁻¹ highlighted in blue, imidazole signals at 1063 cm ⁻¹ and 663 cm ⁻¹ highlighted in red. Spectra on DMAc12 were smoothed by taking the average transmittance of the surrounding six wavenumbers.	57
Figure 37: Top-view SEM images of IM membranes synthesized using different conditions, left: on top of PAN PX, right: on top of DMAc15. Increasing reaction time clearly has an influence on the observed structures.	58

Figure 38: Performance of the 1-MIM membranes synthesized using different conditions: concentrations of 0.5N, 2N, type 1S and 2S, reaction times of 1 h and 3 h. Filtration conditions: 10 bar, 5 mM NaCl aqueous solution.	60
Figure 39: Performance of 1-MIM membranes synthesized under different conditions. White background: membranes with DMAc12 support, blue background: membranes with a DMAc15 support. Filtration conditions: 10 bar, 5mM NaCl aqueous solution.	61
Figure 40: ATR-FTIR spectra of 1-MIM membranes on top of a PAN PX support (black lines), and DMAc12 support (blue lines). Spectra on DMAc12 were smoothed by taking the average transmittance of the surrounding six wavenumbers.	62
Figure 41: Top-view SEM images of 1-MIM membranes synthesized using different conditions, left: on top of PAN PX, middle (highlighted in blue): on top of DMAc15, top right (highlighted in red): on top of DMAc12.	63
Figure 42: Performance of 2-MIM membranes synthesized using different conditions: concentrations of 1N, 2N, 4N, type 1S and 2S, reaction times of 1 h and 3 h. Filtration conditions: 10 bar, 5 mM NaCl aqueous solution.	65
Figure 43: Performance of 2-MIM membranes synthesized under different conditions. White background: membranes with DMAc12 support, blue background: membranes with a DMAc15 support. Filtration conditions: 10 bar, 5mM NaCl aqueous solution.	66
Figure 44: Top-view SEM images of 2-MIM membranes synthesized using different conditions, on top of PAN PX (white background), on top of DMAc15 (blue background).	67
Figure 45: ATR-FTIR spectra of DABCO membranes on top of a DMAc12 support. The spectra were smoothed by taking the average transmittance of the surrounding six wavenumbers. C=O band around 1715 cm ⁻¹ highlighted in red.....	69
Figure 46: CO ₂ /N ₂ separation factor and CO ₂ permeance of membranes synthesized with TMHD, TMPD, and 1-MIM.	72
Figure 47: CO ₂ /N ₂ separation factor and CO ₂ permeance of membranes synthesized with TMHD. The selectivity of a pure PDMS layer is visualized with the orange dotted line.	74
Figure 48: CO ₂ /N ₂ separation factor and CO ₂ permeance of membranes synthesized with 1-MIM. The selectivity of a pure PDMS layer is visualized with the orange dotted line.	75
Figure 49: CO ₂ /N ₂ separation factor and CO ₂ permeance of membranes synthesized with MBDA and MBI. The selectivity of a pure PDMS layer is visualized with the orange dotted line.	76
Figure 50: Design of the IIP set-up used for membrane synthesis ¹²⁵	97
Figure 51: Overview of the chemical structures of all the used initiators.	97
Figure 52: Reference vial tests for initiators used to synthesize RO membranes. Most left: EPON 5 w/v% EPON in toluene on top of pure MQ water. Other pictures: pure toluene on top of 1N aqueous initiator solution.	98
Figure 53: Mean pore diameter and total pore area of three support layers: DMAc12, 15 PAN PX. These values are obtained through gas liquid porometry.	98
Figure 54: Membrane coupons after MB filtration. Left: TMHD-initiated TFC membranes, right: all other membranes.	99
Figure 55: Adsorption capacity of multiple TFC membranes and DMAc12. Y axis: adsorption capacity in mg dye/g membrane. X axis: time.	99

Figure 56: The occurrence of N in multiple TFC membranes and DMAc15. These values are obtained through XPS-analysis. Y axis: atom percentage of a certain bond. No nitrile signals were detected for the TFC membranes.....	100
Figure 57: Zoomed-in view on lower concentrations for the occurrence of N in multiple TFC membranes and DMAc15. Y axis: atom percentage of a certain bond.	100
Figure 58: Zeta potential curve of multiple TFC and support membranes.Y-axis: Zeta potential (mV), X-axis: pH.	101
Figure 59: Static contact angle measurements for multiple TFC and support membranes. Red bars depict membranes with a PAN PX support, blue bars depict membranes with a DMAc15 support.	101
Figure 60: ATR-FTIR spectra of 2-MIM membranes on top of a PAN PX support (black lines), and DMAc12 support (blue lines). Spectra on DMAc12 were smoothed by taking the average transmittance of the surrounding six wavenumbers.	102
Figure 61: Performance of the DABCO membranes at different synthesis conditions: concentrations of 0.5N; 2N; type 1S and 2S; reaction times of 1 h and 3 h. Filtration conditions: 10 bar, 5 mM NaCl aqueous solution.	102
Figure 62: DABCO-mediated conversion of terminal epoxides to methyl ketones. From 166	103
Figure 63: Performance of the Me6Tren membranes at different synthesis conditions: concentrations of 0.5N; 2N; type 1S and 2S; reaction times of 1 h and 3 h. Filtration conditions: 10 bar, 5 mM NaCl aqueous solution.	103
Figure 64: ATR-FTIR spectra of Me6Tren membranes on top of a DMAc12 support. The spectra were smoothed by taking the average transmittance of the surrounding six wavenumbers. C=O band around 1715 cm ⁻¹ highlighted in red.....	103
Figure 65: MB performance of 1S (left graph) and 2S (right graph) membranes synthesized on DMAc12 with different initiators. 1S membrane initiator conc: TMHD: 1N, IM: 4N, 1-MIM: 2N, 2-MIM: 4N, DABCO&Me6Tren: 2N. 2S membrane initiator conc: TMHD: 1N, IM: 1N, 1-MIM: 0.5N, 2-MIM: 1N, DABCO&Me6Tren: 0.5N. All reaction steps were of 1 h. Filtration conditions: 10 bar, 15 μM methylene blue aqueous solution.....	104
Figure 66: Top-view SEM images of DABCO (white background) and Me6Tren (blue background) synthesized with different conditions, all on top of DMAc12. 1S and 2S NI membranes are depicted at the bottom right corner.....	105
Figure 67: ATR-FTIR spectra of 2N 2S 1h membranes made with TMHD, TMPD, and 1-MIM. The epoxide signal is highlighted in purple.....	107
Figure 68: ATR-FTIR spectra of TMHD synthesized with different conditions. The epoxide signal is highlighted in purple.....	107
Figure 69: ATR-FTIR spectra of MBI and MBDA 1N 2S 1H membranes	108

List of Tables

Table 1: Overview of pressure-driven membrane processes ^{17,26,28,33} . SP= symmetric porous, AP= asymmetric porous, TFC = thin-film composite.....	9
Table 2: Overview of system characteristics and relevant initiator properties linked to them.....	52
Table 3: Overview of a set of properties of the initiators used for all membranes - ¹⁵⁶ . * Depict predicted values.....	53
Table 4: Partial solubility parameter (PSP) of water with EPON and PAN, and the calculated R_a . Smaller R_a values indicate stronger interactions ¹⁴⁵ . PSP of PAN and EPON is calculated using the Hoftyzer and Van Krevelen (1976) method ¹⁴⁴	102
Table 5: Vials experiments regarding the GS membrane synthesis. Upper phase: 1N initiator in toluene, lower phase: 5 w/v% PEGDE in MQ water. If there is no extra information at a specific time, this means nothing changed compared to what was visible before. Pictures were taken after 1 week.	106

Context and thesis goals

Nobel prize holder Richard Smalley published a list of humanity's top 10 challenges for the next 50 years. Numbers one, two, and four on this list are respectively energy, water and environment¹. It is clear that a lot of these challenges are intertwined. With a continuously growing world population, resources that were once abundant like unpolluted, potable water are becoming more and more scarce. As 71% of the earth's surface is covered by water, of which 96,5% is saline, seawater could be used in order to produce more fresh water as it becomes less available through surface waterbodies or groundwater².

This has been done for a very long time. In ancient Greece, the concepts of boiling seawater or using filtration media were first applied to purify water^{3,4}. The scale of these techniques evolved over time and in the 20th century, large-scale thermal water desalination plants were constructed. This is an effective way to produce clean water, but the process is very energy intensive, hence contributing to humanity's number one challenge. Later in that century, the first reverse osmosis (RO) membrane plants were constructed to purify water in a less energy intensive way. Comparing RO to thermal desalination, it scores better on social, economic, and environmental aspects and is the better solution when fossil fuels are used as energy source. That is why in 2019, RO technology contributed to 65% of the worldwide desalination capacity⁵.

The most common desalination membranes have a polyamide selective layer, allowing relatively high fluxes while maintaining a high salt rejection. As a downside, they lack in chemical robustness, as they are sensitive to substances such as chlorine. This is often added to water as a disinfectant, making it an important factor for membrane failure¹¹⁹. This sparked a quest to find more chemically robust membranes, and in 2019 Verbeke *et al.* proposed the use of epoxide-based membranes. This is a new type of membrane which utilizes the intrinsic stability of ether bonds. These stable and robust membranes are promising for different applications in addition to reverse osmosis, like acid mine leachates or the dairy industry.

Until now, the synthesis of these membranes remains time consuming, and more or less a black-box process. To move away from this trial-and-error approach to optimize these membranes, it is necessary to conduct fundamental research on the synthesis parameters. With the intention of shedding some light on the black box, the influence of the initiator on the synthesis-structure-performance relationship of these chemically robust epoxide membranes was studied in this work. By increasing the fundamental understanding of the system, a more economically feasible synthesis process could be obtained, which could on its turn help the scale-up of these membranes.

PART 1: LITERATURE REVIEW

1.1 MEMBRANE TECHNOLOGY

1.1.1 Principle

A membrane can be defined as a selective semi-permeable barrier between two phases⁶⁻⁹. The feed is the unmodified solution that comes in contact with the membrane. As illustrated in Figure 1, a part of the feed molecules will go through the membrane and will form the permeate stream, whilst the retentate is the stream that is retained by the membrane¹⁰. The permeate can but does not necessarily need to have the same phase as the retentate. Through certain interactions which for example depend on the membranes chemical and morphological structure, a selectivity will be exhibited towards certain compounds. A visualization of a membrane separation is given in Figure 1, where the green molecules pass through the membrane with less resistance than the yellow ones. A gradient applied across the membrane will act as a driving force for the separation process. Such driving forces can be gradients in temperature, pressure, concentration, which all relate to gradients in electrochemical potential^{6-9, 21}.

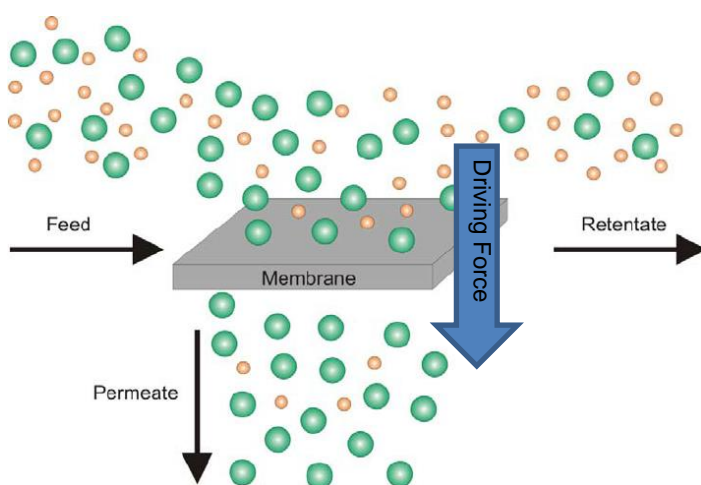


Figure 1: A schematical representation of the principles of membrane separation. Adapted from⁹.

The extent of the driving force (F) will be determined by the difference in potential (ΔX) at both sides of the membrane divided by its thickness (l), given by:

$$F = \frac{\Delta X}{l} \quad 1$$

Chemical potential (μ) and electrical potential (E) are two typical potentials that are used in membrane technology⁸. An equilibrium will be reached ($\Delta X = 0$) when no external forces are applied over the membrane. However, during membrane processes, reaching equilibrium will be prevented by the presence of a constant driving force, resulting in a constant flux in time⁷.⁸. This proportional relationship between the driving force (F) and steady state permeate flux (J) can be given by:

$$J = A * F \quad 2$$

where A is the proportionality factor (units depend on driving force), a measure of the diffusion resistance of the membrane⁶.

1.1.2 Membrane performance characterization

In membrane research, it is important to determine several performance parameters in order to compare different membranes. Several parameters can provide useful information about the performance of a membrane, of which the most important ones are discussed below.

1.1.2.1 Permeability of a membrane

To achieve a commercially viable membrane, components must pass through the membrane at an adequate rate. Hence, two parameters are defined to describe this rate of transported through a membrane. The first one, used in liquid separation applications, is the flux (J), which is given by:

$$J = A * \frac{\Delta X}{l} \quad 3$$

where A is a proportionality factor, ΔX is the potential gradient over the membrane and l is the membrane thickness (m). As the thickness can be seen in the denominator, a thinner membrane will have a higher flux than a thick membrane⁶. A more specific way of expressing the flux (L/m² h bar, often denoted briefly as LMH/bar) is by the equation

$$J = \frac{1}{A \times \Delta P} * \frac{dQ}{dt} \quad 4$$

Where A is the membrane surface area (m²), ΔP is the pressure gradient over the membrane, Q is the permeate volume (L) and t is the time (h).

For gas separations, the flux of a desired component i can be given by:

$$J_i = \frac{P_i}{l} (P_f * x_i - P_p * y_i) \quad 5$$

where P_i is the intrinsic permeability (see 1.1.4.1) of the membrane material for component i (in Barrer; $\frac{10^{-10} \text{ cm}^3(\text{STP})\text{cm}}{\text{cm}^2\text{s cmHg}}$), P_f and P_p are the pressures in the feed and permeate and x_i and y_i are the mole fraction of component i in the feed and permeate respectively¹¹. The $P_f * x_i$ and $P_p * y_i$ terms are the partial pressures of the component i in each phase. Because thickness measurements of the dense layer can be hard or inaccurate, permeance ($\frac{P_i}{l}$) can be used instead of permeability³⁴. Permeance has the unit GPU (gas permeation unit) with $1 \text{ GPU} = \frac{10^{-6} \text{ cm}^3(\text{STP})}{\text{cm}^2\text{s cmHg}}$. Often, the flux through a membrane can be measured and the permeability or permeance will have to be calculated. This can be done by rewriting equation 5 to

$$P_i = \frac{J_i \times l}{\Delta P} \quad 6$$

where P_i is the permeability (barrer), J_i the flux, ΔP the difference in partial pressure across the membrane and l the membrane thickness. Dividing this P_i by l equals the permeance of the membrane¹².

1.1.2.2 Separation capability

To determine the capability of the membrane to distinguish between different compounds in a stream, three parameters can be defined. The first one, the rejection coefficient R , is defined as:

$$R = \frac{C_r - C_p}{C_r} * 100\% \quad 7$$

where R is the % rejection (dimensionless), C_r is the concentration in the retentate and C_p is the concentration in the permeate. This R is used in liquid separation applications, often for dilute mixtures of a solvent and a solute⁶. For some applications, the retentate and feed concentration differ substantially, e.g., in dead end filtrations due to concentration polarization, discussed in part 1.1.6¹⁷.

The next two parameters are more often used for gas separations, starting with the separation factor (or mixed-gas selectivity) α , defined as:

$$\alpha_{A/B} = \frac{y_A/y_B}{x_A/x_B} \quad 8$$

when component A is permeating preferentially. y_A and y_B are the concentrations of components A and B in the permeate, x_A and x_B the concentrations of components A and B in the feed. These can be mass- or molar concentrations, or even weight, mole or volume fractions⁶.

A third parameter is the ideal selectivity which is represented by α_{ab} , defined as

$$\alpha_{ab} = \frac{P_a}{P_b} \quad 9$$

where P_a and P_b are the pure gas permeabilities¹³. An advantage of using the ideal selectivity is that only single gas measurements are required. A disadvantage is that it can deviate substantially from the separation factor, because the presence of a certain gas sometimes influences transport of other gases (depends on molecular properties like size and mass) due to, e.g., swelling of the membrane¹⁴⁻¹⁶.

1.1.2.3 Molecular weight cut-off (MWCO)

The MWCO is another representation of the selectivity of a membrane, often used to characterize membranes with larger pore sizes and for membrane classification in general¹⁷. It is defined as the minimum molecular weight (MW, in Dalton) of a test solute that is retained for 90% by the membrane¹⁸. The determination is done by fitting a so called “cut-off curve”, where the retention of the membrane is plotted for different MW solutes (Figure 2)²⁰. Depending on the application of the membrane, the cut-off curve should be rather sharp or not.

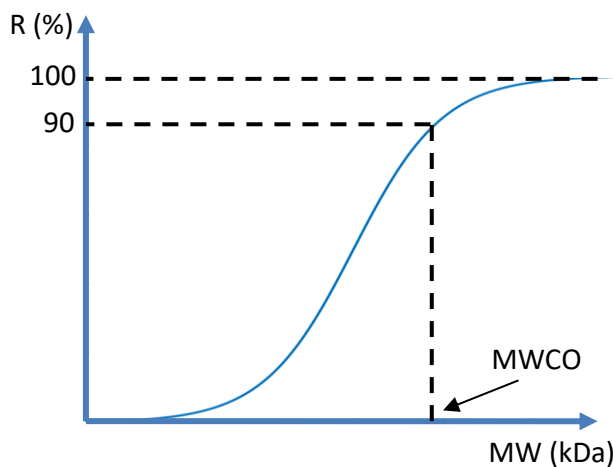


Figure 2: Cut-off curve of a membrane to determine the MWCO.

1.1.3 Classification

There are multiple ways to classify membranes. The first, most general way is to distinguish based on the origin of the membrane, namely natural (e.g., cell membranes) and synthetic membranes. The advantage of synthetic membranes is that they can be tailored for specific applications. A more detailed classification of these synthetic membranes can be based on the material (organic or inorganic), the charge, the pore size, the driving force, and the morphology^{6, 17}. In the next part, morphology will be explained in more detail, and the driving force and pore size will be elaborated on in section 1.1.5. *Morphology*

A general classification based on morphology is depicted in Figure 3. Membranes can be either symmetric (isotropic) or asymmetric (anisotropic) and can be neutral or charged. Symmetric membranes can be porous or dense^{9, 23}. Typical thicknesses for symmetric membranes are in the range of 10-200 μm . Thin membranes with respective high fluxes are desired.

Because there is a limit to how thin these membranes can be made, a major breakthrough in membrane technology was the development of asymmetric membranes. They combine the high fluxes of thin membranes with the, in general, higher selectivities of dense membranes. In porous asymmetric membranes, porosity and pore size vary across the membrane, with a “skinlayer” of narrow pores of very limited thickness ($<0.5 \mu\text{m}$) which will determine the selectivity of the membrane, on top of a more open support layer (50-150 μm). For thin-film composite (TFC) membranes, the dense toplayer and support layer are made from different materials (more in depth in part 1.2)⁶. Another benefit of the thin toplayer is that it makes it economically feasible to use more expensive monomers with superior characteristics. In contrast to these TFC membranes, for integrally skinned asymmetric membranes the two layers are made from the same material²¹.

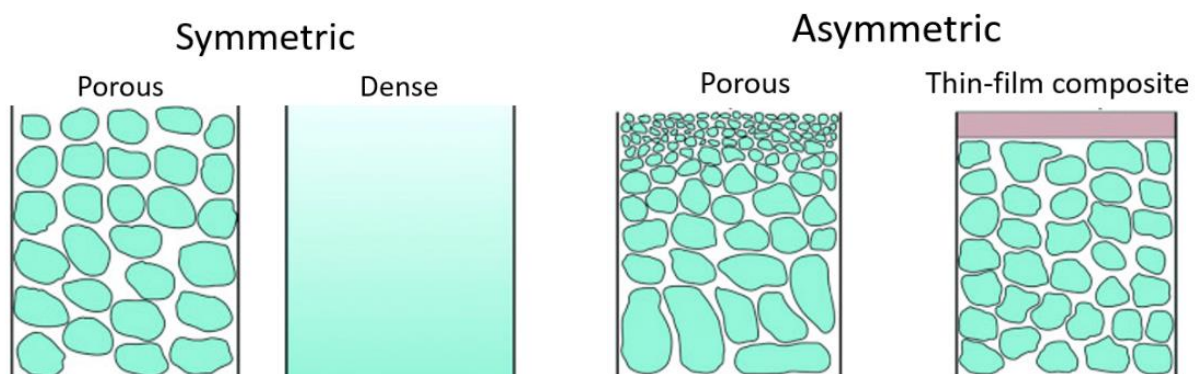


Figure 3: Representation of different membrane morphologies. Adapted from²¹.

1.1.4 Transport through membranes

Transport through the membrane is, among others, determined by the direction of flow, the size of the pores, interactions between the membrane and feed molecules, and the differences in properties of these molecules will determine the selectivity of the membrane¹⁷. Transport through porous and dense membranes is based on different mechanisms (Figure 4). The two main models to explain these mechanisms are respectively the pore flow model (based on convective transport) and the solution-diffusion (SD) model (based on diffusive transport)^{22, 23}. In short, selectivity is achieved by size exclusion of molecules (the pore is too small for the molecule) in the pore flow model, and by different rates of solution and diffusion of molecules through the polymeric membrane material in the SD model. These models differ in their underlying assumptions. In the SD model, a constant pressure is assumed over the membrane

and that the chemical potential gradient of the permeant is represented by a concentration gradient. For the pore flow model on the other hand, it is the other way around: a constant concentration is present, while the pressure gradient induces the chemical potential gradient²⁴. As dense membranes are used in this work, only the solution-diffusion model will be further considered.

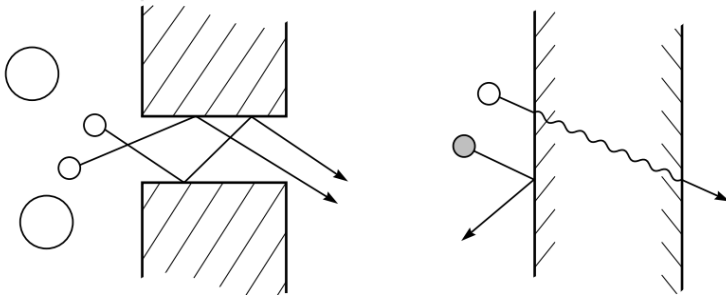


Figure 4: The two main membrane transport mechanisms: pore flow vs solution-diffusion. Adapted from²¹.

1.1.4.1 Solution-diffusion (SD)

The SD model can be used to describe transport through dense membranes used for, e.g., RO, dialysis, GS, and pervaporation (PV)^{25, 26, 27}.

When the pores of a membrane become small, the nature of pores changes from static to dynamic. The term dynamic is used because pore diameters smaller than 5 Å enter the range of thermal motion of the membrane's polymer chains²⁸. These membranes will be called non-porous or dense, and the dynamic pores are described in terms of free volume at a molecular level³³.

Transport of both solvent and solute based on the SD model consists of 3 steps^{25, 33}. First, the permeant dissolves into the polymer at the high chemical potential side of the membrane. Secondly, it diffuses through the membrane down a concentration gradient. It will move from free volume element to free volume element which is possible because of the moving polymer chains. Lastly, desorption happens at the low chemical potential side of the membrane. The diffusion step will be the rate limiting step of this process in most cases. Separation of molecules is possible by both a difference in dissolution and diffusion rates. As the membrane is separating molecules based on subtle differences in characteristics, making sure the membrane is fully intact is of big importance, since defects will result in non-selective convective transport through the membrane³³.

When gases are separated using a dense membrane, the gas molecules will sorb and condense on the membrane before they are able to move through it and will eventually evaporate to appear as a gas again at the other side of the membrane. This sorption depends

on the ability of the gas to condensate and to mix with the membrane polymer²⁹. Permeation of these gas molecules through the membrane will happen with a certain permeability (P in Barrer), which is the result of the product of the solubility (S in $\frac{\text{cm}^3(\text{STP})}{\text{cm}^3\text{cmHg}}$) and the diffusivity (D in $\frac{\text{m}^2}{\text{s}}$) of the permeant:

$$P = S * D \quad 10$$

S and D are respectively thermodynamic and kinetic parameters. They both have an exponential dependence on temperature and are specific for different membrane materials^{33, 34}. Smaller molecules will have higher D values but lower S values, while the reverse is true for larger molecules³³.

In literature, the terms diffusivity selectivity and solubility selectivity are often used. This first term indicates the polymer's size sieving ability, which always favors the smaller molecule^{16, 29}. The second term is important for separation of molecules with similar size and can be tailored by introducing specific functional groups in the polymer that increase the solubility of the target molecule. Careful design is needed because the sensitivity of D towards polymer structure is generally larger, and changes more radically than S ²⁹. For more rubbery polymers though, D is less sensitive to the permeant size than for glassy polymers, meaning differences in solubility selectivity will dominate²⁹. Finally, more permeable polymers are often less selective, which is why upper bound lines can be defined in permeability-selectivity plots to represent the tradeoff between them¹⁶.

1.1.5 Membrane Processes

The separation mechanism of a membrane can be subdivided into classes based on the driving force. As previously mentioned, this can be pressure, temperature, concentration (activity/fugacity) and electrical potential. Only pressure- and concentration-driven membrane processes will be elaborated upon as these are the relevant driving forces for this thesis. Other membrane processes are extensively discussed in papers and books (references 17, 23, 30, and 34).

1.1.5.1 Pressure-driven membrane processes (PDMPs)

Pressure-driven membrane processes can be classified according to pore size (Table 1), but also according to the size of retained species²³. A short overview of the different kinds of membranes using pressure as a driving force is given here.

Microfiltration (MF) membranes are often used to filter out suspended solids and bacteria ($MW > 100$ kDa)^{21, 23}. Ultrafiltration (UF) can be used to retain dissolved macromolecules like

proteins from solutions (MW>10 kDa)³⁰. When the pores get even smaller and the nanofiltration (NF) range is reached, multivalent ions and dissolved organic solutes (>100-200 Da) are retained. Finally, reverse osmosis (RO) membranes can be used to retain most ions and permeate almost exclusively water molecules. This increase in rejection of compounds goes hand in hand with a drastic decrease in permeance (Table 1). Size exclusion due to molecular sieving will be the separation mechanism for the membranes with the biggest pores (MF, UF), and the solution-diffusion model will explain the mechanism for membranes with the smallest pores (NF, RO). In reality, there is no hard distinction between these processes, as the change from MF towards RO is gradual. This explains why in literature, one paper can refer to a “dense ultrafiltration membrane”, while another can refer to an “open nanofiltration membrane”, while both refer to a membrane with similar performance.

Table 1: Overview of pressure-driven membrane processes^{17,26,28,33}. SP= symmetric porous, AP= asymmetric porous, TFC = thin-film composite.

Membrane Process	Membrane Type	Separation Mechanism	Pressure (bar)	Pore Size (nm)	Permeance (l/m ² h.bar)
Microfiltration	SP, AP	Sieving	<2	100-10000	>50
Ultrafiltration	AP	Sieving	2-10	10-100	10-50
Nanofiltration	AP, TFC	Solution-diffusion	10-30	0.5-5	1.4-12
Reverse Osmosis	AP, TFC	Solution-diffusion	35-100	<1	0.05-1.4

Since RO membranes are able to remove monovalent ions from a solution, they are currently used for sea and brackish water desalination, producing around 1% of globally consumed fresh water³¹. High pressures are required for this process (Table 1). This is because of the osmotic pressure that builds up between the concentrated feed side and the diluted permeate side (Figure 5). To let water flow through the membrane from the concentrated to the diluted side, a pressure is required which exceeds the osmotic pressure. The resulting solvent (water) flux is given by:

$$J_A = A(\Delta p - \sigma \Delta \pi_m) \quad 11$$

where J_A is the solvent flux, A is the water permeation coefficient, σ is a correction factor because the membrane does not achieve 100% rejection, Δp is the applied hydraulic pressure, and $\Delta \pi_m$ osmotic pressure gradient across the membrane active layer between the feed and permeate sides^{17, 33, 34, 35}.

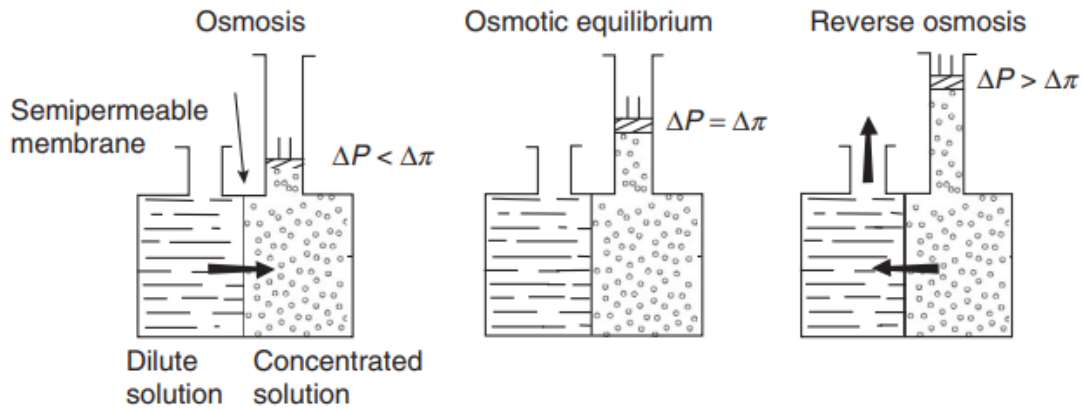


Figure 5: Graphical illustration of osmotic phenomena. From³².

The osmotic pressure (π , in Pa*10⁻³) can be calculated with following formula:

$$\pi = i * c * R * T \quad 12$$

where i is the number of osmotically active solute particles, c is the solute concentration (mol/L), R is the universal gas constant (8.31446 Nm/mol K), and T is the absolute temperature (K)³⁶. As a relevant example, the sea water in the Mediterranean Sea ($c = 0,68$ mol/L, $T = 290$ K)^{37,38} has an osmotic pressure of 32,8 bar. As the pressure needed to desalinate sea water is high, brackish water is often preferred for desalination because the lower salt concentrations result in lower required operating pressures.

The solute flux is given by a different equation:

$$J_B = B\Delta C_s \quad 13$$

Where B is the solute permeability coefficient and ΔC_s is difference in solute concentration over the membrane³⁵.

1.1.5.2 Concentration-driven membrane processes (CDMPs)

The driving force for CDMPs will be a concentration gradient, or better: a gradient in activity of the component over the membrane. Examples of CDMPs are dialysis, forward osmosis, PV and GS^{17, 39}. These GS membranes can be used in industry, as a lot of attention is being paid to reducing atmospheric carbon dioxide (CO₂) due to global climate change. Membranes are being installed to separate CO₂ from the exhaust gasses to avoid its release into the atmosphere. Some other typical commercial applications of GS are H₂ separation, supplying O₂ or N₂ enriched air and CO₂-removal from natural gas^{6, 30, 33, 29}.

For gasses, the driving force is actually a gradient of fugacity (f), which is the effective pressure, or “escaping tendency” of the gas⁴⁰. For an ideal gas, fugacity is equal to the partial pressure of the gas in the feed stream. For real gasses at high pressure, the difference between fugacity

and pressure becomes important ($f/P=0,71$ for $P=60$ bar)³³. Depending on the application, gas pressures used in GS can range between 1 and 100 bar^{17, 41 - 44}. To increase the concentration of the permeant, the total pressure needs to increase. In fact, concentration and applied pressure are more or less proportional to each other for gas separations using membranes^{17,23}. Therefore, most of the coming examples could also have been discussed under the PDMPs. PV and GS both require a fugacity gradient across the membrane and the separation mechanism is based on the SD model when dense membranes are used. Exceptionally, porous membranes can be used for GS as well, which will allow Knudsen flow (pores of 10-100 nm) or molecular sieving (pores of 0,5-10 nm)^{17, 6}.

1.1.6 Membrane fouling and concentration polarization

The performance of most membranes does not stay constant over their lifetime, as the flux and selectivity are often noticed to change over time. This can be attributed to membrane fouling, which will decrease the flux through the membrane due to an increased flow resistance and is a problem that all pressure-driven membrane processes face⁴⁵. A difference can be made between reversible and irreversible fouling, which respectively refer to a more loosely, and tightly attached foulant on the membrane surface. The former can be cleaned physically, while the latter requires chemical cleaning⁴⁶.

Membrane fouling can be classified in different ways. Here, the classification of Du *et al.*⁴⁷ is followed. Internal fouling, also known as “pore blocking”, is caused by adsorption of solutes within the pores of the membrane. External fouling, also called “cake formation”, is caused by deposition of particles and molecules on the membrane surface due to the pressure difference between the feed and the permeate sides.

Concentration polarization is another class of membrane fouling and refers to the accumulation (or depletion) of solutes and ions near the membrane surface as a result of selective transport^{47,48,50}. This can cause certain species to exceed their saturation concentrations, resulting in the formation of precipitates⁴⁹. However, the main reason for a decrease in flux are not these precipitates, but the need for an increased driving force. A boundary layer is formed where concentrations become higher than in the bulk solution (Figure 6). This will induce a reverse diffusive flux, lowering the actual flux through the membrane. To maintain a constant flux, the pressure will have to increase with time. The effect on retention depends on the solute size. It can become higher because large molecules prevent one another to go through this concentrated boundary layer, but it can also be lower for example for salts due to the high local concentrations³³.

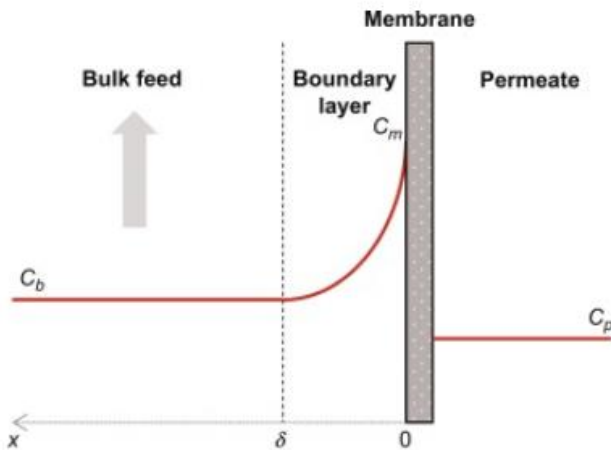


Figure 6: Concentration profile with concentration polarization. Adapted from⁵⁰.

There are ways to prevent membrane fouling. By implementing pretreatment measures like sand filters, impurities and large molecules can already be eliminated from the process⁵¹. Other methods include improving the membranes structural properties, applying cleaning procedures, backwashing, improving turbulence over the membrane by using patterned membranes or by applying crossflow^{33, 52}.

1.2 THIN FILM COMPOSITE MEMBRANES

A TFC membrane is an asymmetric membrane made from two or more layered materials. It generally consists of a nonwoven fabric backing, a porous base layer (polysulfone (PSF), polyimide (PI), polyvinylidene fluoride (PVDF) or polyether ether ketone (PEEK) UF membranes) which serves as a mechanically strong support layer, and a thin selective layer. The microporous support layer is often synthesized using the phase inversion technique and the selective layer for liquid separation applications by interfacial polymerization (IP), and for gas separation applications by coating techniques (dip-, spin-, drop coating)⁵³. As mentioned earlier, the materials that make up the three layers are different and thus can be optimized individually to obtain a membrane with specific properties⁵⁴.

Polyamide (PA) TFC membranes are widely used in RO for desalination. A cross section of such a membrane is depicted in Figure 7. A polyester nonwoven is used to provide extra mechanical stability, and the microporous substrate is used as an intermediate layer to provide a more gradual change in pore sizes. It also serves an important role in regulating transport pathways of water and solutes through the membrane, and furthermore, in IP, dictates the formation of the PA film to some extent⁵⁶. Because of this importance of the microporous substrate, multiple ways to fine-tune its properties have been applied such as incorporating nanomaterials, blending substrate polymers, and the like⁵⁷. To improve the membrane

performance further, alternative monomers can be used during IP, modifications can be made to the membrane surface, and the polymerization reactions can be optimized⁵⁸.

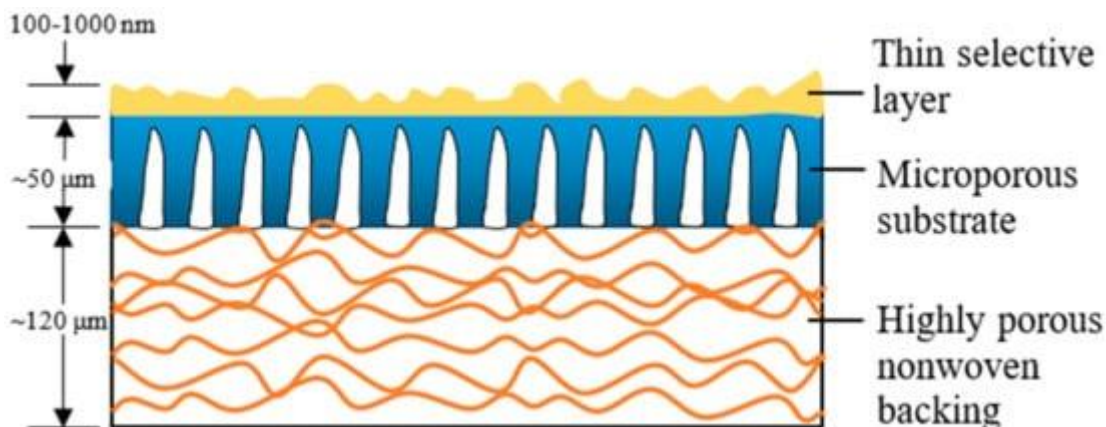


Figure 7: Schematic representation of the PA TFC membrane structure. From⁵⁵.

1.2.1 Phase inversion

Phase inversion is a technique widely used in the commercial production of stand-alone MF and UF membranes. This makes it a suitable technique to produce support layers for TFC membranes. The technique is based on the transition from a homogeneous liquid polymeric casting solution into a solid membrane in a controlled manner^{6,21,59}. This transformation occurs as a result of a demixing process, that changes the thermodynamically stable single phase casting solution into a polymer rich phase, which will solidify to form the solid matrix, and a polymer lean phase, which can be washed out to form the membrane pores^{6,21}. Multiple methods exist to induce this demixing process, such as solvent evaporation, thermal precipitation (cooling down of cast film) and immersion precipitation (immersion in nonsolvent)⁶⁰. The latter, also known as nonsolvent-induced phase separation (NIPS), is capable of forming different membrane morphologies by tweaking several synthesis parameters, such as casting temperature and composition of the nonsolvent bath, making it a popular method for asymmetric membrane formation^{59,61}. As this method will be used to make support layers in this work, the mechanisms playing a role in NIPS are discussed below.

1.2.1.1 Mechanisms of NIPS

A dope solution is cast and subsequently submerged in a nonsolvent bath where the solvent will leave the solution, and phase separation will be induced. To fully understand the NIPS mechanism, its kinetic and thermodynamic aspects must be considered. To visualize the latter, a ternary phase diagram (Figure 8), where polymer, solvent, and nonsolvent are represented by the corners of the diagram, is often used. Every mixture of those three components is a point in the triangle. The binodal line separates the thermodynamically stable monophasic

region from the metastable region. In this metastable region, demixing will allow a polymer rich and a polymer lean phase to form according to a “nucleation and growth” mechanism. These two phases are in equilibrium with each other, and their composition is shown by the point where the binodal and the tie-line cross. The metastable region is separated from the thermodynamically unstable region by the spinodal curve. In this regime, the two phases will form co-continuously and can alter to form nuclei⁶⁰.

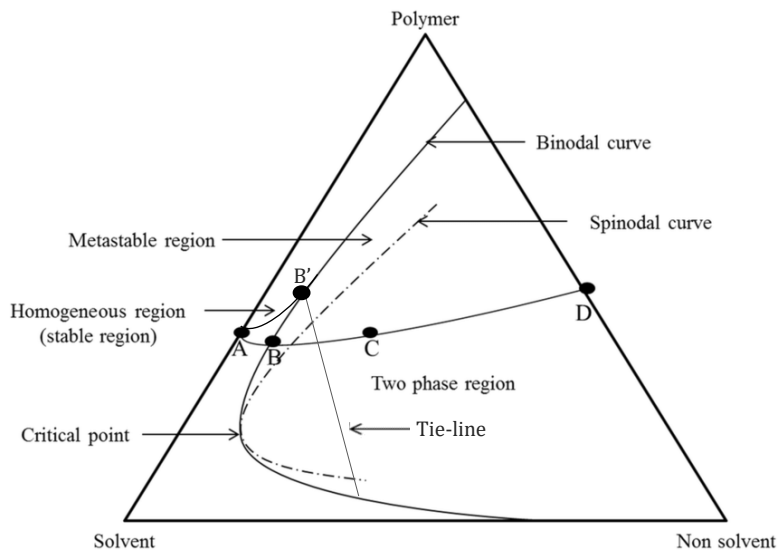


Figure 8: Ternary phase diagram. Adapted from⁶².

If a cast polymer solution has composition A on Figure 8, different paths can be followed during the immersion in the nonsolvent bath. If the path goes from A to B' within $t < 1$ second, the demixing will happen slowly and is thus called “delayed demixing”. This will result in rather dense, sponge-like morphologies, causing the membrane to have rather low permeances but high rejections (Figure 9). If the path goes from A to B to C within $t < 1$ second, the unstable region will be reached quickly (point C), causing demixing to happen fast. This process is called “instantaneous demixing”. A more open (more permeable) membrane will be formed with finger-like macrovoids in the substructure and with generally a lower rejection^{60,65}.

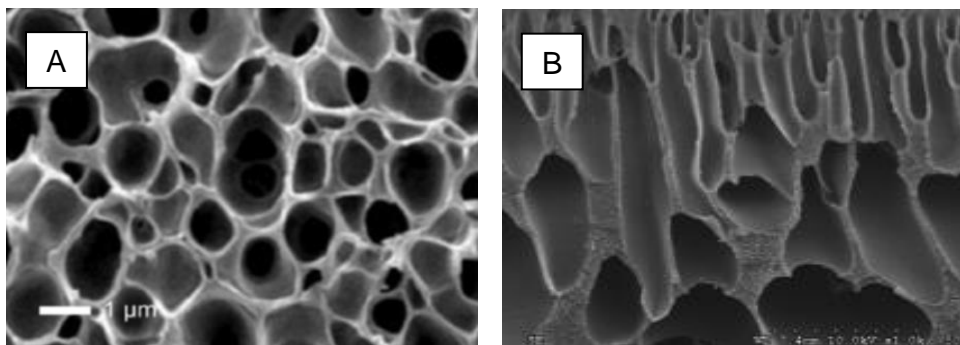


Figure 9: Sponge-like (A)⁶³ and finger-like (B)⁶⁴ membrane morphology.

Although the phase diagram is a useful tool to study the thermodynamics of the system, it does not provide any information about the kinetics. The mass transfer rate between solvent and nonsolvent determines the kinetics of the demixing process, which depend on, amongst others, the viscosity and the chemical potential gradient. When a cast film is immersed in a nonsolvent coagulation bath, the gradient at the top part of the film will be the largest, resulting in the highest exchange rate. With time, the exchange rates slow down because the gradient gets smaller and because a top layer is formed which adds resistance to mass transfer⁶⁰. When more viscous solutions are used, these rates are lower as well.

1.2.1.2 Parameters of influence

As mentioned earlier, a lot of different membrane morphologies can be formed using the NIPS technique. Changes in morphology mostly originate from the diffusion speed of the solvent and nonsolvent in or out of the cast film⁶⁰. There are several parameters that when adjusted slightly can result in a different performance of the membrane. These parameters will not be discussed in depth as it would be out of the scope of this work, hence only an overview will be given of some important parameters. A more detailed discussion of these parameters is demonstrated by papers like 60 and 65. A list of important parameters^{21, 60, 65}:

- Choice of polymer: pretreatment (MW, drying...), concentration, and hydrophilicity (for water purification)
- Choice of solvent: determined by polymer (Hansen solubility parameters), viscosity, and interaction with nonsolvent.
- Choice of nonsolvent: determined by viscosity, interaction and miscibility with solvent.
- Additives
- Casting conditions: evaporation time, temperature, casting speed, impregnation of support, relative humidity, membrane thickness
- Precipitation conditions, composition of coagulation bath, temperature, residence time in coagulation bath
- Post-treatment: annealing, drying, solvent treatment, crosslinking

1.2.2 Interfacial polymerization

In conventional IP, two monomers are dissolved into two immiscible phases. Typical monomers used in the synthesis of PA membranes are trimesoyl chloride (TMC) in the organic phase, and m-phenylenediamine (MPD, for RO membranes) or piperazine (PIP, for NF membranes) in the aqueous phase^{55, 66, 67}. The pores of the support layer are impregnated with the aqueous monomer solution, and the organic monomer solution is added on top. The monomers will diffuse to the interface and can react with each other through a step-growth copolymerization

(see 1.3.3.1) to form an interfacial crosslinked polymer film which will be the selective layer. The formed polymer network will be confined to the interphase due to its low solubility in both phases⁶⁸. The amine is applied in a higher concentration to ensure complete polymerization. The supply of reactants through the forming layer is low, resulting in a self-terminating reaction which leads to a very thin polymer film⁶⁹. Next, a heat treatment can be performed for further polymerization and for better adhesion between the support and selective layer⁷⁰. The final membrane performance will depend on various factors during the synthesis process, such as concentration, reaction time, post treatment, and properties of the support layer⁶⁹.

As mentioned in the introduction about TFC membranes, the influence of the support on the toplayer formation is quite important. The support layers which are being used are just regular UF membranes with their own limitations. For example, it is important to assess the stability of the support material in relation to the feed solution regarding application optimization. Regarding the synthesis, a large distribution in pore sizes can be present in these membranes, causing the IP solutions to penetrate deeper into some pores than others resulting in a PA layer that varies in thickness, or that is defective⁷¹. This variation in pore sizes and porosity can also affect the availability of monomer at the interface, along with the interactions between monomer and support. The surface hydrophilicity is also important to ensure good adhesion between the PA layer and support layer. For a hydrophilic support, the most dense layer in the PA film will be formed at the interface of the PA film and the support with an outward growth direction of PA, while for hydrophobic support layers the densest layer will be formed at the top surface of the PA layer with an inward growth direction (Figure 10)⁷².

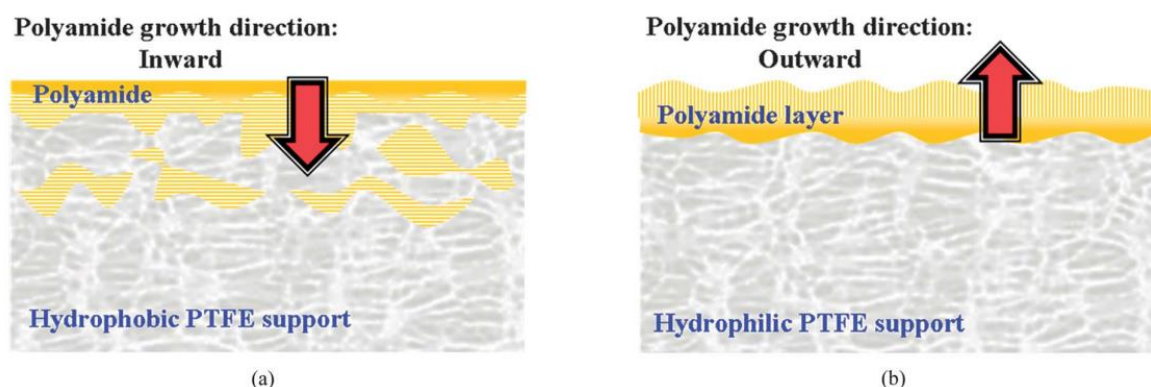


Figure 10: Selective PA layer growth. A) hydrophobic PTFE membrane, first immersed in organic phase, then aqueous phase. B) hydrophilic PTFE membrane, first immersed in aqueous phase, then organic phase. From⁷².

The surface morphology of typical MPD-TMC-based membranes is described by a “ridge-and-valley” (R&V) structure, while for PIP-TMC-based membranes it is a more globular structure (Figure 11)^{55, 73, 74}. There is still debate in literature about the desirability of these R&V structures are desirable, as they often indicate high NaCl rejections, and could enhance the

surface area to generate higher fluxes⁷⁵. A downside could be an increased colloidal fouling behavior due to this increased surface roughness⁷⁶. To promote R&V formation, rougher and more porous supports could be used as they provide a larger reactive area between the IP solutions. More hydrophilic supports could allow deeper penetration of aqueous phase into the support, hence forming the PA layer deeper inside of the support resulting in a smoother surface⁷⁵.

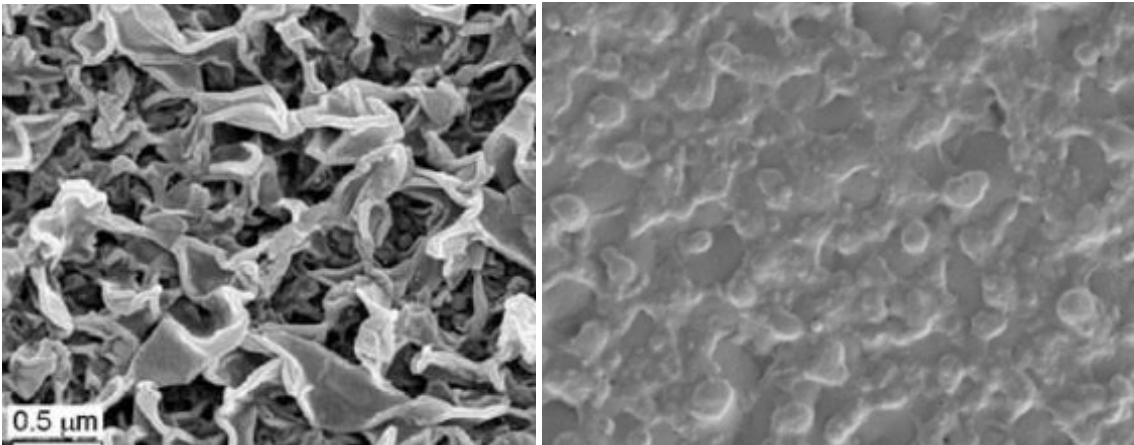


Figure 11: Left) Surface ridge-and-valley structure of PA layer, typical for MPD-TMC membranes. From⁷³. Right) surface globular structure, typical for PIP-TMC membranes. From⁷⁷.

1.2.3 Interfacial initiation of polymerization (IIP)

In IIP, the process is slightly different compared to conventional IP. Instead of a reaction between two monomers, now a monomer and an initiator are dissolved into two immiscible phases (Figure 12). The chain-growth polymerization reaction (see 1.3.3.2) is initiated by the initiator at the interface and proceeds in the organic phase, in which the monomer is dissolved. In contrast to conventional IP, the reaction is not self-terminating (it can continue as long as there is monomer available), and the polymer will mainly consist of one monomer and the initiator will be built in at chain ends and during crosslinking⁷⁹. In section 1.3, the IIP system will be applied to the synthesis of epoxide-based membranes for which the reactions will be discussed more in detail.

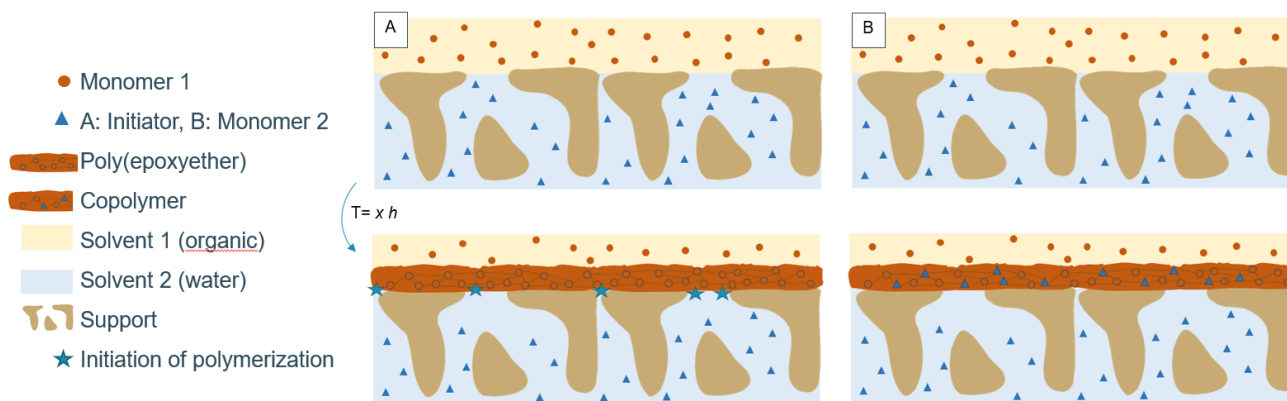


Figure 12: Schematic representation of A) IIP B) conventional IP.

1.3 POLY(EPOXYETHER) MEMBRANES

In the search for stable and robust membranes, epoxides have recently received attention. Although epoxide bulk chemistry is well-established, the application of epoxides in membrane technology is new. Verbeke *et al.*⁷⁹ published a first paper of a series in 2019 about transferring epoxide bulk chemistry to interfacial synthesis of TFC membranes. In the upcoming part, the characteristics (stability, reactivity) of these epoxides, how they compare to normal ethers, how they can be used, and which polymerization pathways can be followed to synthesize a membrane with them, will be discussed in depth.

1.3.1 Ether Characteristics

The ether bond is a C-O-C linkage, which can rotate rather easily. To assess the reactivity/stability of organic molecules, the leaving group, which will need to accept electrons to be able to leave the molecule, plays an important role. For alcohols and ethers for example, those leaving groups (O-H and O-R respectively) are similar strong bases which want to donate electrons, making them less reactive and requiring them to be activated to undergo a substitution or elimination reaction⁸⁰.

As a result, ethers are generally quite stable. Alkyl phenyl ethers decompose around 400 °C and under normal circumstances most ethers only react with hydrogen halides. Reactivity towards the C-O bond cleavage is similar in ethers as in alcohols (similar leaving group)^{80, 81}. Ethers will need to be activated by protonation before undergoing a nucleophilic substitution. Acids like HBr or HI will be able to do this but HCl will not because Cl⁻ is too poor a nucleophile in water (polar protic solvent) compared to Br⁻ and I⁻. Even in those cases, the reactions still require heating in order for them to have a sufficiently high rate^{80, 82}. Acids are often used for cleaning in, *e.g.*, reverse osmosis water desalination practices, but are also present in feed streams of other applications like mine leachates. Alkaline chemicals can be added as well in,

e.g., cleaning in place (CIP) membrane cleaning systems to remove organic foulants⁸³. The lack of reaction with most of these acids and bases makes ethers a better choice of material for a membrane than the less stable polyamide for example.

1.3.2 Epoxides

Even though epoxides (or oxiranes) could be classified as ethers, their reactivity is completely different. This is because of their characteristic form: a three membered ring consisting of two carbon atoms and an oxygen atom. The carbon atoms in this arrangement have a sp³ hybridization which means the ideal bond angle would be 109,5°. In reality, this angle is only 60°, resulting in a lot of ring strain which makes epoxides reactive⁸⁴.

Epoxides can be made by a chemical conversion of an alkene through the chlorohydrin or hydroperoxide routes. The chlorohydrin process (Figure 13) was introduced during the first world war in Germany. In this process, propylene for example can react with chlorine, and this product reacts with calcium hydroxide to be dechlorinated and form the epoxide⁸⁵.

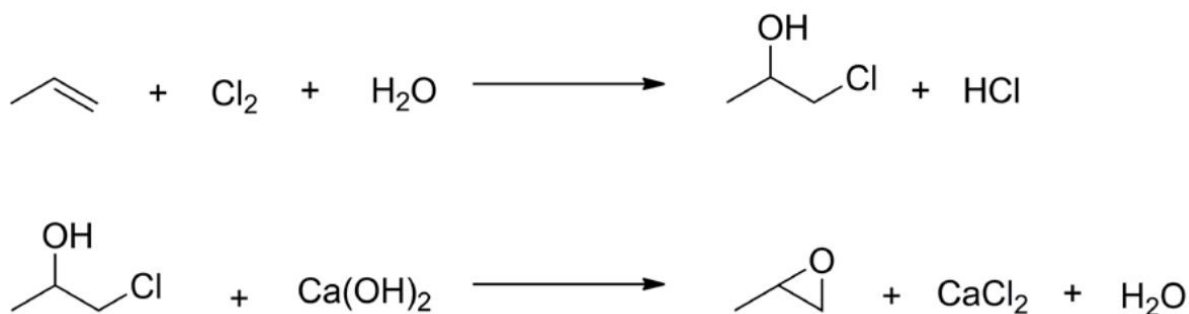


Figure 13: Chemical reactions occurring in the chlorohydrin process. From⁸⁵

A more efficient pathway is the direct oxidation of ethylene to ethylene oxide by using a silver catalyst⁸⁶. An alkene can also react with hydroperoxide in the presence of a metal catalyst. The chlorohydrin and hydroperoxide reactions are carried out on an industrial scale but generate a lot of acid and chlorinated waste⁸⁷.

Epoxides can be bought as the pure compound as such, or as epoxy resins, consisting of prepolymers which are made by condensation reactions⁸⁸. These epoxy resins are thermosets, implying that the curing of the prepolymers is irreversible, and an insoluble, rigid polymer network can be formed. Multifunctional curing agents (a broad range of nucleophiles^{89, 90, 91}) can be used to form strong networks⁹². These cured networks as well as the prepolymers are both denoted as 'epoxy resin'¹¹².

1.3.3 Polymerization

The driving force of epoxide polymerization is the strain on the oxirane ring^{93, 94}. Epoxides can polymerize through different mechanisms, of which the most important for this thesis will be discussed below. They will mostly react through a S_N1 mechanism in acidic environments and through a S_N2 mechanism in neutral or basic environments^{95, 96}. Because amines were used as initiators in this work, most examples are applied to them. Amines are bases, which results in an S_N2 mechanism for the ring opening of epoxides.

1.3.3.1 Step growth

To be able to have a step growth reaction, two different functional groups are needed. These can be on two different monomers, or both on the same one. The polymer chain grows by addition reactions occurring in discrete steps between monomers, oligomers and polymers but this is a slow process most of the time⁹⁷. It lacks a termination step, which means that polymers can keep on reacting as long as there are reactive groups left⁹⁷.

Strong nucleophiles such as primary or secondary amines can open the epoxide ring by performing a nucleophilic substitution reaction (Figure 14)⁹⁸. This is also called “nucleophilic ring-opening polymerization” (NROP), and is a step growth polymerization reaction. The direct attack will happen according to the S_N2 mechanism, meaning that the nitrogen will attack the least sterically hindered carbon atom of the oxirane ring⁹⁹. The product of these reactions are β -alkanol-amines (Figure 14). Secondary amines show lower reactivities than the primary amines because of the increased sterical hindrance. The crosslinking reaction, which will form a poly(β -alkanol-amine) polymer is accelerated by the presence of hydroxyls^{100, 101}. Tertiary amines resulting from these reactions are most often too sterically hindered to contribute to further homopolymerization reactions¹⁰².

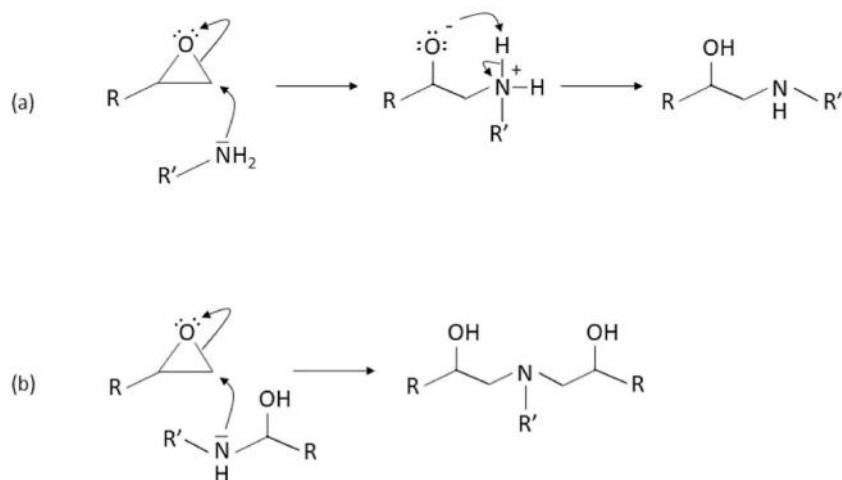


Figure 14: Reaction mechanism for step-growth polymerization in presence of (a) primary amines and (b) secondary amines. From⁹⁸.

If the epoxide is not bifunctional, only very short chains will be able to form (Figure 14), while when multifunctional monomers are used, a large, interconnected network can be formed (Figure 15)¹⁰³.

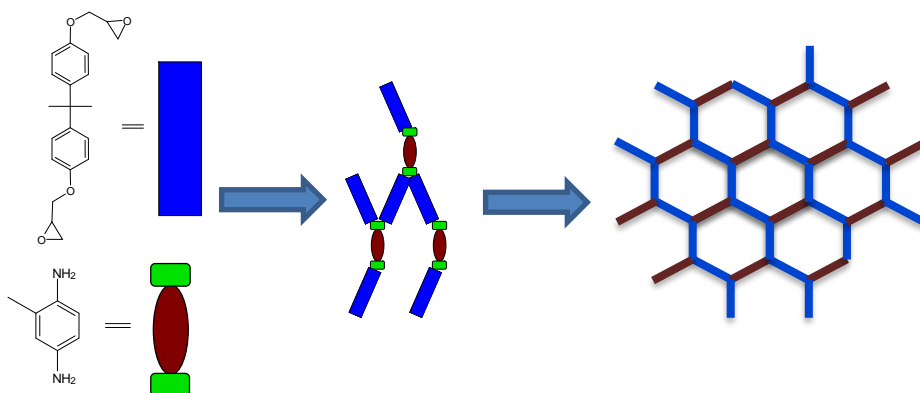


Figure 15: Polymer network formation via step growth polymerization. Adapted from¹⁰³

1.3.3.2 Chain growth

In contrast to the discrete reactions happening in the step growth reactions, chain growth reactions depend on the amount of active sites (chain ends)⁹⁷. The polymerization process contains three steps: initiation, propagation and (in most cases) termination¹⁰². Initiation and propagation include nucleophilic substitution reactions^{93,97}. A visual representation of this mechanism is provided in Figure 16 to be able to easily compare this mechanism to the step growth polymerization mechanism.

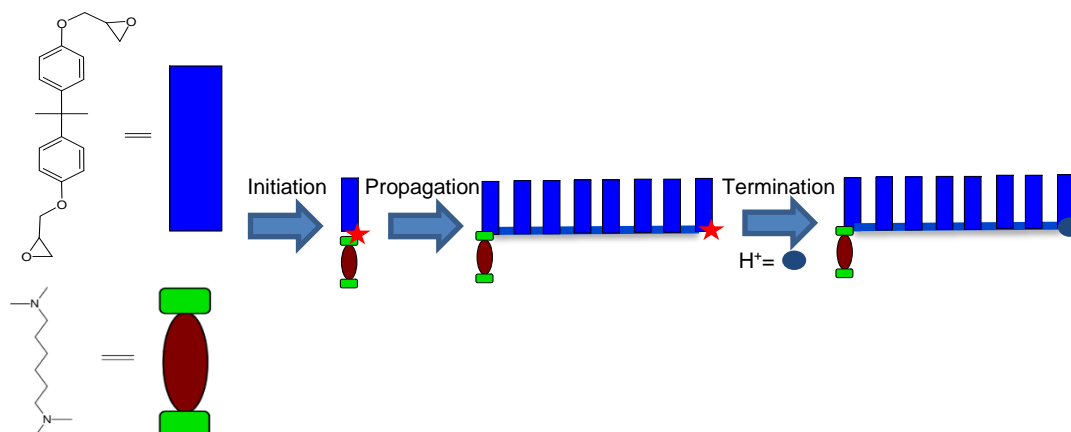


Figure 16: Polymer network formation via chain growth polymerization.

1.3.3.2.1 Anionic ring-opening polymerization

An example of oxirane ring opening chain growth polymerization is the anionic ring-opening polymerization (AROP). Requirements for this kind of chain growth homopolymerization are the presence of Lewis acid catalysts, Lewis bases like tertiary amines or inorganic bases like

sodium hydroxide¹⁰². There have been a lot of studies about this AROP but there is still no universally accepted mechanism agreed upon.

The mechanism starts with an initiation step, where an anion is formed which will be the propagating species. Reaction 1a depicts a direct attack on the amine on the least sterically hindered carbon atom through a S_N2 reaction mechanism to form a zwitterion^{93, 104}. Some researchers conclude from kinetic experiments that proton donors are necessary for this reaction to happen, as the phenyl glycidyl ether (PGE) polymerization virtually did not occur when using dimethylbenzylamine (DMBA) as an initiator in the absence of a proton donor¹⁰⁵. In that case, the proton donor will activate the epoxy ring by constructing a hydrogen bond and thus forming a donor-acceptor complex with the epoxy compound, as depicted by reactions 1b. The amine can attack the carbon atom and through a trimolecular transition state, the active site will be formed^{100, 101, 105}. Other researchers believe the tertiary amine does not need an external proton donor to open the ring, which they explain by isomerization of the epoxy compound resulting in an unsaturated alcohol¹⁰⁶. In reaction 1c, the amine gets protonated by a proton donating compound to yield a reactive alkoxide which will be the propagating species. In any case, the anion that is formed will be stabilized by electron-withdrawing groups¹⁰⁷. The polymerization is believed to be autocatalytic because of this zwitterion/alkoxide formation as active catalysts in the process. These two species are only stable at relatively low temperatures (under 60 °C for ethylene oxide)¹⁰¹.

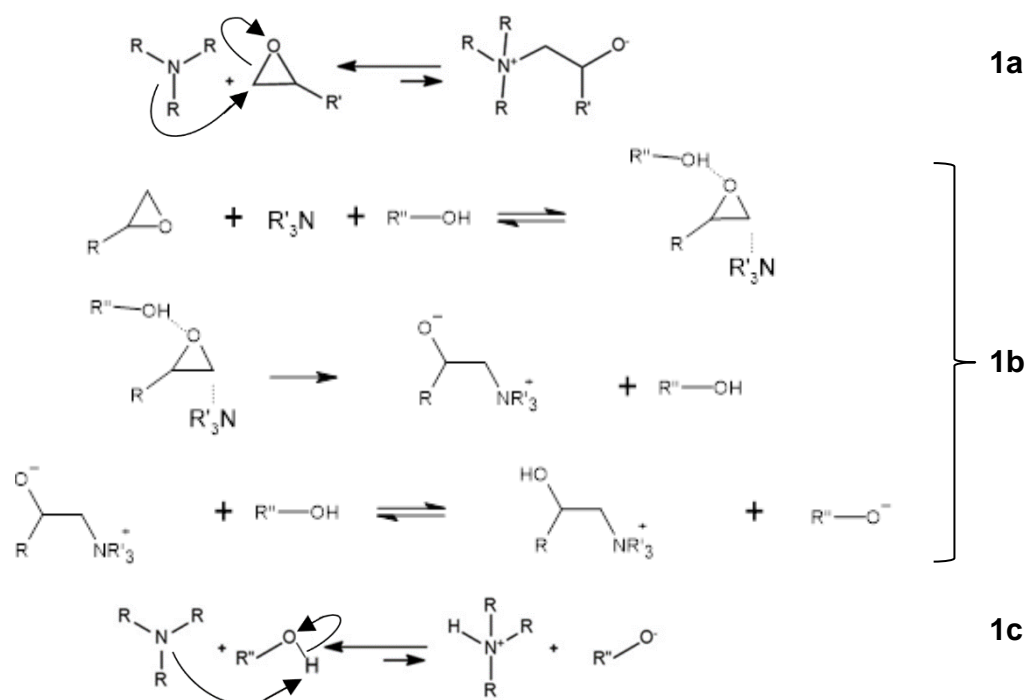


Figure 17: Possible reaction mechanisms for anionic ring-opening polymerization of epoxides initiated by a tertiary amines, including donor-acceptor complex formation by a proton donor to form the propagating species. Adapted from^{100, 79}

The propagation step is the second step in the reaction mechanism. The reactive alkoxide formed during the initiation step will continue reacting with new epoxides resulting in a growing polymer (Figure 18)^{93, 101, 104}. It is often shown that the presence of hydroxyl containing compounds speeds up the polymerization rate, but the effect of an increased amine concentration is observed to have a larger effect on the polymerization rate (consumption of monomer) than the same increase of, e.g., alcohol concentration¹⁰⁸. The structure of the co-catalyst (hydroxyl containing compound) seems to have a very small effect on this acceleration effect. Another important trend is the inverse relationship that is usually seen between catalyst concentration and molecular weight of the polymer chain^{106, 108}.

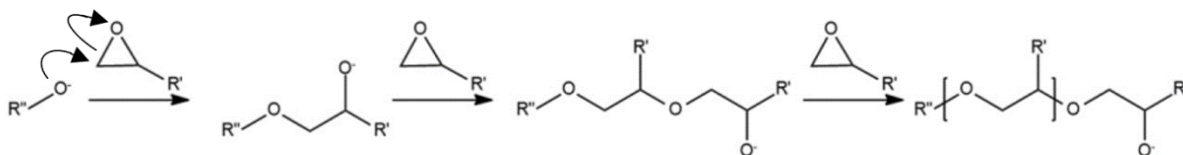


Figure 18: Propagation step in the AROP of epoxides with a tertiary amine as initiator.

The last step in the process is a termination step in which active species are consumed in an irreversible way¹¹⁰. This can happen by a zwitterion or proton donor that reacts with the alkoxide. As can be seen in Figure 19, the hydroxyl concentration will remain constant¹⁰¹.

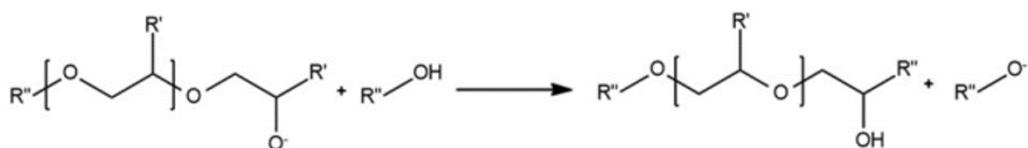


Figure 19: Termination step in the AROP of epoxides with a tertiary amine as initiator

Downsides of these AROP reactions are the low reaction rates with long induction periods and the relatively short chains produced because of transfer reactions^{93, 101, 110}. These transfer reactions can happen as side reactions in this process, resulting in allyloxy compounds as depicted in Figure 20⁹⁴.

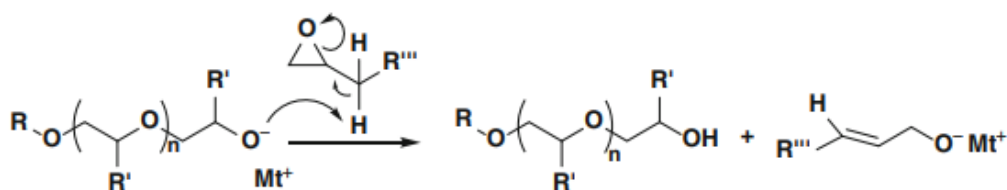


Figure 20: Transfer reaction of the propagating alkoxide and epoxide monomer. Adapted from⁹⁴.

1.3.3.2.2 Initiators for AROP

As mentioned earlier, inorganic bases like sodium hydroxide but also alkali metal derivatives (mainly alkoxides) or organoaluminium based initiators can be used^{102,94,109}. When using inorganic bases for polymerization, the resulting polymers will be of low MW⁹⁷. In order to get polymerization initiated with alkali metal alkoxides, an aprotic and apolar medium (e.g., dimethyl sulfoxide (DMSO), dimethylformamide (DMF)) should be used to be able to dissociate the active species⁹⁴. However, the system used in this thesis consists of a water and a toluene phase and therefore it is not possible to use alkoxides. Some extra attention needs to be paid to tertiary amines as initiators because they will be used in this work. The important groups are imidazoles, alkanolamines, aromatic and, aliphatic amines. The aliphatic tertiary amines have mostly been studied until now.

Aromatics

An amine group has a positive mesomeric effect on the phenyl ring when it is directly attached to it, making the free electron pair less available to execute nucleophilic attacks¹⁷⁸. Hence, purely based on nucleophilicity, aromatic amine initiators are expected to have lower initiation rates than aliphatic initiators. However, it could be interesting to use initiators containing aromatic rings in certain systems as it would decrease the solubility in the aqueous phase. When a defined reaction zone is desired and no further diffusion of the initiator in the aqueous phase is wanted, the use of an aromatic initiator could be an option.

Imidazoles

Imidazoles have a secondary and a tertiary amine group, which could potentially react through different reaction mechanisms (Figure 21). The tertiary amine (3-(N)) is the active nucleophile that reacts to form an alkoxide adduct, which would be the true catalyst of the reactions with epoxides¹¹⁰. Through a H⁺ transfer reaction, a neutral molecule is obtained, of which the 1-(N) nitrogen likely shows similar reactivity as the 3-(N) nitrogen towards the epoxide group and forms a zwitterion¹¹¹. The formed alkoxide will then propagate the polymerization¹⁵⁷.

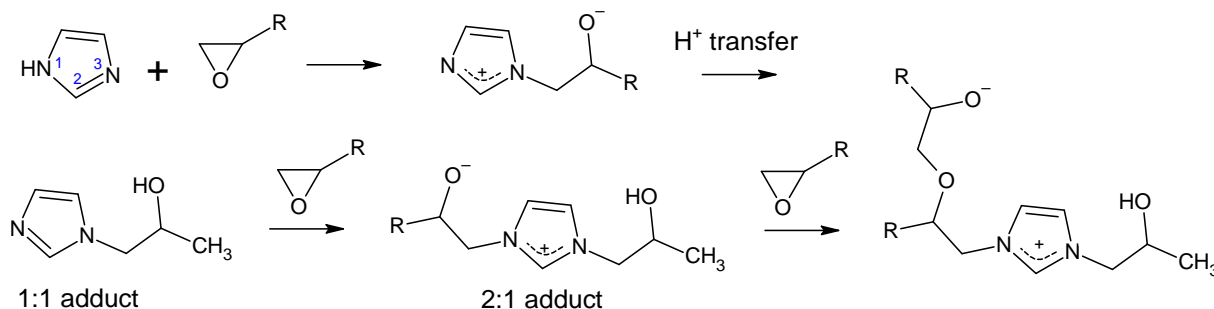


Figure 21: Generally accepted reaction mechanisms of imidazoles with an epoxy resin. Adapted from¹⁵⁷.

Berger and Lohse (1985), on the contrary, describe differences in conversion and time dependencies between polymerization catalyzed by 2-ethyl, 4-methyl imidazole and 1-methyl imidazole, suggesting different starting mechanisms when epoxides are polymerized by imidazoles with or without secondary amines¹¹³. Depending on the rate of the proton transfer, this could be explained by the fact that 1-(N) substituted imidazoles directly form a 1:1 adduct containing the reactive alkoxide compared to the unsubstituted imidazoles, if proton transfer happens quickly, only form a 2:1 adduct containing the reactive alkoxide group¹¹². The polymerization rate and degree of polymerization is observed to increase with increasing catalyst (alcohol) concentrations¹¹³.

Alkanolamines

Alkanolamines contain a hydroxy group, making the 1b reactions in Figure 17 the most plausible initiation mechanism. It could be expected that the polymerization has a higher rate than the polymerization with an aliphatic tertiary amine as initiator because of the presence of these hydroxy groups. When initiator concentrations increase, more epoxy groups can be activated resulting in a higher crosslinking degree and (crosslinking) reaction rate, and a shorter induction time¹¹⁴.

1.3.4 Advantages of PEE membranes

1.3.4.1 Liquid separation applications

The water that is purified in industrial RO plants often contains salts, bacteria, and suspended solids. Aforementioned, this can cause membrane fouling, causing adverse effects on the separation process like membrane plugging, which results in an increased energy use and a reduced membrane lifetime. Chemical pretreatment is because of these issues an important step in industrial RO plants. Caustic chemicals like NaOH can be added resulting in a decreased solubility of certain compounds like organic carbon (TOC), silica, and boron. Acids like HCl or H₂SO₄ are often added in order to reduce membrane plugging by, *e.g.*, increasing calcium carbonate (CaCO₃) solubility, hence reducing CaCO₃ scaling¹¹⁵. There are different reasons why H₂SO₄ is preferably used over HCl, *e.g.*, it reduces corrosion of the piping network and pressure vessels¹¹⁵. Another downside of HCl is that when it used, a lot of precaution must be taken to eliminate all free chlorine in the feed after the acid treatment, as it would oxidize the common PA RO membranes¹¹⁵. Other factors that affect the lifetime of RO membranes are hydrolysis, operating pressure, bacterial attack and chemical degradation¹¹⁶. Given this information, an innovative RO membrane should be able to handle certain acids, bases, free chlorine, and high pressures.

The polyether polymer chains are, as mentioned earlier, quite stable. In some cases, these ether groups are still susceptible to an attack, *e.g.*, when an ether oxygen is directly attached to an aromatic ring (benzyl ethers)⁸¹. Both HCl and H₂SO₄ will not react strongly with ethers because of the weak nucleophilicity of their anions, resulting in a preference of SN1 reactions over SN2 reactions^{80, 81, 82}. Only for concentrated H₂SO₄, a reaction could occur. Besides this stability for acids used in RO, ether bonds are also very stable towards bases, oxidizing and reducing agents⁷⁹. Polyethers also have a high hydrolytic stability^{117, 118}.

1.3.4.2 Gas separation applications

In order to reach high selectivities, one can choose for a membrane with high diffusivity- or solubility selectivity²⁹. The first will always favor the smaller molecule, however a high P and α are desired for CO₂/light gas (CH₄, N₂, H₂) separation, which can be accomplished by optimizing the flexible membrane material towards solubility selectivity by choosing a polymer containing a lot of polar groups¹⁶. Ether oxygens have been proven to provide good CO₂ separation as well as permeation properties²⁹.

1.3.4.3 General advantages

Some additional advantages are:

- a) By crosslinking the chains with tertiary amines, positive charges will be built in, and the membranes will achieve charge-based rejection mechanisms¹¹⁹.
- b) There is a wide range in epoxy monomers available for the synthesis of these PEE membranes, often produced at large scale, hence giving the opportunity to easily tune the membranes.
- c) The epoxide chemistry is well established. A lot of research has already been done about the reactivity and curing, which is helpful in understanding processes that are happening during synthesis or membrane performance.

PART 2: MATERIALS AND METHODS

2.1 MATERIALS

2.1.1 Support layer

2.1.1.1 Commercial PAN support

The commercial PAN support used in this work is a PX UF PAN-based membrane (MWCO 400 000 Da), purchased from Synder Filtration. This membrane requires a pre-treatment to remove a pore blocking agent. The chemicals used in the pretreatment are:

- 2-Propanol (IPA), ACS reagent, 99+%, Chem-lab NV
- Deionized water (DI water)

2.1.1.2 In-house synthesized PAN support

PAN supports were also synthesized in-house on top of a non-woven support. These non-wovens were polyester based Hollytex 3329 purchased from Kavon Filter Products Co. and the polyethylene terephthalate/polybutylene terephthalate (PET/PBT) Novatexx 2483 purchased from Freudenberg Filtration Technologies were used. The chemicals required during the synthesis steps are:

- Polyacrylonitrile (PAN), MW = 150 000 g/mol, Sigma-Aldrich
- 1-methyl-2-pyrrolidone (NMP), 99% (extra pure), Acros Organics
- *N, N*-Dimethylacetamide (DMAc), 99% (pure), Acros Organics
- DI water

2.1.2 Selective layer

2.1.2.1 Monomers and initiators

The EPON™ resin 1031 by Hexion (denoted as EPON) is used in the RO system as the epoxide monomer, while poly(ethylene)glycol diglycidyl ether (MW=512 g/mol) by Sigma-Aldrich (denoted as PEGDE) is used in the GS system.

EPON, or tetraphenolethane tetraglycidylether (Figure 22, A), is a solid multifunctional epoxy resin, able to form a dense crosslinked polymer. EPON has an epoxy-equivalent-weight (EEW, *i.e.*, the weight of the resin per epoxide group) of 195-230 g/eq¹²⁰. The resin should contain low levels of ionic impurities and has an excellent thermal stability. It is often used in laminate applications, structural composites and adhesives¹²¹.

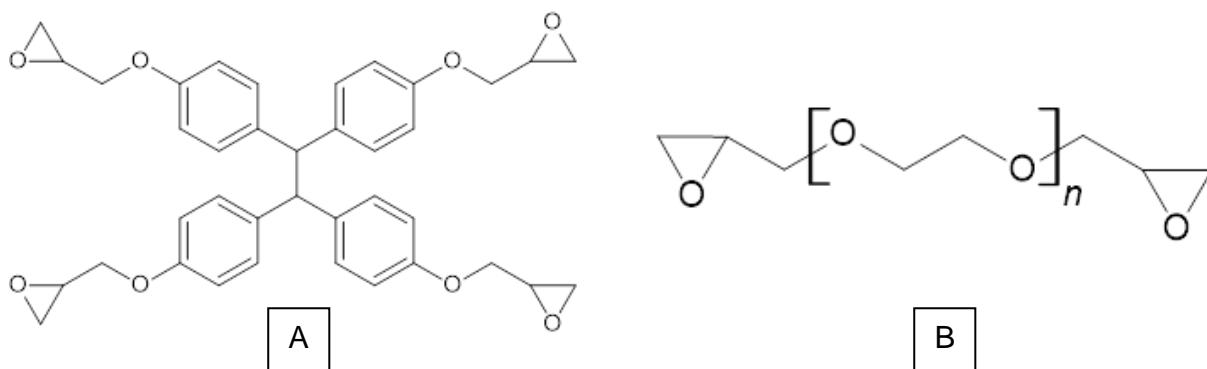


Figure 22: A: EPON structure, B: PEGDE structure.

PEGDE, or poly(ethylene glycol) diglycidyl ether (Figure 22, B), is a viscous fluid which is highly soluble in water and produced by polymerizing ethylene oxide^{122,123,124}.

In addition to these two monomers, the following chemicals were used during the synthesis of the TFC membrane:

- *N, N, N', N'*-Tetramethyl-1,6-hexanediamine (TMHD), >98%, Tokyo Chemical Industry Co., LTD.
- *N, N, N', N'*-Tetramethyl-1,3-propanediamine (TMPD), 99+%, Acros Organics™
- Imidazole (IM), 99%, ThermoFischer (Kandel) GmbH.
- 1-Methylimidazole (1-MIM), >99%, Tokyo Chemical Industry Co., LTD.
- 2-Methylimidazole (2-MIM), 99%, Sigma-Aldrich
- 1,4-Diazabicyclo[2.2.2]octane (DABCO), >98%, Tokyo Chemical Industry Co., LTD.
- Tris(2-dimethylaminoethyl)amine (Me6Tren), 98+%, ThermoFischer (Kandel) GmbH
- 1-Methylbenzimidazole (1-MBI), >98%, Tokyo Chemical Industry Co., LTD.
- 4,4'-Methylenebis(*N, N*-dimethylaniline) (MBDA), 98%, Acros Organics™
- Toluene, >=99%, Fisher Scientific
- Milli-Q (MQ) water (18.2 MΩ.cm at 25 °C)

2.1.3 Spin coating

The chemicals used for spin coating the sealing layer on top of the GS membranes are:

- SYLGARD™ 184 Silicone Elastomer Base, The Dow Chemical Company.
- SYLGARD™ 184 Silicone Elastomer Curing Agent, The Dow Chemical Company.
- n-heptane, 99+%, Chem-lab NV

2.1.4 Feed solutions for filtration experiments

Pure water flux measurements and rejection tests were performed using:

- Milli-Q (MQ) water (18.2 MΩ.cm at 25 °C)
- Sodium chloride (NaCl), Fisher Scientific

2.1.5 Gas separation experiments

The gases used for gas separations are:

- Carbon dioxide (CO₂), >99.995%, Air Liquide
- Methane (CH₄), >99.995%, Air Liquide
- Nitrogen (N₂), >99.995%, Air Liquide

2.1.6 Zeta potential measurements

The chemicals used during zeta potential measurements are:

- Potassium chloride (KCl), 99.995% (metals basis), Thermo Scientific Alfa Aesar
- Hydrogen Chloride (HCl), 37%, A.C.S. Reagent, VWR
- Potassium Hydroxide (KOH), 99.98% (metals basis), 85% min, Thermo Scientific™

2.1.7 Porometry

To prepare samples for the gas liquid porometry measurements, following chemicals were used:

- Porefil 250, fluorinated hydrocarbon wetting fluid, Porometer
- Ethanol, 99+%, Fisher Scientific

2.2 METHODS

2.2.1 Commercial PAN support pretreatment

To prevent pore collapse, commercial membranes are often treated with pore conservers. Before use, these conserving chemicals must be washed out the PAN PX support. This is done by immersing the membranes in a 1L beaker containing a mixture of 75 v% DI water and 25 v% IPA. After 15 mins, the membranes are turned around in the beaker to ensure every part of the membrane is wetted. After 15 more mins, the mixture is discarded and the beaker containing the membranes is filled and emptied 3 times with DI water. Then, the membranes remain for 20 mins in the beaker filled with DI water before storing them in a DI water filled plastic container in a refrigerator for later use.

2.2.2 In-house PAN support synthesis

The commercial PAN PX support that was used is likely a polyvinyl acetate (PVAc)-PAN blend, although the exact composition is unclear. To avoid the observed significant differences between different batches of the same type of commercial support, PAN supports were cast in-house. First, the PAN polymer powder was dried in the oven at 100 °C for at least 24 h to evaporate any adsorbed water. Dope solutions were made by weighing PAN into a vial and

filling a small Duran bottle with solvent (NMP or DMAc). The solvent was stirred at 700 rpm at 60 °C when the PAN was added all at once from the vial into the bottle, to achieve a homogeneous dispersion of the dope solution. Then the stirring was gradually decreased down to 50 rpm while maintaining the heating at 60 °C. The PAN solution was left overnight to dissolve, removed from the stirring plate and left to degas overnight. Hereafter, the dope solution was cast with a wet-film thickness of 250 µm on a solvent impregnated non-woven using a film coating device (MEMCASTTM, Porometer) at a certain speed (3 cm/s for 12 wt% PAN in DMAc, and 1 cm/s for 15 wt% PAN in DMAc) at room temperature. The non-woven was attached to a glass plate using tape and was dabbed with a paper tissue to remove excess solvent. Immediately after casting the glass plate was submerged into the nonsolvent bath filled with DI water at room temperature. After 20 mins, the cast membranes were transferred into plastic containers filled with DI water for storage in a refrigerator. Every time when casting, the relative air humidity was measured using a memory hygrometer/thermometer (Traceable® Products). This protocol was adapted from reference¹²⁵.

2.2.3 Initiator concentration calculation

To compare other initiators to TMHD, molar equivalents of amine groups rather than similar w/v% were used. In a 1 w/v% solution of TMHD in water, 0,0058 moles TMHD or 2 x 0,0058 moles of amine groups are present. A 1N concentration is equal to the amine molar equivalent to 1 w/v% TMHD, 2N to 2 w/v% TMHD and 4N to 4 w/v% TMHD. One active amine group was used in concentration calculations for the 1-MIM, two for TMHD, IM, 2-MIM, DABCO, TMPD, and MBDA, three for Me6Tren.

2.2.4 Support-free interfacial polymerization

To check whether film formation was possible, vial tests were carried out for the different initiator-monomer pairs. In a glass vial, a bottom phase of 5 w/v% PEGDE in MQ water and a top phase of 1N amine solution in toluene were contacted to mimic the GS system. For the RO system, a bottom phase of 1N amine solution in MQ water and a top phase of 1.5 w/v% EPON in toluene were contacted. After certain time intervals (1 h, 2 h, 1 day, 3 days, 1 week), a visual check was performed to verify whether a film was formed at the interface.

2.2.5 Selective layer synthesis

The toplayer synthesis allows for tuning of various parameters. In this study, mostly initiator concentration and reaction time were varied.

2.2.5.1 Reverse osmosis membrane

Two kinds of selective layers can be synthesized using the protocol of Verbeke *et al.*⁷⁹: the one-step (1S)- and two-step (2S) membranes. To synthesize this 1S membrane, the PAN support is impregnated for 1h in a slowly stirred aqueous initiator solution. If the initiator is sensitive to light, the cylinder was wrapped in aluminum foil. After impregnation, excess liquid on top of the membrane was blown off using compressed air. Next, the membrane was fixed in a specifically designed IP setup (Appendix, Figure 50, active area of 88 cm²), and about 50 mL of 1.5 w/v% EPON in toluene was poured slowly into one of the corners of the setup. A glass lid was placed on top of the setup to prevent toluene evaporation. After allowing the reaction to proceed for a fixed duration, the EPON solution was discarded, and 25 mL of toluene was poured into the corner and the setup was slightly rocked to remove unreacted monomers from the formed membrane. After this washing step, the membrane was removed from the setup, dried at room temperature for 5-10 mins, and placed in DI water for 1 h to remove excess initiator. Finally, the membrane was stored in a plastic container filled with DI water in a refrigerator until further use.

To synthesize the 2S membrane, the impregnation and the first EPON step are similar to the 1S membrane. After this first EPON step, however, the solution is now replaced with a fresh 50mL of 1.5 w/v% EPON solution. After an additional hour of reaction, the solution is discarded, and the membrane washed with toluene. Subsequently, 50 mL of the aqueous initiator solution is applied and left to react for 1h. This solution is then discarded, the membrane washed with toluene, and subsequently dried for 5-10 mins. The membrane is then placed in DI water, and finally stored in a refrigerator as for a 1S membrane.

2.2.5.2 Gas separation membrane

The synthesis of the GS membranes is similar to the RO membranes, with the difference that some phases are inversed, and the IP setups are slightly bigger (active area of 112 cm²). For 1S membrane synthesis a 5 w/v% of PEGDE in MQ water solution is used for impregnation, and about 75 mL of initiator in toluene solution was poured into one of the corners of the setup. The membranes were washed by applying three glass pipets of about 4 mL toluene homogeneously over the membrane, and slightly rocking the setup. Hereafter, the membrane was removed from the IP setup and again rinsed with toluene using a glass pipet. The membrane was fixed on a glass plate and dried overnight. Next, the membranes were

immersed in toluene for 18 h in order to remove alle unreacted monomers. Finally, the membranes were dried and stored in a box protected from dust.

For the 2S membranes, the impregnation, PEGDE and washing step are similar to the 1S membrane, but now 75 mL of fresh 5 w/v% solution of PEGDE in toluene was added again to react for 1 h. After a toluene washing step, 75 mL of initiator in toluene solution was added again for an additional hour of reaction. Finally, a toluene washing step, membrane drying, immersion in toluene and storage were conducted similarly to the 1S membrane.

2.2.6 Solvent annealing of supports

To check whether toluene anneals the support membrane, exactly the same process is done as the synthesis of a selective layer, but without monomer or initiator. The supports can be 1S- or 2S annealed.

2.2.7 Spin coating

As the performance of GS membranes is sensitive to defects, it is necessary to apply a PDMS-sealing layer on top of the TFC membranes, sealing any potential defects allowing convective transport of gasses. The PDMS layer should be sufficiently thin, in order to not significantly alter the membrane permeance.

The PDMS sealing layer was applied using spincoating (Erichsen spincoater), using an adapted protocol from Nikolaeva *et al.*¹²⁶. A 20 wt% PDMS with a 1:10 curing to base agent solution in heptane was prepared¹²⁷. This solution was pre-cured for 1 h in an oil bath at 70°C whilst stirring. After being allowed to cool for 30 mins, 2 mL of cooled off solution was applied the membrane surface using a micropipette prior to spinning for 1 min at 1000 rpm. This procedure was repeated 3 times, always leaving 10 mins between every spinning step.

2.2.8 Adsorption tests

Methylene blue adsorption tests were performed to measure the adsorption capacity (q_t) of different types of membranes according to an adapted protocol from Bull (2022)¹²⁸. A membrane coupon was cut and excess water was dabbed off using a paper towel upon weighing. This coupon was then immersed in 50 mL of 15 μ M aqueous methylene blue solution in a glass beaker which was sealed off to avoid evaporation. The solution was stirred at 300 rpm using a magnetic stirring plate, and after certain time intervals, a 2 mL sample was taken using a micropipette, of which the absorbance was measured using a UV-VIS spectrophotometer. The adsorption capacity at time t (q_t , mg/g) was plotted against the time and calculated according to

$$q_t = \frac{\sum_{n=0}^{n=t} V_n (c_{n-1} - c_n)}{m}$$

14

where c_0 and c_t are the dye concentrations (mg/L) in the liquid phase at time 0 and time t , V_0 and V_t are the volume (L) of the solution at time 0 and time t , and m is the mass of the membrane coupon (g). One reference experiment was included, for which all the steps were the same, except no membrane coupon was added to the dye solution. Since no substantial change (*i.e.*, background adsorption) in dye concentration was observed for the control experiment, there was no need to correct the observed “adsorbed” dye mass in order to calculate the membrane adsorption capacity.

2.2.9 Membrane characterization

2.2.9.1 Gas liquid porometry

The pore size and pore size distribution of a membrane can be derived by measuring the gas (N_2) pressure needed to displace a certain wetting fluid present in the pores¹²⁹. The higher the pressure, the smaller the pores can be which will be emptied. This will result in an increasing gas flux through the membrane until all pores are empty, as of when the gas flux will increase linearly with the pressure. First, a wet membrane sample is immersed in pure ethanol for at least 2 h in order to replace all water. This is required as the surface tension of ethanol is lower than of water, which will make it easier to be replaced by porefil (a fluorinated hydrocarbon wetting fluid) in the next step. This replacement is done by completely immersing the membrane sample in porefil and placing this in the vacuum oven for 2 h at room temperature. Afterwards, the membrane sample is placed in the PoroluxTM (Porometer), and a wet curve is measured, representing the gas flow through the membrane in function of the applied pressure. At the highest pressure, all pores should have been emptied, so that the dry curve of the membrane can be measured subsequently. Based on the data of those two curves, information about the largest, mean, and smallest pores can be calculated as well as, total pore number and surface porosity.

2.2.9.2 Liquid filtration experiments

Liquid filtration experiments were done using a SpiderTM (Porometer) high throughput membrane testing module. In this dead-end filtration setup, 16 membrane coupons (active filtration area of 1.54 cm²) could be tested under the exact same conditions. 4 coupons of the same membrane were measured in order to provide statistically adequate results and compensate for any defect coupons. To measure the pure water flux (for support layers), MQ water was used as feed and a pressure of 1 bar was applied (pressurized N_2). To measure salt

rejections, a 5 mM NaCl in MQ water solution at 10 bars was used, stirred at 350 rpm during the filtrations to reduce concentration polarization.

After allowing the membranes to reach steady state, permeate was collected in glass vials for a certain amount of time in order to calculate permeance and rejection using equations 4 and 7, where dQ can be calculated from the amount of mass collected in the time interval and the density of the permeate, and C_r is the retentate concentration the end of collecting permeate in the vial. Salt concentrations were determined by conductivity measurements using a Consort™ C3010 multiparameter analyzer.

2.2.9.3 Gas separation experiments

Gas separation experiments were done using a high throughput gas separation device (HTGS™ (Porometer)), where 16 membrane coupons (active filtration area of 1.54 cm²) could be tested under the same conditions. For all separations the same conditions were used: a temperature of 35 °C and 2 bars of upstream pressure of a 25/75 CO₂/N₂ mixture. The membranes were left overnight in the HTGS in order to initially reach steady state. When the feed composition was changed to 100% CO₂ or N₂, steady state was checked by measuring the selectivity of the least permeable membrane every half hour for at least 1.5 h. When the deviation between two consecutive measurements was less than 1%, steady state was assumed. Hereafter, the selectivity and permeance of the other coupons were measured. Selectivity was measured using a compact gas chromatograph with a Porabond Q/ RT-Q-bond column (Interscience). Permeance was measured by capturing the permeate gas in a known, constant volume while measuring the change in pressure. To calculate the selectivity, equations 8 and 9 were used.

Formulas used for respectively mixed-gas and pure-gas permeability (barrer) are:

$$P_{i,mixed} = 10^{10} \frac{y_i \times V \times l}{x_i \times p_{up} \times A \times R \times T} \frac{dp}{dt} \quad 15$$

$$P_{i,pure} = 10^{10} \frac{V \times l}{p_{up} \times A \times R \times T} \frac{dp}{dt} \quad 16$$

where y_i and x_i are the mole fraction of component i in the downstream and upstream respectively, V is the downstream volume (cm³), l is the membrane thickness (cm), p_{up} is the upstream pressure (Torr), A is the membrane permeation area (cm²), R is the gas constant, and T is the temperature (K)^{12, 127}.

2.2.9.4 Attenuated total reflectance Fourier-transform infrared spectroscopy (ATR-FTIR)

ATR-FTIR was used as a qualitative characterization technique to determine the membrane chemical composition. To minimize interference with water, the membranes were dried for at least 24 h atmospherically before measuring the spectrum. A Bruker Alpha FTIR Spectrometer was used, equipped with a diamond crystal and a single point MCT detector. A spectrum was recorded between 400 and 4000 cm^{-1} with a resolution of 2 cm^{-1} by taking the average of 32 scans with a scanning depth between 0.5 and 2 μm ¹³⁰.

2.2.9.5 Scanning electron microscopy (SEM)

SEM was used to visualize the surface morphology of the selective layer and cross section of the support layers. Small pieces of dried membrane were fixed on a sample holder by carbon tape. A JEOL JFC-1300 Auto Fine Coater was used to coat the samples twice for 30 seconds with a 60/40 Au/Pd coating, to prevent charge accumulation what could result in image artifacts¹³¹. The measurements were conducted on a JEOL JSM-6010 LV scanning electron microscope, operated with acceleration voltage of 10 keV.

2.2.9.6 Contact angle measurements

Contact angle measurements were performed with a Krüss DSA 10-Mk2 Drop Shape Analysis System in order to characterize the hydrophilicity of the membrane surface. A water droplet of 4 μL was formed at the tip of a needle, and subsequently put into contact with membrane surface. Through a set of lenses, the Drop Shape Analysis System measured the contact angle between the membrane surface and the water droplet for 30 seconds (static contact angle). Afterwards, the needle was inserted in the droplet without touching the membrane, and continuously inserted water at 6,32 $\mu\text{L}/\text{min}$. These “advancing” contact angles were measured again for about 30 seconds. By using this advancing contact angle method, more consistent results should be retrieved from the same membrane sheet as surface inhomogeneities will have less influence^{132, 133}.

2.2.9.7 X-ray photoelectron spectroscopy (XPS)

By irradiating the membrane surface with an X-ray beam, electrons from the top 1-10 nm of sample will be ejected with a certain kinetic energy. By measuring these ejected photoelectrons, a quantitative elemental composition as well as binding energies of the atoms present at the membrane surface can be derived¹³⁴. To record sample spectra, an X-ray photoelectron spectrometer (Axis Supra, Kratos) with a monochromatic Al $K\alpha$ ($h\nu = 1.4867$ keV, 10 mA emission) X-ray source, hemispherical analyzer, hybrid (magnetic/electrostatic) optics and a multichannel plate and delay line detector (DLD) with a take-off angle of 90° was used. To hold the pass energy at a constant value, the hemispherical analyzer was set in Fixed

Analyzer Transmission (FAT) mode. All the survey scans were taken at a pass energy of 160 eV and high-resolution scans at a pass energy of 20 eV, all under charge neutralization conditions using a low energy electron gun within the field of the magnetic lens. The spectra were processed using the CasaXPS software¹⁴⁸. Obtained results are preliminary due to time constraints.

2.2.9.8 Zeta potential

Zeta potential measurements were performed on a SurPass 3 (Anton Paar). The samples, which were stored in water, were blotted at the non-woven side with tissue paper to allow good attachment to the sample holder. The samples were then cut in squares of 20 x 10 mm and subsequently attached to the sample holders of the same dimensions with carbon tape. Each zeta potential measurement was performed using 150 mL of 1 mM KCl solution (in MQ water), which was first acidified to pH 2 with a 0.1 M HCl solution. Argon gas was used to purge the electrolyte solution to reduce the buffering effect and resulting pH drift of dissolved CO₂. Before starting the pH scan, the sample was allowed to stabilize in the acidified electrolyte solution by performing 10 rinse steps at 600-200 mbar, at which time the gap height was adjusted to a value between 90-110 μm . Once the sample was stabilized, the pH scan was initiated. Each step consisted out of 2 rinse cycles, followed by 4 zeta potential measurements (600-200 mbar, all values above 500 mbar were discarded to reduce measurement errors). The pH was varied in steps of 1.5 and titration was performed using a 0.1 M KOH solution. All data points with a correlation coefficient lower than 0.9 between the measured value and predicted value of the Helmholtz-Smoluchowski equation were discarded.

PART 3: RESULTS AND DISCUSSION

In order to study the role of the initiator on the epoxide-based membrane synthesis and performance, a strategically chosen set of initiators was defined. For RO membranes, the initiators should be soluble in water, while for GS membranes, they should be soluble in toluene. As these systems significantly differ from each other, the influence of the initiator on the synthesis-structure-performance relationship of these two classes of membranes is discussed separately.

A standardized testing procedure was used for every initiator. First, support-free interfacial polymerization via simple vial tests was conducted to verify whether a film formed at the interface. Second, a set of membranes was synthesized by keeping the monomer concentration constant, but by varying the type of membrane (1S or 2S), the reaction time (1 or 3 h), and the initiator concentration (0.5N, 1N, 2N, 4N). These synthesis conditions are represented by a membrane code, e.g., PAN PX TMHD 1N 1S 1h, where the first part represents the support on which the toplayer is synthesized (here PAN PX), the second part the initiator (here TMHD), and the third part the specific synthesis conditions (a concentration of 1N in a 1S-type membrane with a reaction step of 1 h). Third, ATR-FTIR measurements were performed to verify the occurrence of polymerization, with as key attention points the decrease of epoxide absorption bands and the increase in alkyl ether and initiator related bands. When there were signs of polymerization, filtration experiments were carried out. Finally, more physicochemical characterization techniques like SEM, contact angle, zeta potential, and XPS were executed in order to establish the membrane synthesis-structure-performance relationship. In addition, differences in performance originating from varying synthesis conditions for the same initiator, were examined.

3.1 RO SYSTEM

3.1.1 Support-free interfacial polymerization tests

Although limited, vial tests can provide rudimentary information about an interfacial reaction¹³⁵. First of all, it provides information on the occurrence of polymerization. Furthermore, the evolution of a formed film can be tracked in time, giving information about the speed at which the polymerization process occurs. Care must be taken when interpreting these results as this is only a proxy for the real system. Indeed, there is no support layer present, nor is there a possibility to perform a densification step, and visual observations might not always be accurate. Reference experiments are conducted in which either EPON or the initiator is omitted

from the system. When EPON is omitted, no film is observed. However when the initiator is omitted, a thin, transparent film is observed (Appendix, Figure 52), likely to be a layer of deposited EPON molecules at the water-toluene interface due to the interactions with glycidyl ether functional groups. For all the studied initiators, film formation is observed within 2 h (Figure 23), suggesting that all amines are able to initiate the epoxide ring-opening polymerization. In the TMHD vial test, film formation is observed after 30 mins, in the 2-MIM vial test after 1 h, and in the other tests after 2 h. After one week, morphologically similar thin, white films which are confined to the interface can be observed for all initiators. For TMHD, a thick, yellow film which is rather spread out over both phases is formed up to an extent where it starts to sink into the aqueous phase. The thickness of the film can be attributed to the high dissolution of TMHD into both phases, or its higher nucleophilicity.

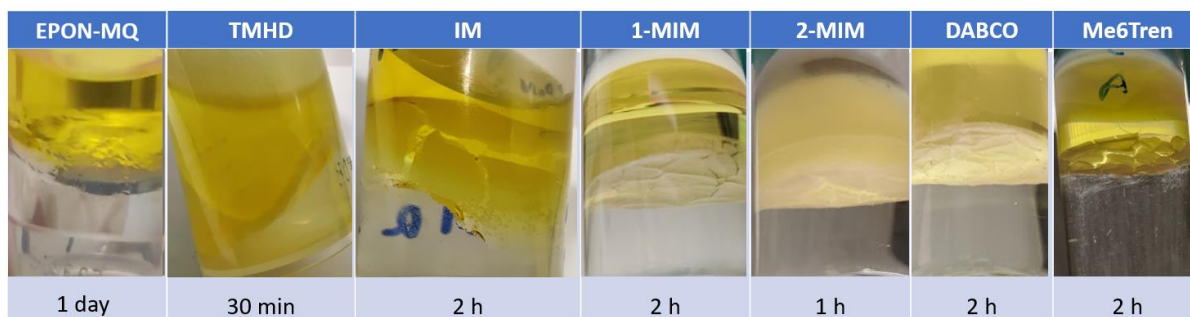


Figure 23: Overview of the vial tests with different initiators for the RO membranes. Upper phase: 1.5 w/v% EPON in toluene, lower phase: 1N initiator in MQ water. Most left picture: reference experiment: no initiator added in the water phase. Pictures are taken after one week of reaction. At the bottom, the time after which film formation is first visually observed has been provided.

This is in line with the short time after which the film can visually be seen, indicating a relatively high polymerization rate. The thin film formed using the other initiators could be the result of a more confined reaction zone as the other initiators are less toluene soluble (in-depth physicochemical property comparison in specific initiator sections), or the formed films being less permeable for the initiators (which are less flexible than TMHD) hence inhibiting the film formation faster¹³⁶. As this results in a thin synthesized selective layer, it might be an interesting characteristic for IIP. However, the time after which first signs of film formation were observed are higher, making them less attractive for IIP.

3.1.2 Defining the reference system: TMHD

As a film is formed in every vial experiment, the initiators appear to be promising candidates for membrane synthesis. The EPON-TMHD system has already been studied thoroughly, hence this is defined as the reference system, as such a system is necessary to compare membranes synthesized with new initiators with^{79,119,169}.

Besides the synthesized toplayer, other effects like unreacted monomer adsorption or solvent annealing of the support layer can also contribute to the observed salt rejection.^{169, 137, 138}. Hence, a baseline needs to be established which signifies this background rejection due to non-toplayer effects, which was done by synthesizing a membrane according to the 2S synthesis procedure, but without the initiator was added in the aqueous phase so that no polymerization could occur (*i.e.*, no initiator (NI) membranes).

3.1.2.1 Membrane performance on PAN PX

Reference 1S and 2S membranes were synthesized on a commercial PAN PX support (further denoted as PAN PX) using TMHD as the initiator. These have a NaCl rejection of respectively 38% and 85% with concurrent water permeances of ~0.5 and 0.1 LMH/bar (Figure 24). The salt rejection of the 2S membrane is comparable to what is reported in literature (81%), but the permeance is drastically lower¹¹⁹. Similarly as previously observed in literature, it seems that the 2S densification and re-initiation step is crucial in order to obtain high salt rejection. Remarkably, the baseline NI membrane has rejection of ~41% and a permeance of 0.56 LMH/bar (Figure 24, NI). This performance does not differ significantly from the 1S TMHD membrane.

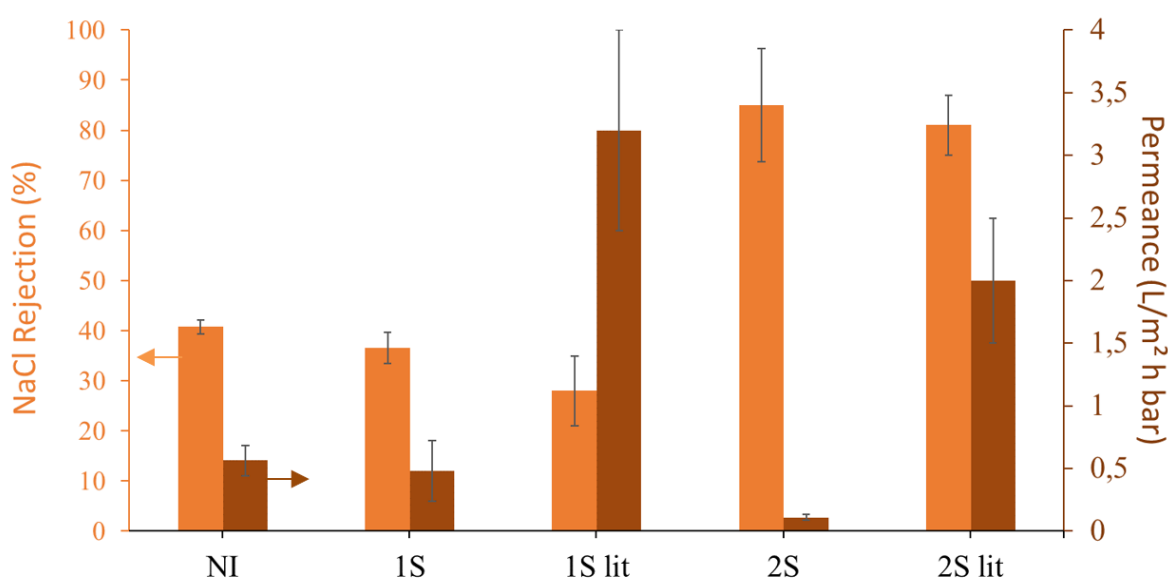


Figure 24: Performance of 1S and 2S membranes synthesized with TMHD as the initiator at a concentration of 1N, with reaction steps of 1 h. Literature performance of the 1S and 2S membranes are depicted as “1S lit” and “2S lit”¹¹⁹. Filtration conditions: 10 bar, 5 mM NaCl aqueous solution.

Problems related to PAN PX and optimization of in-house cast support

Firstly, the flux of all the epoxide-based TFC membranes is low compared to previous results. Since the synthesis procedure is identical, the performance of a pristine, and solvent annealed (2.2.6) PAN PX support was determined (Figure 25). The permeance is respectively 16.5 and

11 LMH/bar, which is extremely low for an ultrafiltration membrane and also lower than the previously used batch of this PAN PX, showing permeances of respectively ~140 (pristine) and ~100 (solvent annealed) LMH/bar¹²⁵. The low permeance of this support layer combined with the rather low total pore area of ~2% (50% smaller than the previous PAN PX batch), can lead to the observed small permeances of the overall TFC membrane. Indeed, the so-called “funnel effect” predicts that the permeate will have to be transported laterally in the toplayer along a longer path before it can reach a pore of the support layer and be removed, compared to more open support layers¹³⁹.

The second problem related to the support membrane is observed for the NI membrane. Ideally, the rejection of this membrane would be close to zero with a permeance close to that of the solvent annealed support so that deviations from this baseline value for the TFC membranes can be attributed to the presence of a toplayer. However, EPON adsorption seems to significantly contribute to the salt rejection of this membrane (Figure 25). This could be explained by the low total pore area of the support (~2%)¹²⁵. Support pores are more likely to be covered and as such be “sealed” by EPON adsorption when the surface porosity is low, further reducing the permeance from an already intrinsically low value¹⁴⁰.

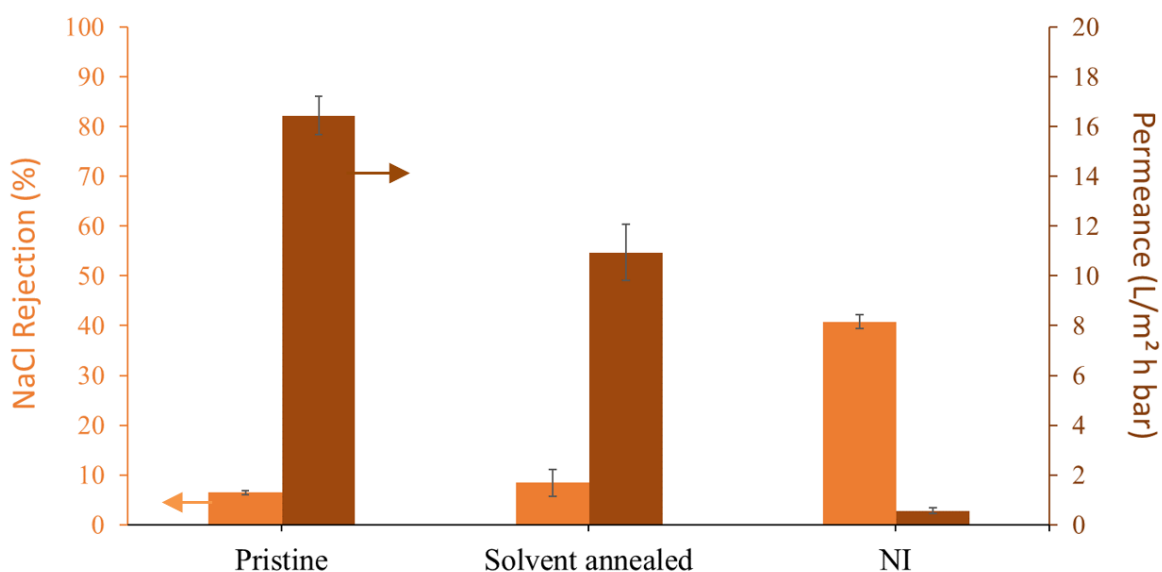


Figure 25: Performance of the PAN PX support. Pristine refers to a washed PAN PX membrane, Solvent annealed to a synthesis procedure of a 2S membrane but without EPON or initiator present in the toluene and water phase. Filtration conditions: 10 bar, 5 mM NaCl aqueous solution.

The problematic adsorption can also partly be attributed to the fact that the PAN PX support is likely a PAN-PVAc blend, as suggested by ATR-FTIR absorption bands at 1735 cm⁻¹ and 1235 cm⁻¹, corresponding to respectively C=O and C-O stretches (Figure 27)^{148, 173}. The presence of PVAc can slightly increase the hydrophilicity of the membrane, which might increase EPON

adsorption. However, as the exact composition of the membrane is not revealed by the manufacturers but definitely affects the interaction between the solvent, the initiators and EPON, it was decided to move away from commercial supports and cast PAN support membranes in-house.

3.1.2.2 TFC membrane performance on in-house cast supports

Synthesizing in-house support membranes allows control of the exact chemical composition and ideally performance. Two PAN supports are made, of which the dope solutions consist of 12 wt% PAN (further denoted as DMAc12 support) and 15 wt% in DMAc (further denoted as DMAc15 support), with varying porosities (Appendix, Figure 53) based on the work of Lenaerts (2021).

For the DMAc12 support, the performance of the pristine, solvent annealed, and NI membranes were measured. No NI membrane was made on the DMAc15 membrane because similar performance was expected as the DMAc 12 NI membrane because of their similar chemical composition. Both pristine membranes have no salt selectivity, but the DMAc12 membrane (pristine and solvent annealed) has a permeance larger than 100 LMH/bar while the permeance of the DMAc15 membrane is 65 LMH/bar (Figure 26). The baseline, DMAc12 NI membrane experiences a drop in permeance, but the rejection remains low (1.65%), fulfilling the desired criteria for a good support.

The rejection is again low for the 1S TFC membrane (9% on DMAc12, 2% on DMAc15) and high for the 2S membrane (62% on DMAc12, 82% on DMAc15). The 2S membrane performance is now comparable to the previously mentioned results in literature, as the permeance of both 2S membranes is ~2.5 LMH/bar. The DMAc15 support seems to be a better support layer than DMAc12 for this system, since the rejection of the 2S 1h membrane is 33% higher.

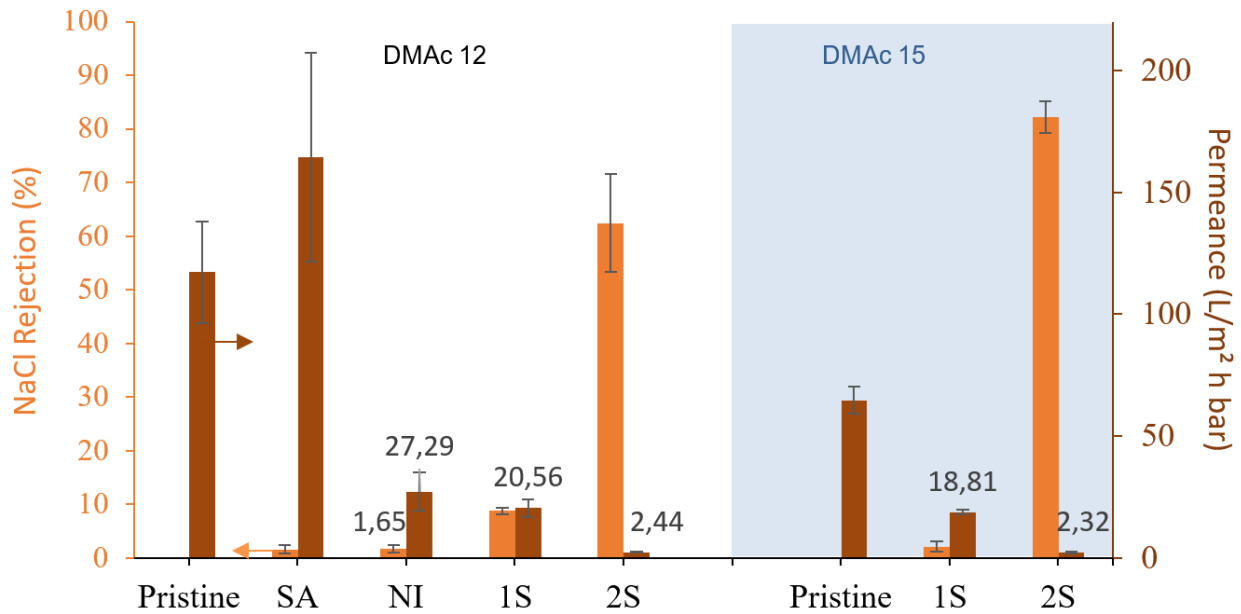


Figure 26: Performance of support membranes and membranes synthesized with TMHD as the initiator at a concentration of 1N, with reaction steps of 1 h. SA is short for solvent annealed. White background: membranes with DMac12 support, blue background: membranes with a DMac15 support. Filtration conditions solvent annealed and NI membrane: 10 bar, 5 mM NaCl aqueous solution. Pristine: 1 bar, pure water.

3.1.2.3 Physicochemical characterization

For these in-house cast supports, FTIR measurements reveal characteristic PAN absorption bands around 2245 cm^{-1} (nitrile stretch), 1450 cm^{-1} (methylene C-H bend), and 1370 cm^{-1} (methyne C-H bending)¹⁷³. An additional band at 1622 cm^{-1} likely results from residual DMac trapped in the polymer matrix (highlighted in orange in Figure 27). This residual solvent is removed when the support is solvent annealed¹²⁵. The bands at 1735 cm^{-1} and 1235 cm^{-1} which are observed for the PAN PX support are not present anymore.

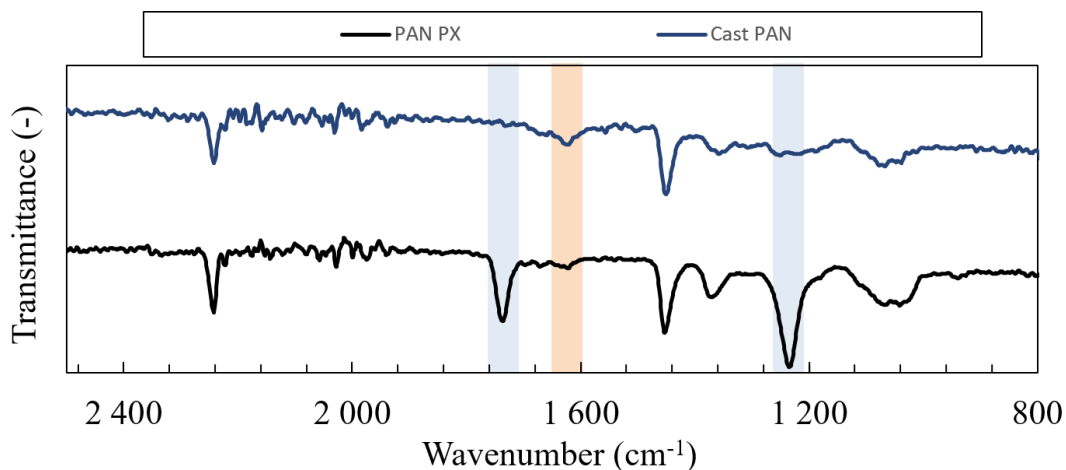


Figure 27: ATR-FTIR spectra of PAN PX and a cast PAN support from a dope solution of PAN in DMac. PVAc absorption bands are highlighted in blue, DMac absorption bands highlighted in orange.

As the scanning depth is between 0.5 and 2 μm and the thickness of the poly(epoxyether) toplayer is only expected to be around 160 nm, both the absorption bands of this toplayer and of the PAN support are expected to be observed for the spectra^{119, 130}. Characteristic bands for the EPON monomer can be observed at 1606 cm^{-1} (C=C-C aromatic ring stretch), 1508 cm^{-1} (C=C-C aromatic ring stretch), 1226 cm^{-1} (asymmetric C-O-C stretch of aryl alkyl ethers), 1175 cm^{-1} , with some lower intensity bands in the range from 1150 cm^{-1} to 1085 cm^{-1} (asymmetrical C-O-C stretching vibrations), 1028 cm^{-1} (EPON: symmetric C-O-C stretch of aryl alkyl ethers), 968 cm^{-1} , 910 cm^{-1} (C-O stretching of oxirane group), 830 cm^{-1} (C-H bending of para-substituted aromatics), 750 cm^{-1} (methylene C-H rocking bend) (Figure 28)^{141, 142, 172, 173}.

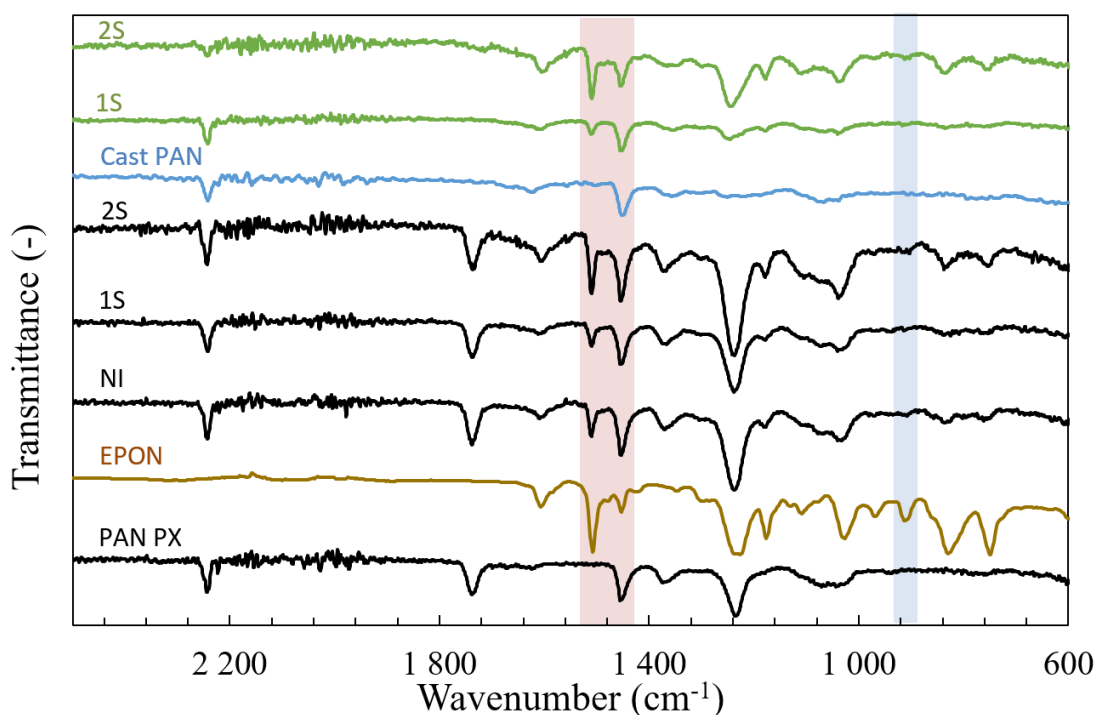


Figure 28: ATR-FTIR spectrum of the supports, pure EPON monomer, NI membrane, TMHD 1N 1&2S 1h membranes. Black lines are used are for membranes containing a PAN PX support, green lines for membranes with a DMAc12 support. The cast PAN spectrum is equal for DMAc12 and DMAc15. Epoxide signal highlighted in blue. Signals around 1508 cm^{-1} and 1450 cm^{-1} highlighted in red. The membrane spectra are scaled towards the PAN nitrile signal at 2245 cm^{-1} .

Since FTIR is a qualitative rather than quantitative characterization method, only the relative difference in intensity of 2 bands can give a means to compare the abundance of a chemical bond. For example, the band at 1508 cm^{-1} (aromatic ring stretch) for the NI membrane is about half of the intensity of the band at 1450 cm^{-1} (methylene C-H bend), while for TMHD 2S (on PAN PX), these bands have about the same intensity. This might indicate a higher presence of EPON in the TMHD 2S membranes since the band at 1508 cm^{-1} is only a characteristic band of the EPON monomer.

Apart from checking absorption bands related to EPON, it is also important to investigate whether it polymerized, which would be visible as a decrease or disappearance of the epoxide band around 910 cm^{-1} . Neither the NI, TMHD 1S or 2S membranes seem to have this band. EPON is expected to polymerize when TMHD is added, but for the NI membrane no initiator is added, hence no reaction is expected. As other EPON bands are relatively weak, e.g., at 830 cm^{-1} and 750 cm^{-1} , the small epoxide band might have disappeared in the noise of the spectrum, similar to the TMHD 1S membrane. Alternatively, unreacted epoxide groups could potentially hydrolyze and form two alcohols, however no substantial alcohol band around 3400 cm^{-1} is observed. Determining initiator related absorption bands can also be informative, however none could be distinguished as these might coincide with EPON bands.

Top-view SEM images were taken in order to characterize the surface morphology of the membranes. For TFC membranes made on different supports, there is a clear difference between the 1S and the 2S membrane, with the 1S membrane exhibiting smaller, ring like structures accompanied by small but rather bulky structures (

Figure 29). The 2S TFC membranes show larger bulky protrusions on top of a relatively flat surface, in agreement with literature¹¹⁹. The DMAC12 1S and 2S NI membranes depict annular structures which are more pronounced on the 2S NI membrane. On PAN PX, the NI membranes contain rather flat, delineated structures but they are less circular than the structures on the 1S membrane. To find out whether the structures on the NI membrane are the result of EPON adsorption on the support surface, the membrane was placed in toluene for 18 h. During this time, adsorbed EPON should redissolve and not be visible on the surface anymore. Indeed, the structures disappear after this toluene washing step, and only some prints remain on the surface. Earlier research indicated that the bulky protrusions for the TMHD EPON TFC membranes remained after toluene washing¹⁴³.

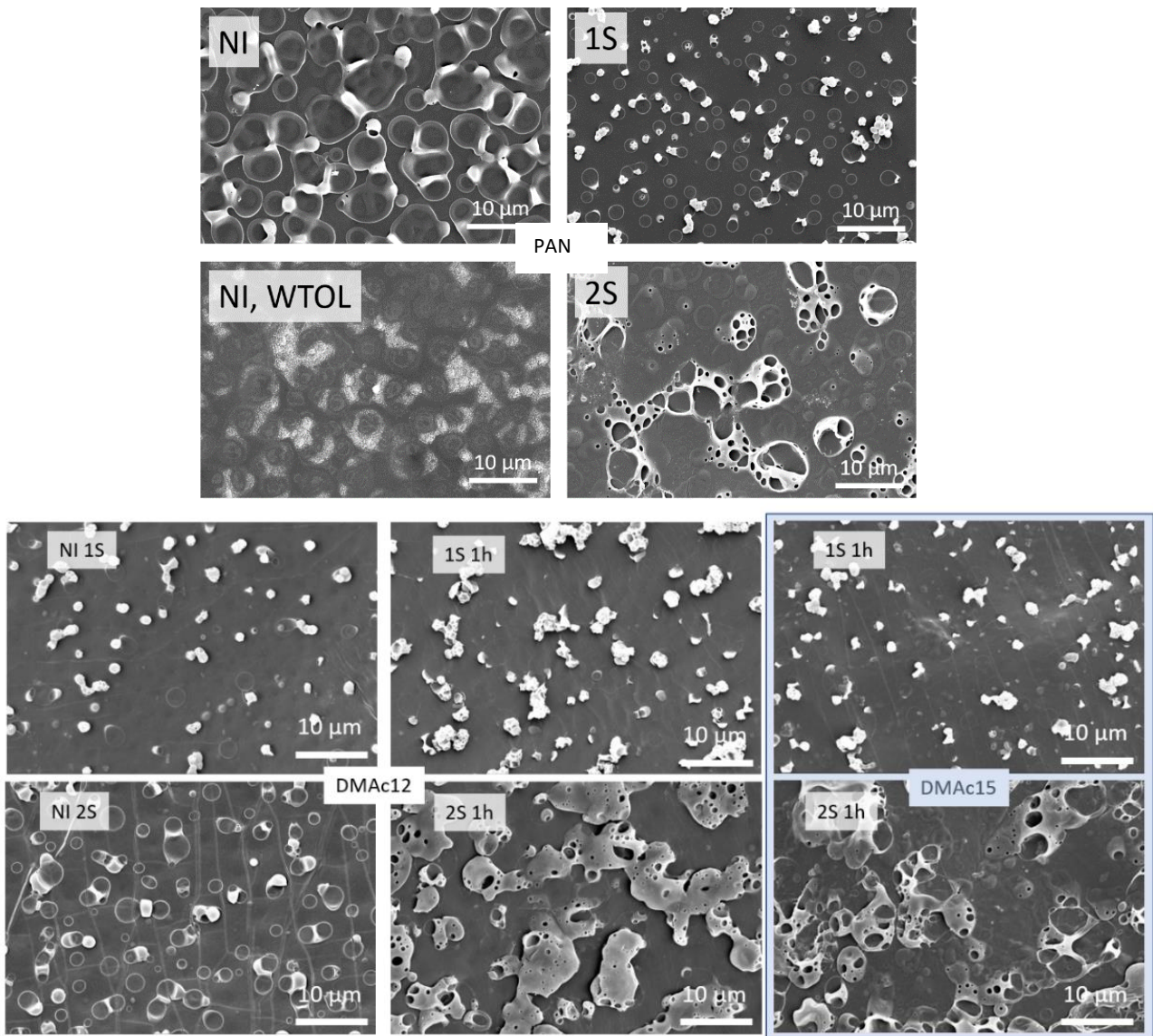


Figure 29: Top-view SEM images of membranes synthesized with a 1N concentration of TMHD. Top four images: on PAN PX. NI WTOL relates to a 2S NI membrane washed in toluene for 18 h. Bottom 6 images on in-house cast supports: white background: on DMAc12, blue background: on DMAc15.

Additionally, contact angle measurements were performed, where a significant difference can be observed between the DMAc support, NI, and 1&2S 1h TMHD membranes (Appendix, Figure 59). The support has the lowest angle, indicating it is the most hydrophilic. The observed differences can be explained using the Hansen solubility parameters (HSP), which can be used to compare interactions between PAN or EPON with water. The solubility parameter distance R_a between water and PAN is 35.5, and the distance between water and EPON 40.4 (Appendix, Table 4). The lower this R_a is, the higher the affinity of the two compounds, meaning water has more affinity for PAN than for EPON, and thus it makes sense the contact angle for the NI membrane is larger than the support^{144, 145}. The contact angle of TMHD 1&2S 1h membranes is somewhere between the NI and the support. Its increased hydrophilicity compared to the NI membrane is likely due to charge incorporation. However, it should be

noted that the contact angle is also dependent on other surface characteristics such as surface porosity or pore size, which might influence comparison between different membranes¹³².

3.1.3 Changing the reaction time during TMHD 2S synthesis

The current synthesis time of a 2S epoxide-based TFC membrane is 4 hours, which challenges the scale-up of these membranes. In an attempt to shorten synthesis time, a reaction time experiment was set up to verify whether selective membranes could be made by shortening all synthesis steps.

3.1.3.1 Membrane performance

5 mM NaCl filtration

Additional 2S membranes were made on the in-house cast supports, where all the steps during the synthesis were 20, or 40 mins compared to the 1 h reaction steps used for the reference membrane. Here again, DMAc15 appears to be a more suitable support compared to DMAc12 as the rejection of the 2S 20m membrane is larger when it is made on DMAc15 instead of DMAc12 (Figure 30). It is clear that on both supports, the permeance of the 2S 20m membrane is lower than the 1S 1h membrane, even though the total synthesis time is equal. In addition, the permeance decreases almost linearly with increasing reaction times for the DMAc12 membranes, indicating more polymerization is happening. However, the only selective membranes are obtained when the synthesis steps are 1 h, total synthesis time cannot be decreased by simply reducing the duration of all synthesis steps.

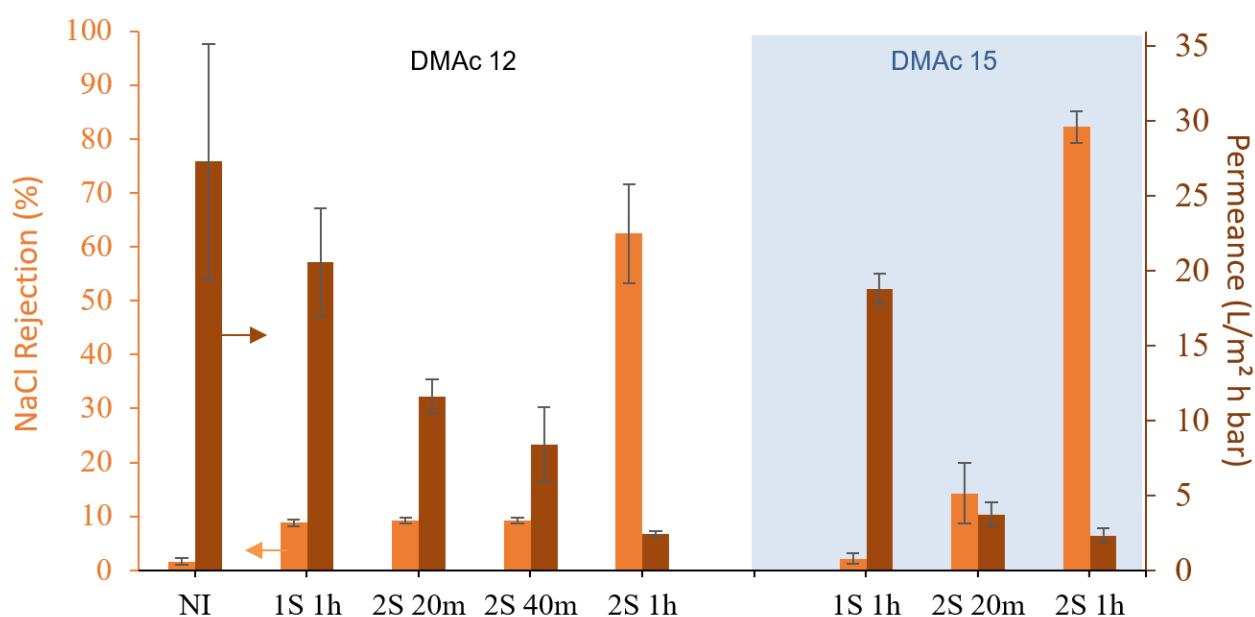


Figure 30: Performance of 1S and 2S membranes synthesized with TMHD at a concentration of 1N, with varying reaction times (20, 40 mins and 1 h) White background: membranes with DMAc12 support, blue background: membranes with a DMAc15 support. Filtration conditions: 10 bar, 5mM NaCl aqueous solution.

15 μM methylene blue filtration

When shortening reaction times, the system might not have had enough time to crosslink, resulting in a rather open polymer structure. In this case, the cut-off range of this layer might be located at higher molecular weights compared to a dense 2S 1h membrane. As a consequence, measurements with NaCl as a solute may be taken below the cut-off range of the membrane resulting in low rejection¹⁴⁶. To verify this hypothesis, filtrations were performed using a higher MW solute, methylene blue (MW=320 Da).

All membranes show high rejections: 92% for the 1S 1h membrane and 99% for the 2S 20&40m membranes, with a permeance of around 5 LMH/bar (Figure 31). However, the NI membrane also has a high rejection and standard deviation, making it difficult to significantly distinguish between the baseline and the TFC membranes. This is most likely a result of MB adsorption¹⁴⁷. A first indication of this is a blue discoloration of the membranes after filtration. This discoloration is less pronounced for the TMHD membranes compared to the NI membrane (Appendix, Figure 54).

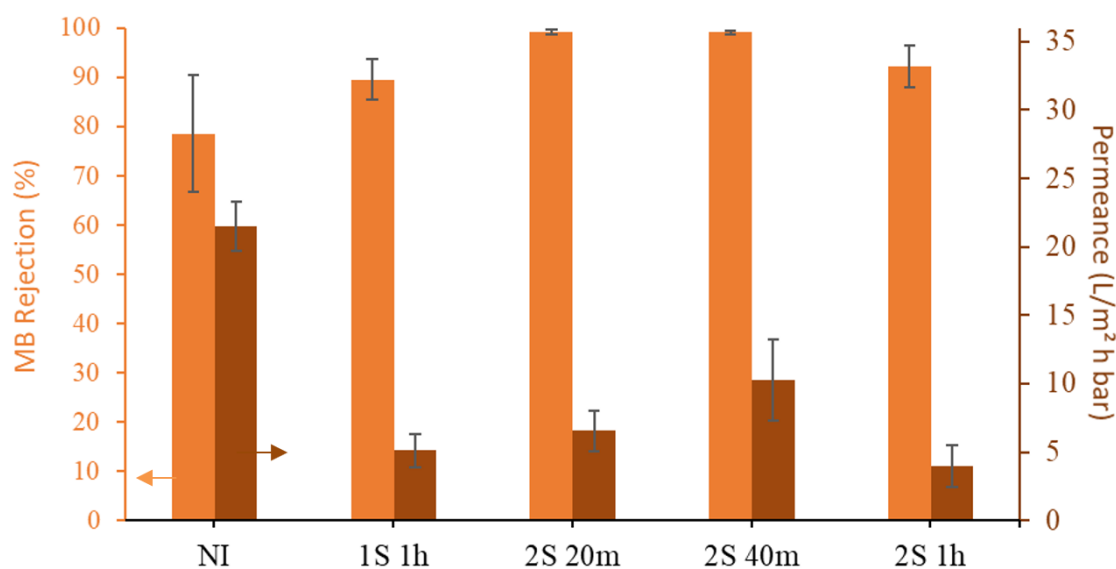


Figure 31: Performance of 1S and 2S membranes synthesized on DMAc12 with TMHD as the initiator at a concentration of 1N, with varying reaction times (20, 40 mins and 1 h). Filtration conditions: 10 bar, 5 mM NaCl aqueous solution.

To get a better understanding of the MB adsorption on the membrane surface, adsorption experiments by immersing the TFC membranes in the dye solution were performed. The average time of a filtration is about 3 h, after which the adsorption capacity (q) of the TMHD 2S 1h membrane is 0.55 mg/g, 1.65 mg/g for the TMHD 1S 1h membrane and 1.88 mg/g for the NI membrane (Appendix, Figure 55). Even though these values are likely overestimations, as the support is also freely available for adsorption, the differences between the membranes

indicate that during the filtration a large part of the rejection is due to adsorption for the 1S 1h and NI membrane compared to the 2S 1h membrane. This is further confirmed by a filtration where 105 μM - instead of 15 μM aqueous MB feed solution was used. For this higher feed concentration, the rejection of the 1S membrane decreases to 22%, as the maximum adsorption capacity is quickly reached compared to a filtration with only 15 μM . For the 2S membrane, the rejection is still 96%.

3.1.3.2 Membrane characterization

On in-house cast support

There is a large difference in performance between the 1S and 2S TMHD TFC membranes, both in the NaCl filtrations (*i.e.*, drop in permeance with increasing reaction times) and in the MB filtrations (*i.e.*, difference in adsorption). This difference can be further explained by XPS measurements (Figure 32). The ammonium content (N^+ , positively charged) in the TMHD 2S 1h membrane is 1.26 at.%, in the TMHD 2S 20m is 0.92 at.% and in the TMHD 1S 1h membrane only 0.2 at.%¹¹⁹. This higher abundance of positively charged groups will decrease adsorption of the positively charged dye MB due to electrostatic repulsion.

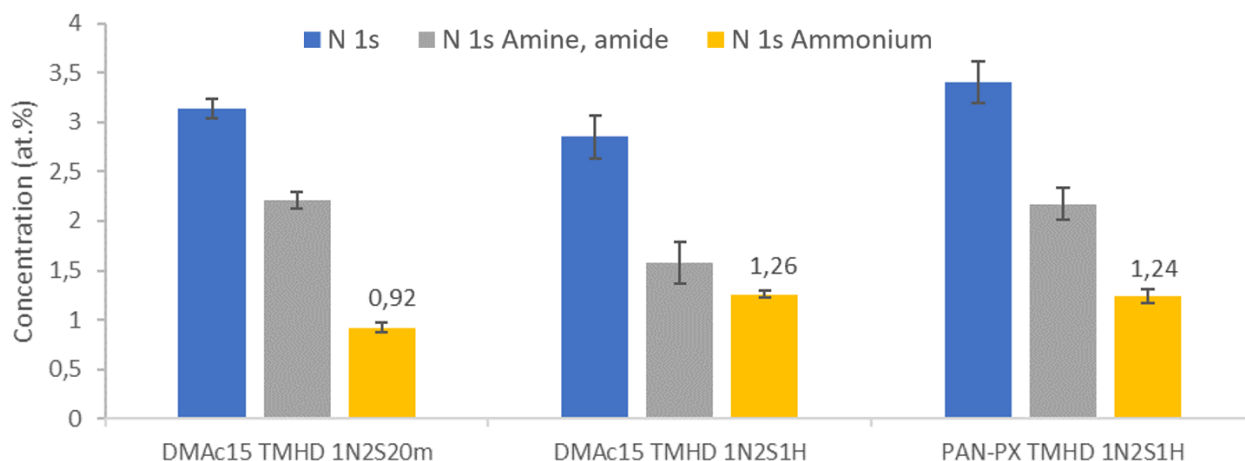


Figure 32: XPS measurements on membranes synthesized with TMHD as an initiator. Two membranes on the left: on DMac15, membrane on the right: on PAN PX. Y axis: atom percentage of a certain bond.

It is however interesting that the 2S 20m membrane, which in total reacts for one hour (*i.e.*, three reaction steps of 20 mins), has an N^+ of 0.92 at.%, and the 1S 1h, which also has a total reaction time of one hour, only has an N^+ content of ~ 0.2 at.%. In addition, the DMac15 2S 20m has an 80% lower salt water permeance than the 1S 1h membrane. These results suggest that the re-initiation and densification step in the 2S synthesis procedure is more important than the 1S IIP step to achieve a dense selective layer.

The following hypothesis is established to explain the importance of the 2S densification step to achieve high salt rejection. The poly(epoxyether) film that forms in the 1S step is expected to have the highest charge density close to the interface, as initiation is most prevalent here. Higher into the toluene phase, less initiation will occur, causing the upper part of the film to have a high density of accessible, reactive epoxide functional groups, but a relatively low charge density and a low crosslinking density. These properties will result in the low salt rejection of the 1S membranes. For the 2S membranes, the epoxide and TMHD solutions are subsequently reapplied onto the 1S film. Reapplication of the epoxide solution is expected to further grow the polymer network and to increase the density of accessible, reactive epoxide functional groups in the film. At this point, the film is solvated by toluene and will remain swollen in the subsequent densification step, where TMHD is added on top of the film. TMHD diffusion into the film is facilitated thanks to the swollen polymer network and the higher contact area compared to the 1S step, where TMHD is only supplied from the pore mouths of the support. TMHD can then react with the high abundance of epoxide groups, resulting in a dense film with a high charge density. Furthermore, TMHD can also still react from the bottom side, so that charge incorporation occurs at both sides of the film. The high charge density and the dense network of the resulting 2S membrane contribute to its high salt rejection.

The ammonium content in the 2S 1h membrane is 1.26 at.%, which is only 30% higher than in the 2S 20m membrane, even though the total reaction time is three times longer. This might indicate that the incorporation of TMHD slows down over time, as the most readily available epoxide groups will already have reacted. The rejection of the 2S 1h membrane is however 400% higher than the 2S 20m membrane, which might be explained by allowing the formation of a denser network through crosslinks between EPON alkoxy and unreacted epoxide groups. This importance of densification in order to achieve salt rejection is in line with literature¹⁴⁸.

The formation of the polymer network was visualized by taking top-view SEM images (Figure 33). The growth and formation of the toplayer can be observed, starting to from the bare support to form a rough surface for the 2S 20m membrane and evolves to a smooth surface for longer reaction times. The typical EPON protrusions seem to appear as small, spherical structures which grow over time into larger polymer structures.

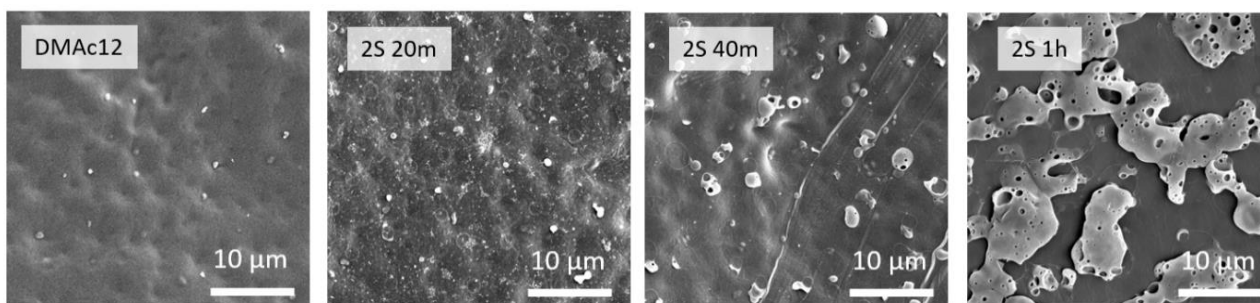


Figure 33: top-view SEM images of the DMAc12 support and 2S membranes synthesized on DMAc12 with TMHD as the initiator at a concentration of 1N, with varying reaction times (20, 40 mins and 1 hour).

Zeta potential measurements were conducted on the membranes to investigate the membrane surface charge within the measured pH range (2-10). The zeta potential of most TFC membranes is negative across this entire range, only for TMHD-initiated 2S 1h membranes it increases more rapidly with decreasing pH and becomes positive, resulting in an iso-electric point (IEP) (Appendix, Figure 58). A negative zeta potential curve can be expected due to the large specific adsorption of hydroxyl groups on the rather hydrophobic PAN chains, as demonstrated by the negative zeta potential for the DMAc15 support¹⁴⁹. This specific hydroxyl adsorption might overshadow certain effects, but by comparing the zeta potential curves of membranes with and without an IEP, some conclusions can be made. For example, the TMHD 2S 20m membrane has a 0.92 at.% ammonium content, but its zeta potential curve remains negative. The zeta potential curve of a membrane containing mostly permanent positive charges (*i.e.*, quaternary ammonium groups, originating from the ROP of EPON), is expected to be positive across the whole pH-range, around a more or less constant value. However, this value could drop towards negative values as a consequence of specific hydroxyl adsorption and hence result in a zeta potential curve as observed for the TMHD 2S 20m membrane. These curves suggest that all the TMHD has reacted at both sides when the reaction steps are 20 mins. In contrast, the steeper zeta potential curve of the TMHD 2S 1h membranes which contains an IEP, suggests the presence of additional pH dependent groups, *i.e.*, dangling tertiary amine groups, which result from TMHD incorporation from only one side.

The fact that the 2S 1h membrane has a higher N⁺ content than the 2S 20m membrane likely indicates that they contain at least the same amount of double-reacted TMHD, and because the readily available reaction sites are already gone, the newly added TMHD in the 2S step might only be incorporated via one side, resulting in dangling tertiary amine groups. These obtained insights could open up new, efficient synthesis routes, where the first reaction steps in the 2S procedure can be shortened, but with a longer final densification and charge incorporation step.

3.1.4 Initiator properties

The performance of membranes synthesized with new initiators will, as beforementioned, be compared with the reference TMHD system defined in 3.1.2. Initiator properties will serve as a tool to explain the differences in membrane performance and physicochemical properties. While many initiator properties can be compared, a selection was made based on their relevance in the interfacial ring-opening polymerization (ROP) (Table 2). However, since the initiators used in this work are rather uncommon molecules, little experimental data about their properties is available in literature. Therefore, numerical values are often predicted by models (e.g., EPISuite, ACD/PhysChem Suite) based on the structure of the molecules (Table 3)¹⁵⁵.

Table 2: Overview of system characteristics and relevant initiator properties linked to them.

System characteristic	Initiator property
SN2 reaction mechanism	Spatial configuration (sterical hindrance)
Nucleophilic substitution reaction	Nucleophilicity (N index, pK _b)
Reaction in organic phase	Toluene solubility
Initiator/crosslinker activity	Functionality
Limited reaction time	Diffusivity, solvation
Reaction near support	Confinement effects, polarizability
Interfacial reaction	Surface tension, interfacial coordination

The nucleophilicity parameter N can be used to compare the nucleophilicity between molecules, but no data is available for the used initiators¹⁵⁰. As a proxy, the pK_b can be used, since basicity (tendency to attack a hydrogen atom) can be seen as a narrower form of nucleophilicity (tendency to attack any atom). The pK_b values are depicted in the table and increase in the order of TMHD \approx TMPD < Me6Tren \approx DABCO < 2-MIM < IM \approx 1-MIM < MBDA \approx MBI⁸⁰. The log(P) (*i.e.*, octanol-water partitioning coefficient, DABCO < IM \approx 1-MIM < 2-MIM < TMPD < Me6Tren < MBI < TMHD < MBDA), the surface tension (TMPD \approx TMHD < Me6Tren < 1-MIM < MBI \approx MBDA \approx 2-MIM < IM), and the toluene solubility can provide information about the presence of the initiator at the interface or in the organic phase, and hence give an indication whether it can initiate the polymerization. As the presence of the PAN support might introduce catalytic initiator-pore wall interactions, there is a possibility that polarizability plays a role as well, which increases in the order of IM < 2-MIM \approx 1-MIM < DABCO < TMPD \approx MBI < TMHD < Me6Tren < MBDA¹⁵¹. The spatial configuration of initiators is also depicted as it has an influence on the nucleophilicity, the diffusivity and the ability to penetrate a polymerized network.

Interactions between the initiator and the support or the interface, or differences in solvation of molecules both in the aqueous and in the organic phase, also alter the behavior of the initiators substantially in addition to intrinsic initiator properties^{165, 179}. Of course, there could be many more parameters influencing the system than there are depicted here. In addition, certain properties are intertwined (e.g., polarity, toluene solubility, log(P)), which further complicates the contribution of a certain initiator property to the observed membrane performance and physicochemical properties.

Table 3: Overview of a set of properties of the initiators used for all membranes^{152 - 156}. * Depict predicted values.

Initiator	pK _b	Log(P)	Surface tension (dyne/cm)	Polarizability (*10 ⁻²⁴ cm ³)	Spatial configuration
TMHD	3.9	1.5*	28.6±3.0*	22.1±0.5*	Flexible
IM	7.05	-0.08	48.6±3.0	7.4±0.5	Rigid, small
1-MIM	7.05	-0.06	35.0±7.0*	10.0±0.5*	Rigid, small
2-MIM	6.14	0.24	43.7±3.0*	9.4±0.5*	Rigid, small
Me6tren	5.01±0.5*	0.77*	32.9±3.0*	28.8±0.5*	Flexible
DABCO	pK _{b1} =5.3 pK _{b2} =11	-0.85*	42.3±5.0	13.3±0.5*	Rigid
TMPD	pK _{b1} =3.9 pK _{b2} =5.9	0.43*	27.2±3.0*	16.6±0.5*	Flexible
MBDA	8.43± 0.12 *	4.37	41.8±3.0*	33.4±0.5*	Semi-flexible, bulky
MBI	8.60±0.10*	1.44*	40.8±7.0*	16.3±0.5*	Rigid

3.1.5 Imidazole (IM)

Imidazoles are often used as catalytic curing agents in epoxide chemistry at elevated temperatures¹¹². Imidazoles without substitutes on the 1-(N) position can act as crosslinkers through a proton transfer mechanism (Figure 21).¹⁵⁷. To verify the effect on the IIP characteristics of introducing a substitute on the 1-(N) nitrogen, and the sterical hindrance

caused by its presence, 1-methylimidazole (1-MIM) and 2-methylimidazole (2-MIM) were also tested (sections 3.1.6 and 3.1.7, respectively) .

3.1.5.1 Membrane performance

On PAN PX

To get a better understanding on the behavior of IM as the initiator, membranes were synthesized using different conditions (*i.e.*, varying reaction times, initiator concentrations, 1S or 2S). Care should be taken when drawing conclusions from this data, as the NI membrane has a rejection of ~40%, which is often not significantly different from the IM-initiated TFC membranes.

Extending the reaction time from 1 to 3 h (2N 1S 1h vs 3h) does not have a significant effect on either rejection or permeance (R~50%, P~0.4 LMH/bar, Figure 34), suggesting that the density and thickness of-, or charge incorporation in the selective layer do not substantially increase over time. This might be explained according to the reaction mechanism (Figure 21): even if IM reacts from both sides, only one positive charge is incorporated due to H⁺ transfer, in comparison to two positive charges for TMHD. Additionally, IM is a short crosslinker, resulting in charges and bulky side groups (*i.e.*, sterical hindrance) to be present unfavorably close to each other, slowing down the start of polymerization. This results in limited polymerization and less thickening of the membrane than, *e.g.*, a membrane initiated by the longer, bifunctional TMHD. Indeed, the rejection of such a TMHD membrane increases slightly when increasing the reaction time, suggesting densification and higher charge incorporation in the selective layer⁷⁹. With increasing IM concentration, the permeance increases (1N 1S 1h vs 4N 1S 1h and 1N 2S 1h vs 4N 2S 1h), reaching a permeance of 1.7 LMH/bar for the 4N 2S 1h membrane. This could be expected as higher initiator concentrations will result in shorter polymer chains, which might not be able to form a dense, selective toplayer.^{106, 108}. Surprisingly, rejections go down when comparing the 1S with the 2S membranes, (53% vs. 42% for 1N), and permeances go up (0.5 vs 0.8 LMH/bar for 1N), while for TMHD the reverse was observed. This drop in rejection is likely due to insufficient polymerization and removal of loose polymer chains by the toluene washing step, as suggested by XPS-data (section in 3.1.5.2)

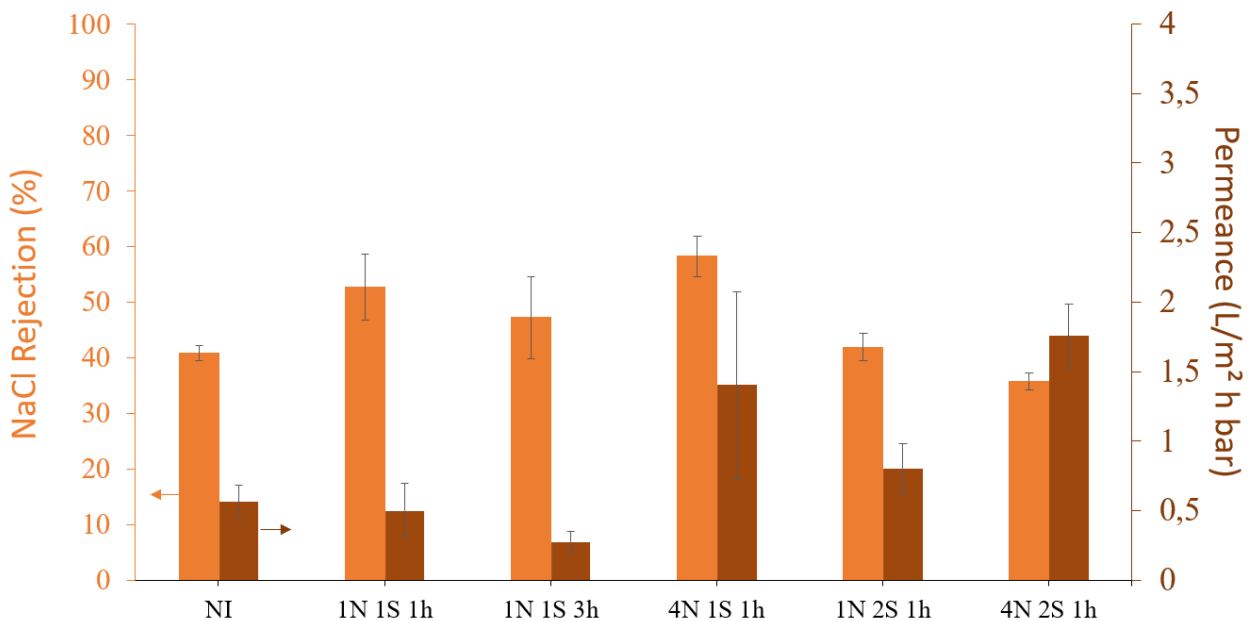


Figure 34: Performance of the IM membranes synthesized using different conditions: concentrations of 1N, 4N, type 1S and 2S, reaction times of 1 h and 3 h. Filtration conditions: 10 bar, 5 mM NaCl aqueous solution.

On in-house cast PAN supports

Some of the most promising membranes made on the PAN PX support were resynthesized on DMAc12 and DMAc15 supports to circumvent the issues related to the high selectivity of the NI membrane (*i.e.*, due to adsorbed EPON). The permeance is on average lower on the DMAc15 support (~19 LMH/bar) than on the DMAc12 (>25 LMH/bar), but none of the membranes made on these in-house cast supports show a rejection over 5%, indicating that no salt selective toplayer was formed (Figure 35). On PAN PX, higher rejections are observed, which can be explained by a number of reasons. The NI membrane on PAN PX already has a high baseline rejection. Only the 1&4N 1S 1h membranes have a significantly higher rejection. Here, the support might play a role in the film formation, *e.g.*, due to interactions between the epoxide and PVAc present in PAN PX but absent in the in-house cast supports, or due to an increased hydrophilicity of PAN PX¹²⁵. Another explanation could be the occurrence of a saponification reaction of the ester group in PVAc, which produces an alcohol and thereby accelerates the polymerization rate^{80, 108}. Additionally, defects in the toplayer will more strongly affect the performance of the TFC membrane on the self-made supports as they have a larger surface porosity than on PAN PX (Appendix, Figure 53).

The MB rejection of the 4N 1S 1h and 1N 2S 1h membranes is also not significantly different from the NI membrane, again indicating the absence of a selective, defect free toplayer (Appendix, Figure 65). The adsorption capacity after 3 h (~1.4 mg/g, Appendix Figure 55) is smaller than the NI membrane but similar to the supports *q* value. After filtration, membrane

coupons had a blue discoloration, indicating significant adsorption occurs which results in similar rejection to the NI membrane.

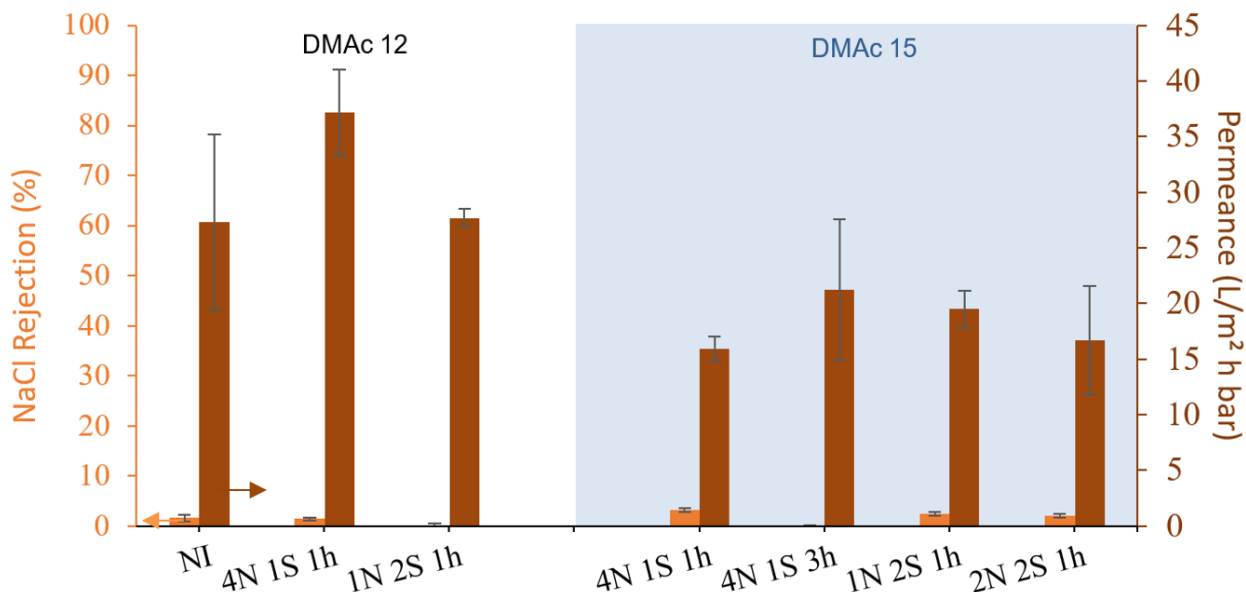


Figure 35: Performance of IM membranes synthesized under different conditions. White background: membranes with DMAc12 support, blue background: membranes with a DMAc15 support. Filtration conditions: 10 bar, 5mM NaCl aqueous solution.

3.1.5.2 Physicochemical characterization

ATR-FTIR

ATR-FTIR measurements were performed in order to confirm IM incorporation and polymerization. Characteristic PAN PX and EPON absorption bands, discussed in 3.1.2.3, are observed for all spectra^{141, 172, 173}. All spectra on PAN PX appear similar except for the 1N 1S 3h membrane, for which the EPON bands are more intense than the PAN PX bands. This can be due to the longer reaction time, allowing more EPON adsorption, which is further implied by the increase of the epoxide band around 910 cm⁻¹, compared to the other membranes. The presence of this band indicates incomplete polymerization. Two new bands appear for multiple membrane samples at 1063 cm⁻¹ and 663 cm⁻¹ (highlighted in red in Figure 36), which can be attributed to IM (likely a C-H out-of-plane-bending and ring deformation out-of-plane-bending, respectively)¹⁶⁰.

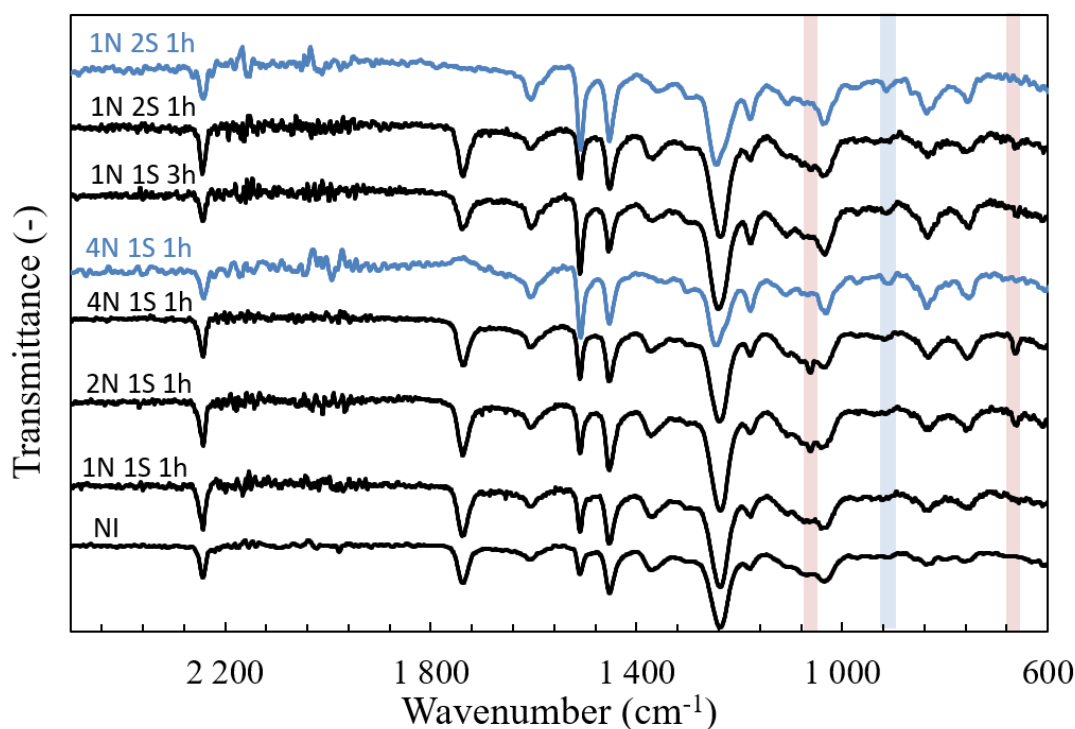


Figure 36: ATR-FTIR spectra of IM membranes on top of a PAN PX support (black lines), or on DMAc12 (blue lines) Epoxide signal at 910 cm^{-1} highlighted in blue, imidazole signals at 1063 cm^{-1} and 663 cm^{-1} highlighted in red. Spectra on DMAc12 were smoothed by taking the average transmittance of the surrounding six wavenumbers.

XPS and zeta potential measurements

XPS-data of the IM membranes (on DMAc15) depict a N^+ content of 0.10 at.% for the 1S (4N, 3h) membrane, and 0.19 at.% for the 2S (2N, 1h) membrane. No nitrile signal was detected for either membrane, suggesting the presence of a homogeneous toplayer of a thickness of at least 10 nm (*i.e.*, XPS measurement depth) (Appendix, Figure 56). This 100% increase in N^+ content for the 2S membrane for IM compared to a 500% increase for TMHD can be explained by the lower charge incorporation of IM due to the proton transfer reaction (Figure 21), compared to TMHD. The lower charge incorporation with IM as initiator is believed to be one of the reasons of the generally low observed salt rejection. The lower N^+ content in absolute values of the 2S membranes (0.19 for IM, 1.26 for TMHD), in other words less incorporation of IM compared to TMHD, might be due to the lower $\log(P)$ or $\text{p}K_b$ (\sim nucleophilicity), hence lower reactivity and availability of IM to initiate the reaction (Table 3). This lower reactivity was also already depicted by the vial tests, where IM only showed first signs of film formation after 2 h, compared to 30 mins for TMHD.

The presence of N^+ in the 1S IM membrane indicates initiation, and the fact that this N^+ content is higher in the 2S membrane suggests re-initiation is likely happening as well. However, as beforementioned, chain propagation will likely only occur from one amine group, which results

in a less dense membrane than when chain propagation is possible from both amine groups like for TMHD. As another toluene rinse step is present in the 2S compared to 1S synthesis procedure, the toplayer might get damaged more severely for such low density and lower crosslinked systems, resulting in the observed slight drop in rejection from the 1S to 2S membranes.

Zeta potential measurements indicate the incorporation of IM as well, as the zeta potential of the IM membrane decreases faster than the NI membrane for high pH (Appendix, Figure 58). This is likely due to a shift in equilibrium between the alcohol and the alkoxide in water.

SEM

A difference in surface morphology can be observed comparing the IM-initiated membranes made on PAN PX and on DMAc15, particularly for longer total synthesis times (1S 3h and 2S 1h membranes). These morphological differences are most likely unrelated to solely IM properties, but rather a combined result of the system-IM interactions¹⁶¹. Globular structures can be observed on the surface of the 1S membranes (Figure 37, both on PAN PX and DMAc15). These structures change significantly when the reaction time is increased from 1 h to 3 h. Especially on the DMAc15 support (4N 1S 3h), it is clear that the protrusions grow substantially, indicating further polymerization. However, these membranes were not salt selective, which was explained earlier, by the lower density of the membranes and lower charge incorporation. In the case of the 2S membranes on DMAc15, annular shapes with globular structures, similar to the ones in the 1S membranes but slightly flattened out, are observed.

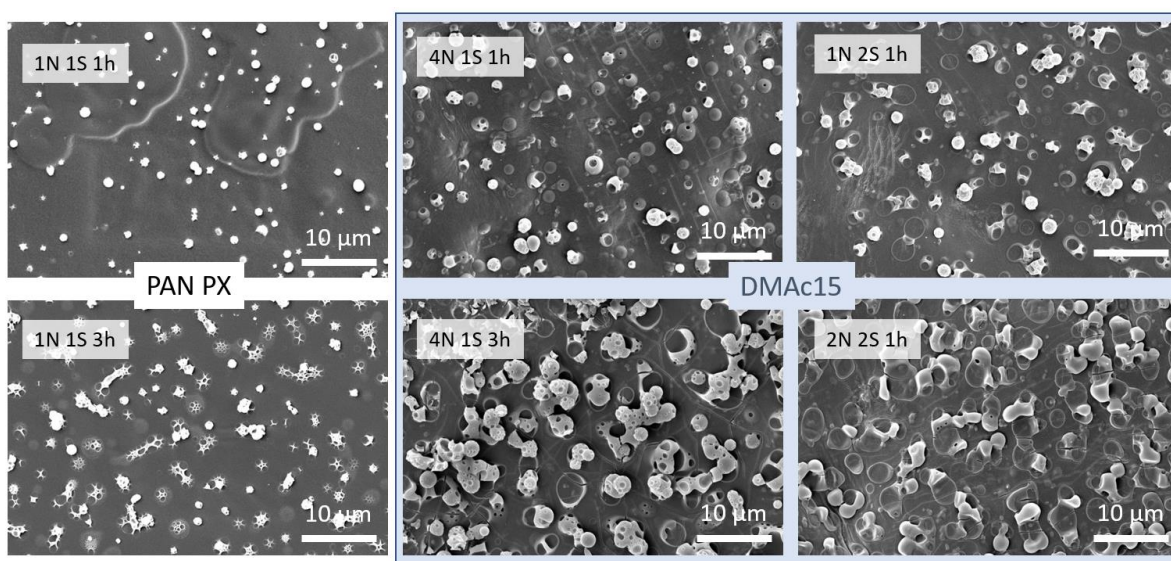


Figure 37: Top-view SEM images of IM membranes synthesized using different conditions, left: on top of PAN PX, right: on top of DMAc15. Increasing reaction time clearly has an influence on the observed structures.

3.1.5.3 Conclusion

To summarize, the ROP of EPON via IM can be confirmed by XPS, zeta potential and FTIR measurements, and polymerization is observed in SEM pictures. However, there is still an epoxide IR absorption band left, indicating incomplete polymerization. Due to the reaction mechanism and relatively low reactivity of IM, likely a low density toplayer with insufficient charges is synthesized to be salt selective on the in-house cast supports. However, a significantly more selective toplayer than the NI membrane was formed on PAN PX, likely due to accelerating effects of PVAc present in only the PAN PX support. Furthermore, MB, a N-containing aromatic dye, is observed to highly adsorb to the NI and the support membrane. This might suggest additional IM could be present on the membrane surface via similar adsorption (e.g., pi-stacking...).

3.1.6 1-Methylimidazole (1-MIM)

To study whether the reactivity of imidazole compounds differ when the 1-(N) nitrogen is a secondary amine or not, membranes were made using 1-MIM as a 1-(N) substituted imidazole initiator (Appendix, Figure 51).

3.1.6.1 Membrane performance

On PAN PX

Similarly as for the IM membranes, care should be taken when interpreting these results as the differences in performance with the NI membrane are small. An elongation of the reaction time (0.5N 1S 1h vs 3h) does not have a significant effect on rejection nor on permeance (R~38%, P~1 LMH/bar, Figure 38), as both remain similar to 1S TMHD reference and the NI membrane. This indicates the lack of polymerization at these low initiator concentrations. For a higher concentration however (1N 1S 1h), a significantly higher rejection (58%) and lower permeance (0.3 LMH/bar) is observed. This permeance is 40% lower than the same membrane synthesized by IM, which can be explained by the reaction mechanism. Proton transfer is not possible for 1-MIM and as a consequence, a reactive alkoxide (which will initiate and propagate the polymerization) is formed directly when 1-MIM reacts with an epoxide group (1:1 adduct, as explained in 1.3.3.2.2), compared to IM which has to react with two epoxide groups in order to generate the reactive alkoxide (2:1 adduct). This suggests the 1-(N) substituted imidazoles (e.g., 1-MIM) are more reactive than their unsubstituted analogues (e.g., IM), resulting in more polymerization, hence denser and thus less permeable membranes for 1-MIM compared to IM¹¹². Furthermore, only these higher initiator concentration membranes (1&2N 1S 1h) have a substantially higher rejection than the NI membrane. Similar as for the IM-synthesized membranes, the performance of the 2S membranes is not better than the 1S membranes,

which is likely due to the lack of a crosslinking ability of 1-MIM, and the removal of loose polymer chains by the toluene washing step.

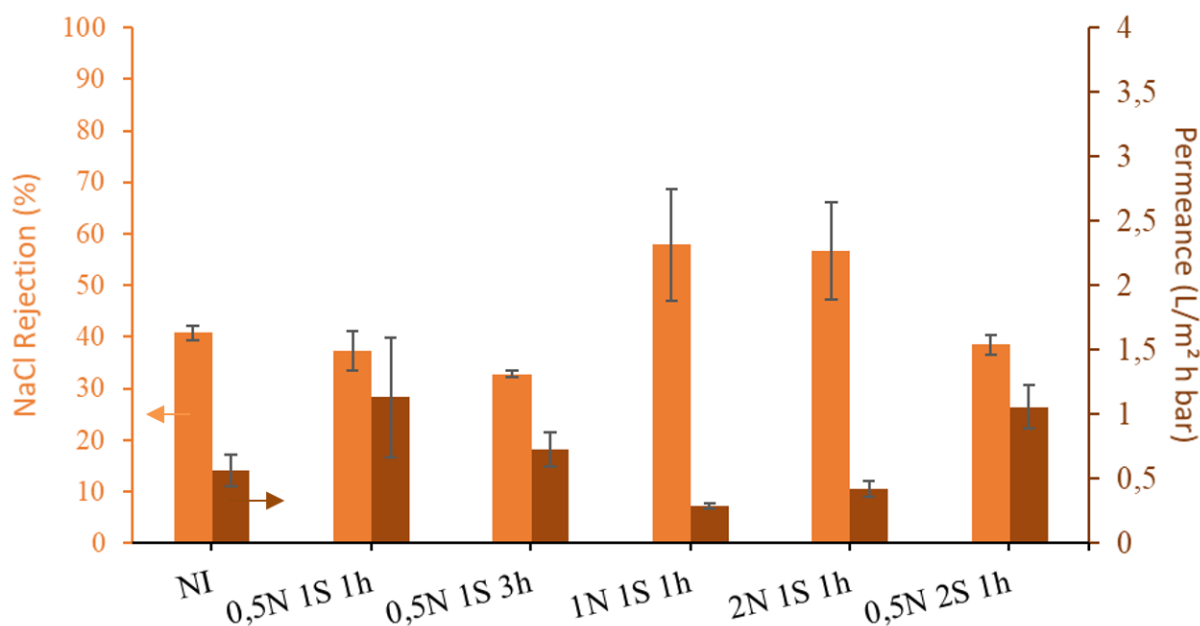


Figure 38: Performance of the 1-MIM membranes synthesized using different conditions: concentrations of 0.5N, 2N, type 1S and 2S, reaction times of 1 h and 3 h. Filtration conditions: 10 bar, 5 mM NaCl aqueous solution.

On in-house cast PAN supports

The most promising membranes made on the PAN PX support were resynthesized on the DMAc12 and DMAc15 supports. The permeances of the TFC membranes made on a DMAc12 support (~16 LMH/bar, Figure 39) are lower than the TMHD 1S membranes (~20 LMH/bar), and the IM membranes (~30 LMH/bar) made on this support. The latter is in line with the reaction mechanism which suggest faster polymerization for 1-MIM compared to IM. Surprisingly, apart for a slightly lower rejection for the DMAc15 membranes (4% on DMAc15 vs 9% on DMAc12), no significant differences are observed in performance between DMAc12 and -15 membranes. Similar to what is observed for IM, the low rejections indicate the absence of a selective layer on in-house cast supports, even though it was present on the PAN PX support (2N 1S 1h membrane). Acceleration effects due to PVAc present in PAN PX are hypothesized to cause this difference.

The MB performance of the 2N 1S 1h and 0.5N 2S 1h membranes are not significantly different from the NI membrane, also suggesting the absence of a dense, defect-free selective toplayer (Appendix, Figure 65). The adsorption capacity after 3 h (~1.4 mg/g, Appendix Figure 55) is identical to the IM membrane, and the blue discoloration of the membrane coupons after filtration suggest adsorption results in the similar MB rejection of 1-MIM and NI membranes.

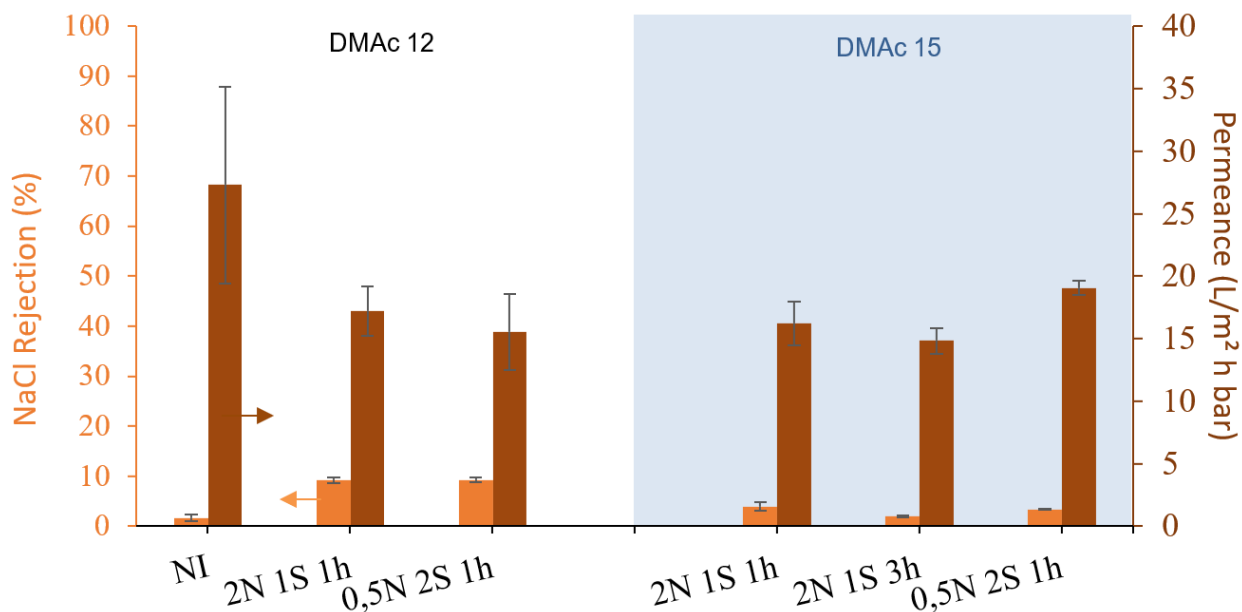


Figure 39: Performance of 1-MIM membranes synthesized under different conditions. White background: membranes with DMac12 support, blue background: membranes with a DMac15 support. Filtration conditions: 10 bar, 5mM NaCl aqueous solution.

3.1.6.2 Physicochemical characterization

ATR-FTIR

The expected characteristic EPON and PAN PX absorption bands are present in the FTIR spectra (as discussed in 3.1.2.3). Remarkably, a higher intensity of EPON bands is observed for the 0.5N 1S 1h membrane than for the 1&2N 1S 1h membranes (Figure 40). As for the IM membranes, the EPON bands become more visible for longer reaction times. For example, the 0.5N 1S 3h and 0.5N 2S 1h membrane show pronounced EPON bands (1508 cm^{-1} and 1240 cm^{-1} are relatively large compared to PAN band at 1450 cm^{-1}), which suggests important EPON adsorption. The presence of epoxide bands for these two membranes indicates incomplete polymerization. For the other membranes, there might not be enough EPON adsorbed in order for the epoxide band to be intense enough, although incomplete polymerization is also likely. There are no other bands present which may indicate 1-MIM presence in the toplayer.

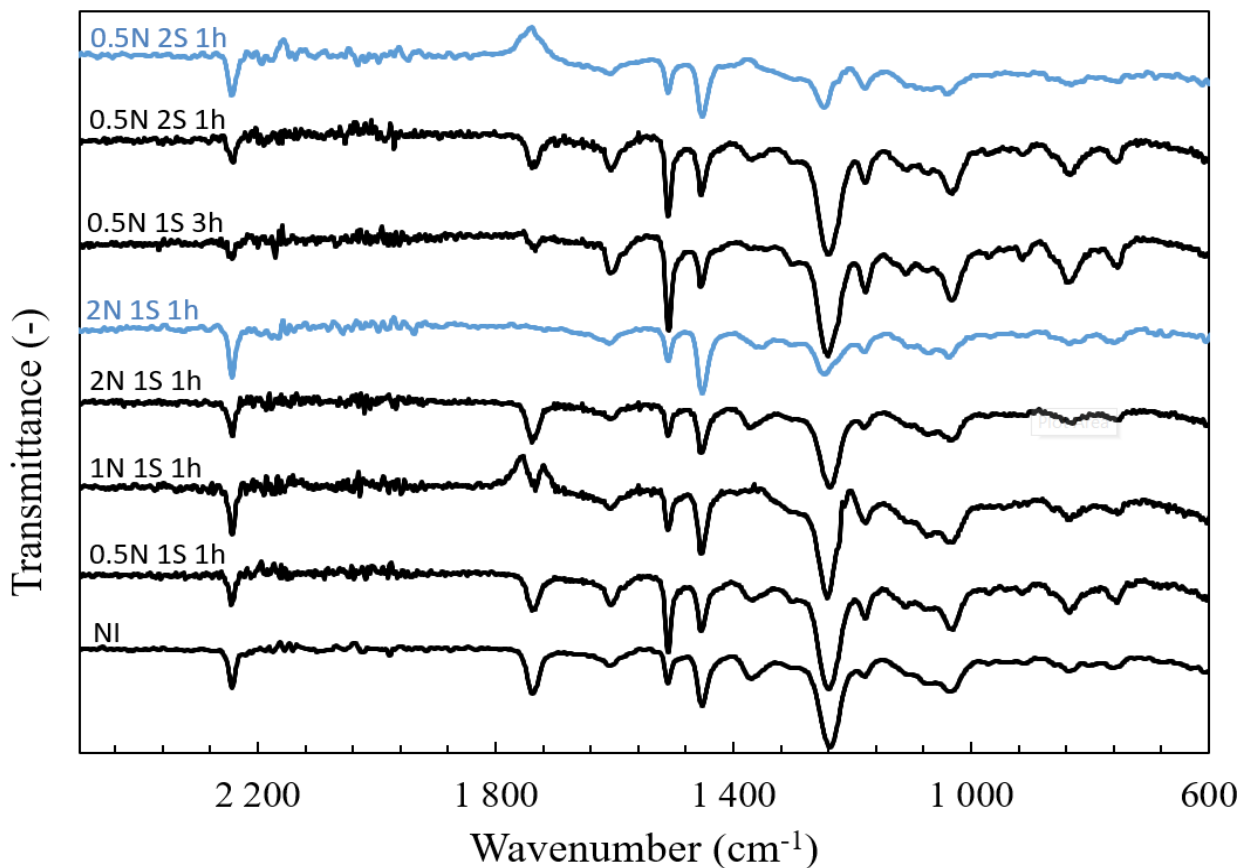


Figure 40: ATR-FTIR spectra of 1-MIM membranes on top of a PAN PX support (black lines), and DMAc12 support (blue lines). Spectra on DMAc12 were smoothed by taking the average transmittance of the surrounding six wavenumbers.

SEM

A clear difference in toplayer morphology can be seen comparing the 1S membranes synthesized with the same reaction time (1 h) on different supports (Figure 41, A, B, C). This difference can be attributed to support parameters like pore size and hydrophilicity, which affect the toplayer by influencing the interactions between the monomer, support, initiator, and solvent^{125, 162}. The typical globular and annular structures expected on a 1S 1h membrane according to the reference membrane TMHD, are present on DMAc15 (Figure 41, B). They are absent on DMAc12 (Figure 41, C), and replaced by punctured annular shapes, and both 1S membranes look different to the NI membrane. The 0.5N 1S 1h membrane on PAN PX shows very distinct annular structures, often accompanied by polymer protrusions, and it is the only membrane with significant salt rejection (57%). All structures change significantly with increasing reaction time, (1h vs 3h membranes Figure 41, D and E), indicating further polymerization. It appears more polymerization occurred on PAN PX compared to on DMAc15, as would be expected due to the PVAc accelerating effects and is line with the filtration results.

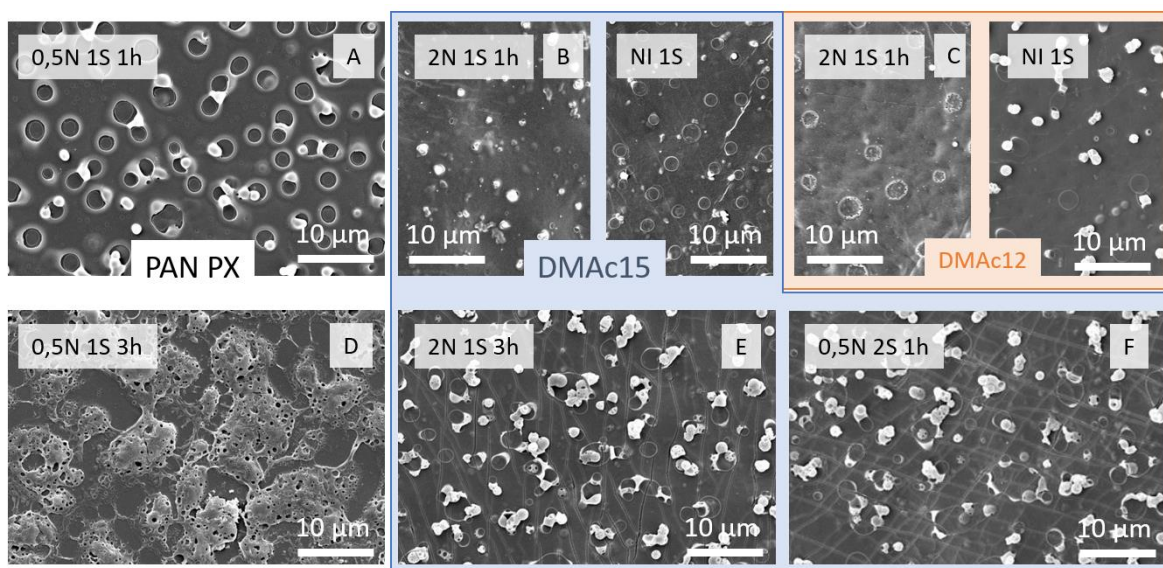


Figure 41: Top-view SEM images of 1-MIM membranes synthesized using different conditions, left: on top of PAN PX, middle (highlighted in blue): on top of DMAc15, top right (highlighted in red): on top of DMAc12.

XPS

To verify the occurrence of initiation by 1-MIM initiation, XPS-measurements were conducted. Remarkably, no N^+ functionalities were detected (Appendix, Figure 57), even though the permeance of the membranes, reaction mechanism, and SEM pictures indicate polymerization. The absence of a N^+ signal might be due to charge neutralization issues during the XPS-measurement or due to sampling at a location where no initiation occurred. Nevertheless, a low N^+ content would be expected anyway as the reactivity of 1-MIM is likely lower than TMHD (pK_b is 7.05 for 1-MIM vs 3.90 for TMHD), and as only one charge can maximally be incorporated per 1-MIM molecule compared to two for TMHD.

3.1.6.3 Conclusion

The salt rejection of TFC membranes synthesized on the in-house cast supports, is low (<10%), compared to when the PAN PX support is used (up to 58%). The reason a selective layer forms on top of PAN PX and not on the in-house cast supports is likely due to the accelerating effect of PVAc, which is only present in PAN PX. The permeance of the 1-MIM-initiated TFC membranes on DMAc12 are lower than the IM-initiated TFC membranes. This is explained by a faster IIP reaction of 1-MIM compared to IM, as the reactive alkoxide is formed as a 1:1 adduct for 1-MIM and as a 2:1 adduct for IM. Polymerization is further confirmed by SEM images, but likely incomplete as epoxide bands are still observed via FTIR. Surprisingly, no N^+ signal was detected using XPS, which is rather contradictory with the other characterization. A low N^+ content is expected, and as charge neutralization difficulties were

experienced during the XPS-measurement, the signal might have been lost in the background noise.

3.1.7 2-Methylimidazole (2-MIM)

To examine whether sterical hindrance has a significant effect on the ROP of EPON via imidazoles, 2-MIM was tested for comparison with IM. A similar reaction mechanism is followed for both IM and 2-MIM, as both will involve a proton transfer and form a 2:1 adduct containing the reactive alkoxide¹¹².

3.1.7.1 Membrane performance

On PAN PX

Careful interpretation of the data is needed as the performance of most 2-MIM membranes is similar to the NI membrane. Longer reaction times (1N 1S 1h vs 3h) only cause a significant decrease in permeance (R remains ~30%, P drops from 2.0 to 0.7 LMH/bar, Figure 42). This might indicate an increased toplayer thickness, but a similar density or charge incorporation compared to the IM membranes, for which both rejection and permeance remained constant with increasing reaction times. The explanation might be found in the reaction mechanism and initiator properties. The methyl group next to the amine groups can have two opposite effects on nucleophilicity: the electron-donating effect of the methyl group would result in an increase, while the sterical hindrance introduced by this methyl group would result in a decrease. As the permeance drops by 40% more when the reaction time increases from 1 h to 3 h for the 2-MIM membranes compared to IM membranes, this might indicate the electron-donating effect outweighs the sterical hindrance effect, resulting in a stronger nucleophile which will promote more polymerization. The fact that the rejection remains similar could be explained by the low charge incorporation by imidazoles, which can maximally incorporate one charge per molecule. However, more research is needed to confirm this difference in nucleophilicity as it is only further substantiated by the permeance of the 4N 1S 1h 2-MIM membrane which is lower than the IM membrane.

The increase in initiator concentration (1N vs 4N 1S 1h) results in an increased rejection (48%) and a decreased permeance (0.4 LMH/bar). This improved selectivity could be due to a higher availability of 2-MIM to initiate the polymerization, as the log(P) for 2-MIM is rather higher (Table 3). Comparing the 1S and 2S membranes, the rejection slightly goes down (32% to 20% for 1N membranes), and permeances remain constant around 2 LMH/bar. Similar to the IM- and 1-MIM-synthesized membranes, this could be due to insufficient polymerization and removal of the loose polymer chains by the toluene washing step.

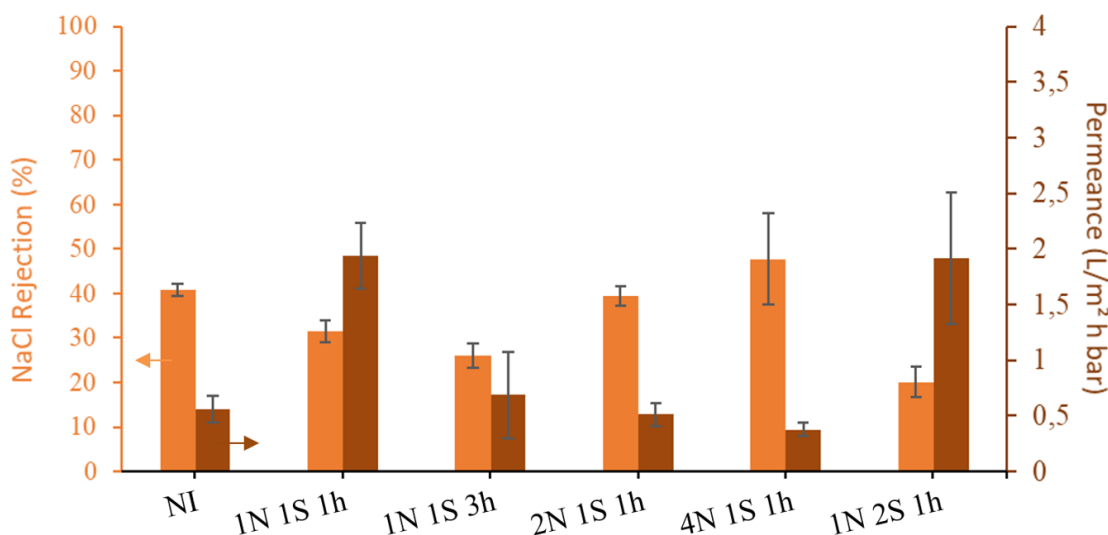


Figure 42: Performance of 2-MIM membranes synthesized using different conditions: concentrations of 1N, 2N, 4N, type 1S and 2S, reaction times of 1 h and 3 h. Filtration conditions: 10 bar, 5 mM NaCl aqueous solution.

On in-house cast PAN supports

The most promising membranes made on the PAN PX support were resynthesized on in-house cast supports. The rejection of the TFC membranes is slightly higher on DMAc12 than on DMAc15 (R~9% and ~4%, respectively, Figure 43), but no salt selective toplayer is formed. In addition, the DMAc12 1S 2-MIM-initiated TFC membrane has a permeance of ~17LMH/bar compared to ~25 LMH/bar when the same membrane is IM-initiated. These results suggest that even though 2-MIM might be a stronger nucleophile than IM, it is less efficient in synthesizing selective toplayers. The increased permeance from 17 to 34 LMH/bar for the 1S and 2S membranes on DMAc12 is similar to what was observed on PAN PX, which might be due to the toluene washing step as well.

MB rejection of the 1S membrane is slightly higher than the NI membrane (92% vs 78%), (Appendix, Figure 65), suggesting a selective layer with a higher MWCO is formed on 1S 2-MIM membranes, so that it can significantly reject MB but not NaCl. MB rejection of the 2S (46%) membrane is lower than the NI membrane. This low rejection compared to the 1S membrane is remarkable and likely due to defect membrane coupons, as defects in the 2S toplayer due to the toluene washing step are unlikely to cause the observed drop in rejection between the 1S and 2S membrane. A blue discoloration was observed on both 1S and 2S 2-MIM membranes ($q \sim 1.4$ mg/g after 3 h) similar to the IM- and 1-MIM-initiated TFC membranes, suggesting significant contribution of adsorption to the overall membrane rejection. The high observed MB adsorption also suggests low charge incorporation, since a higher positive charge content would prevent the adsorption of positively charged MB, and result in a q value closer to that of the charge-abundant TMHD 2S membrane.

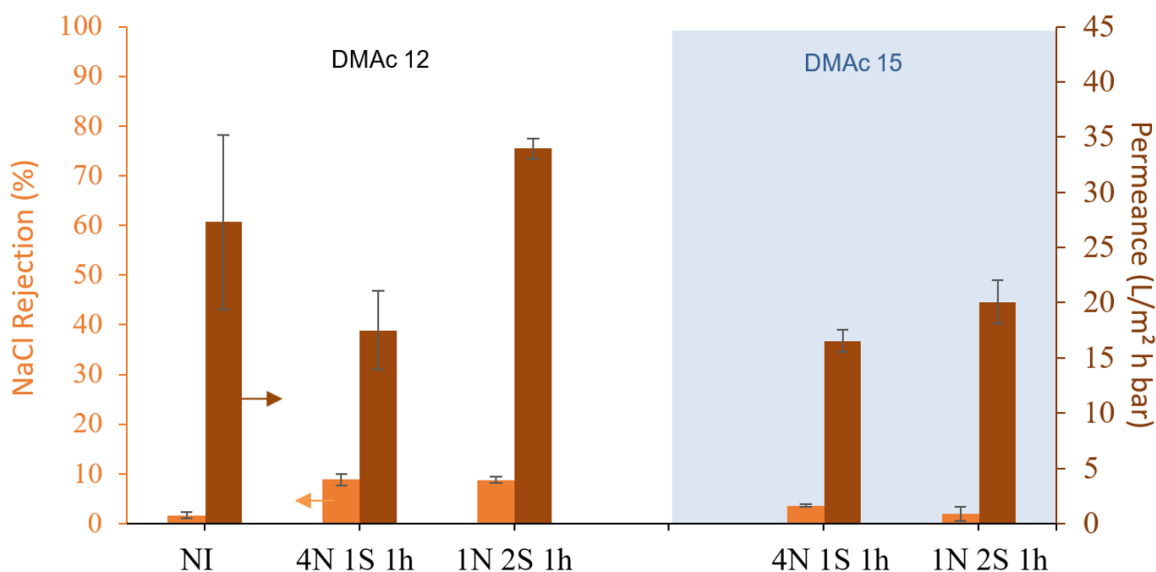


Figure 43: Performance of 2-MIM membranes synthesized under different conditions. White background: membranes with DMAc12 support, blue background: membranes with a DMAc15 support. Filtration conditions: 10 bar, 5mM NaCl aqueous solution.

3.1.7.2 Physicochemical characterization

ATR-FTIR

ATR-FTIR measurements were conducted to investigate the occurrence of polymerization and of 2-MIM incorporation. Similar as for the IM and 1-MIM membranes, the EPON bands (including the epoxide band) become more visible for longer reaction times, indicating incomplete polymerization and the importance of EPON adsorption (Appendix, Figure 60). An interaction effect between the support layer and EPON is also noteworthy in the spectra. EPON bands are less intense when the same membrane is synthesized on DMAc15 support instead of on PAN PX. This can be explained by the presence of PVAc in PAN PX, resulting in an increased hydrophilicity and hence enhanced interactions and adsorption between the support and EPON. Similar to the spectra of membranes synthesized with 1-MIM, no characteristic initiator bands can be observed.

SEM

As the IM&1-MIM 1N 1S 3h membranes were not selective, these were only synthesized for 2-MIM on PAN PX and not on the in-house cast supports. For these 1S membranes on PAN PX, a clear difference is observed in surface structures with increasing the reaction time (1 h vs 3 h, Figure 44). Both the annular structures and polymer clusters grow over time, indicating polymerization. The polymer clusters on top of this 1N 1S 3h PAN PX membrane are larger when initiated with 2-MIM than with IM (Figure 37), further substantiating the hypothesis of higher reaction rate of 2-MIM due to increased nucleophilicity by the methyl group (section 3.1.7.1). Similar to the other initiator membranes, a difference can be noticed in the morphology

of the same membrane, synthesized on two different supports (1N 2S 1h on PAN PX and DMAc15), likely due to the interactions between the monomer, support, initiator, and solvent^{125, 163}. The surface morphology of all 2-MIM membranes is different from the NI membranes, further supporting the occurrence of polymerization.

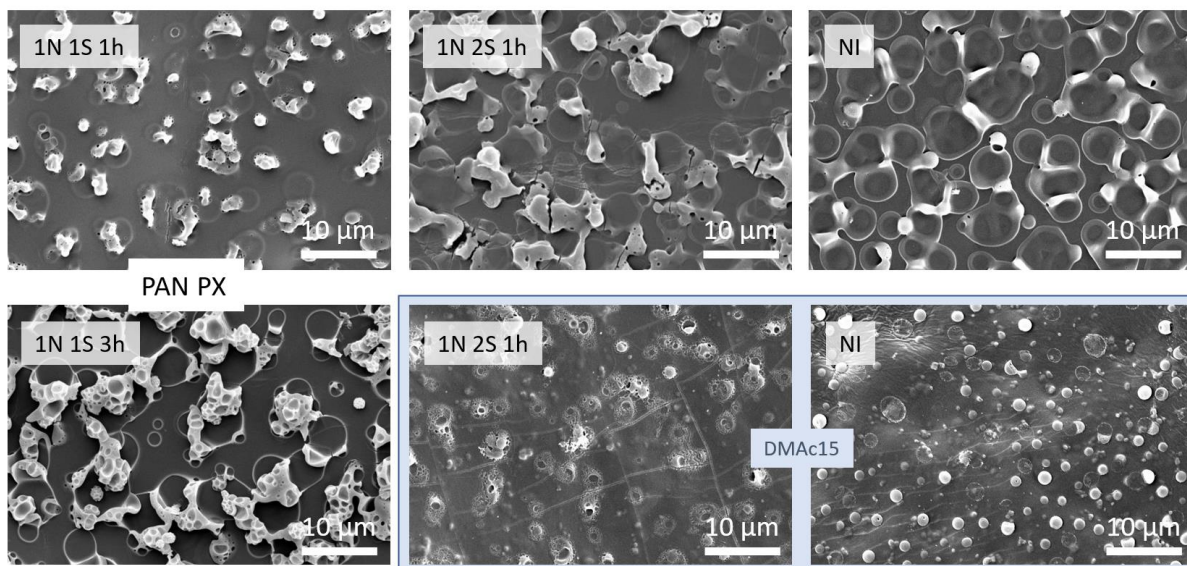


Figure 44: Top-view SEM images of 2-MIM membranes synthesized using different conditions, on top of PAN PX (white background), on top of DMAc15 (blue background).

3.1.7.3 Conclusion

ROP of EPON by sufficiently high (2N) 2-MIM concentration is suggested by filtration results, and by SEM pictures. No selective toplayers were formed, as the rejections were not significantly higher than the NI membrane for the TFC membranes made on PAN PX, and as the rejections were lower than 10% on in-house cast supports. Furthermore, polymerization is not complete, as the epoxide band is still observed in the FTIR spectra, and no salt selectivity is observed.

The larger drop in permeance when reaction times are longer (1h vs 3h) for the 2-MIM membranes than for the IM membranes, suggests that 2-MIM has a higher nucleophilicity than IM and can thus achieve higher degrees of polymerization. This also means that the electron-donating effect of the methyl group in 2-MIM outweighs the sterical hindrance effect. However, this is however only further substantiated by the permeance of the 1S 4N membrane, thus further research is needed to confirm this difference in nucleophilicity.

3.1.8 1,4-diazabicyclo[2.2.2] octane (DABCO) and Tris(2-dimethylaminoethyl)amine (Me6Tren)

DABCO is often used in nucleophilic substitution reactions due to its properties as a nucleophile ($pK_b=5.30$)¹⁶⁴. As high nucleophilicity is believed to be a desired characteristic of

the initiator, its capability to synthesize a membrane was studied. Another relatively strong nucleophile, Me6Tren, was studied as a trifunctional initiator (Appendix, Figure 51). It contains four tertiary amine groups, of which only three are expected to be active in nucleophilic substitution reactions ($pK_b=5.01$), as the N located in the center is too sterically hindered to react. In a single-phase solution, a higher reaction rate would be expected for an initiator with a higher functionality¹⁷⁹. However, vial tests suggested that this is not the case for this biphasic system, as the first signs of film formation were only observed after 2 h for Me6Tren, and after 30 mins for TMHD (Figure 23). This shows that observed trends, kinetics, and even reactions in bulk chemistry cannot easily be extrapolated to interfacial chemistry¹⁶⁵.

3.1.8.1 Membrane performance

On in-house cast PAN supports

Both initiators were only tested on DMAc12 to circumvent the EPON-adsorption related issues of the NI membrane on PAN PX. Remarkably, none of the DABCO-initiated 1S and 2S membranes have a significantly different NaCl performance than the NI membrane ($R\sim 1.5\%$, $P\sim 25$ LMH/bar, Appendix Figure 61), suggesting no substantial polymerization occurs. Since DABCO is a more reactive nucleophile than IM ($pK_b_{DABCO}=5.30 < pK_b_{IM}=7.04$), initiation of polymerization is expected to occur, except when side reactions are happening preventing DABCO to be available in the ROP of EPON. As discussed in section 3.1.8.2, this might be the case as an ether signal is observed in FTIR. The Me6Tren membranes show a slightly lower permeance in general (~ 15 LMH/bar, which is lower than the 1S TMHD reference of ~ 20), indicating the occurrence of polymerization. However, no selective membranes were obtained as the NaCl rejections of all TFC membranes is less than 5%.

Changing from a 1S to a 2S TFC membrane results, similarly to the TMHD membranes, in a decrease of the permeance for the 2S DABCO membrane (19 LMH/bar for salt filtration, 14 LMH/bar for MB filtration, Appendix Figure 65). The MB rejection is rather high (88%), but not significantly different from the NI membrane due to the large standard deviation. This decrease in permeance might be due to additional crosslinking of the toplayer, rather than due to charge incorporation by the initiator, as the second amine group has a low reactivity ($pK_b = 11$). Hence, DABCO can be seen as a monofunctional tertiary amine without crosslinking ability. For Me6Tren, both 1S and 2S membranes have a lower MB rejection lower than the NI membrane (respectively 54% and 37%, vs 78% for the 2S NI membrane, Appendix Figure 65). A possible explanation for this might be that the Me6Tren membranes achieving their maximum membrane adsorption capacity faster, hence less rejection will be observed after a 3 h filtration.

Initiator properties related to the poor membrane performance of both DABCO- and Me6Tren-initiated membranes are discussed in section 3.1.9.

3.1.8.2 Physicochemical characterization

ATR-FTIR

ATR-FTIR measurements show lower intensity of the EPON characteristic absorption bands for higher DABCO concentrations (Figure 45). For both DABCO and Me6Tren, the absence of significant polymerization is suggested by the epoxide bands which are visible on spectra with high EPON band intensities. These signals are likely present in the spectra of the other TFC membranes as well but disappear in the background noise. The DABCO 0.5N 1S 3h and Me6Tren 0.5N 2S 1h (Appendix, Figure 64) membranes have a clear band around 1715 cm^{-1} , which is in the typical range of ketone carbonyl (C=O) stretches¹⁴². The reason this band is present, might be due to the reaction of DABCO with terminal epoxide groups to form methyl ketones (Appendix, Figure 62)¹⁶⁶. However, this reaction has only been observed in literature at higher temperatures, and in pure toluene, making it hard to assess whether this would happen in an interfacial setting at room temperature. The reason why little polymerization is happening for these initiators might be reactions like this, or additional initiator properties playing a role in IIP.

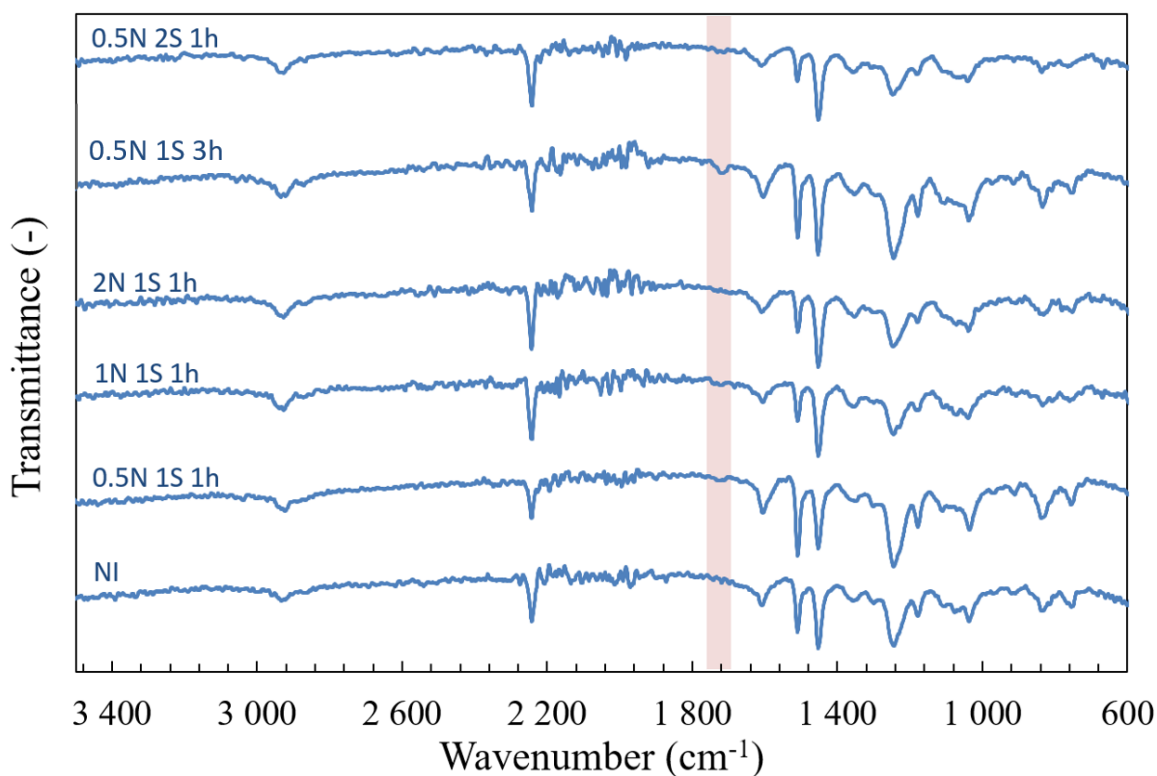


Figure 45: ATR-FTIR spectra of DABCO membranes on top of a DMAc12 support. The spectra were smoothed by taking the average transmittance of the surrounding six wavenumbers. C=O band around 1715 cm^{-1} highlighted in red.

SEM

Top-view SEM images were taken to examine the toplayer morphology of the membranes. No substantial difference is observed between the surface of the 1&2S DABCO membranes (Appendix, Figure 66) and the NI membrane, revealing EPON adsorption might most likely be happening instead of polymerization. The Me6Tren contain a low amount of the spherical polymer structures, except for the 0.5N 1S 3h membrane, but the morphology generally looks similar to the NI membranes as well. This slightly higher abundance of polymer structures could however explain the generally lower permeances in salt filtrations compared to DABCO-initiated membranes.

3.1.8.3 Conclusion

The only indication of polymerization is the generally significantly lower permeances of Me6Tren-initiated TFC membranes than the NI membrane. For DABCO, no indications of the ROP of EPON are observed, as SEM pictures, FTIR measurements, and filtration results all depict the absence of a toplayer. A possible explanation could be the occurrence of unwanted side-reactions, like ketone formation, as an absorption band at 1715 cm^{-1} is observed for the DABCO 0.5N 1S 3h and Me6Tren 0.5N 2S 1h TFC membranes.

3.1.9 Selecting important initiator characteristics for selective layer formation

In order to explain certain performance results, important initiator properties have already been addressed in the sections per specific initiator. It is however interesting to allocate a few key initiator properties which are important in the synthesis of a selective layer. As only TMHD yields selective membranes, the question arises as to what makes TMHD unique compared to the other initiators.

Polarizability does not seem to have a big effect, as imidazoles (low polarizability) and Me6Tren (high polarizability) both show a bad membrane performance. The difference in surface tension between Me6Tren and TMHD is not significant either, and it does not seem to play an important role as the Me6Tren membranes perform poorly. This leaves $\log(P)$ and pK_b (~nucleophilicity) as two selected properties for which TMHD is the most unique, hence suggesting these are important for selective toplayer formation¹⁶⁷. However, a lower nucleophilicity does not mean no initiation is taking place, as film formation was observed during support-free interfacial polymerization for all initiators. Furthermore, imidazole has a relatively low nucleophilicity, but the XPS results still indicate the presence of N^+ groups which are a result of initiation. This might suggest that high nucleophilicity is necessary to obtain *sufficient* polymerization during the synthesis to obtain a selective toplayer.

As mentioned in 3.1.8.1, two pK_b values (5.3 for the first N and 11 for the second N) are allocated to DABCO¹⁶⁸. This suggests that the second N will have a very low nucleophilicity. Hence, DABCO can be seen as a monofunctional tertiary amine, which is not able to form crosslinks, similar to 1-MIM. Even though some polymerization might occur for both initiators, the network may possibly not get dense, crosslinked, and charge-incorporated enough to form a selective. The latter is especially true for imidazoles, as the proton transfer in the reaction mechanism only allows the incorporation of one positive charge per molecule, in comparison to two charges for TMHD¹¹².

It might also be the case that TMHD has the ideal length as a crosslinker, since *N,N,N',N'*-Tetramethyl-1,3-propanediamine (TMPD) has already been tested as an initiator and did not yield a selective toplayer¹⁴⁸. As DABCO is a relatively strong nucleophile but only monofunctional, this could indicate that the ideal length of a crosslinker is only relevant if the initiator has a crosslinking ability. Apart for TMHD, Me6Tren was the only tested initiator with a high nucleophilic character, similar length as TMHD, and with an ability to crosslink. As Me6Tren did not yield selective membranes, the EPON system seems to require a bifunctional initiator with crosslinking abilities, of a length similar to TMHD.

3.2 GS SYSTEM

3.2.1 Introduction

Until now, the focus of the application of the IIP-made epoxide-based membranes has been on liquid separations^{79, 119,169}. However, as ether oxygens have strong interactions with CO₂, it makes sense to extend their application to GS membranes. With this in mind, fundamental research about the synthesis process is needed.

As described in the Materials and Methods section, some of the phases during synthesis of the GS membranes are reversed compared to the synthesis of the RO membranes. This is done with the idea of dissolving the monomer and initiator in their preferred phase, resulting in a reaction zone which is more confined to the interface. In this way, the selective layer could theoretically be synthesized more locally resulting in a thinner and denser layer. Just as for the RO membranes, TMHD is chosen as the reference initiator for the GS membranes, but a different monomer is used in order to increase the amount of ether oxygens in the final network. Instead of using a 1.5 w/v% EPON in toluene solution, 5 w/v% PEGDE in water and toluene solutions are used. A typical separation factor of ~55 and permeance ~10 GPU is expected for selective polyether membranes synthesized according to this process¹⁷⁰.

3.2.2 Support-free interfacial polymerization tests

PEGDE is a polymer which is well soluble in water. Hence, film formation is hard to visually observe, since the reacted polymer can still dissolve into the water phase without exceeding its solubility and precipitating on the interface. For all initiators however, a white turbidity on the interface was observed after, at most, a day (Appendix, Table 5).

3.2.3 TMHD – TMPD – 1-MIM comparison

TMPD is chosen as initiator because it is a smaller molecule, which can potentially penetrate the formed epoxide layer better and thus result in a denser selective layer. As beforementioned, imidazoles are often used in curing of epoxides, hence would be an interesting initiator to test for the GS membrane synthesis¹¹². Toluene solubility of the initiator is required in this system, hence 1-MIM is chosen instead of IM or 2-MIM, which have low toluene solubility. 1-MIM, like TMPD, has a relatively small size, but also has the typical planar structure of imidazoles.

For TMHD, TMPD and 1-MIM, two GS membranes were made (Figure 46). Both of the membranes were of the 2S type with an initiator concentration of 2N. The only difference was the reaction time during synthesis, which varied between 1 h and 2 h. The membranes synthesized with TMHD have the highest measured separation factors ($\alpha_{\text{CO}_2/\text{N}_2}^* \sim 23$) and highest (mixed gas) permeances ($P_{\text{CO}_2/\text{N}_2} \sim 12$ and 33 GPU) of these initiators. The performance of the 1-MIM membranes ($\alpha_{\text{CO}_2/\text{N}_2}^* \sim 15$ and 23, $P_{\text{CO}_2/\text{N}_2} \sim 1$ and 5 GPU) is somewhere between the TMHD and TMPD membranes. The TMPD membranes have a relatively low separation factor (~ 14) combined with a very low permeance (< 1 GPU). As both the TMHD and 1-MIM membranes showed better performance, more synthesis conditions were tested which are discussed in the next parts.

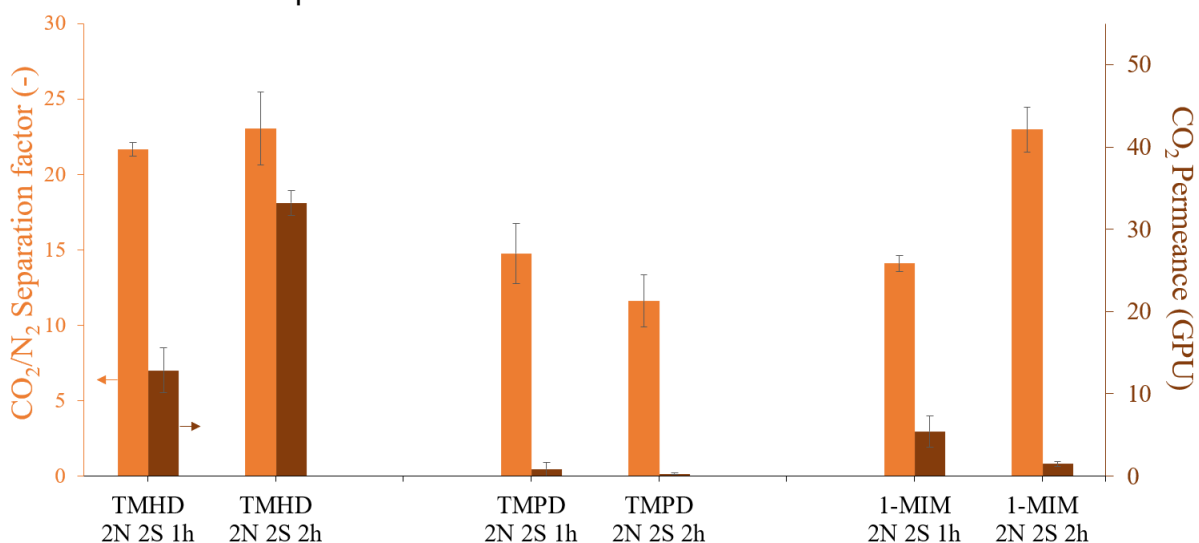


Figure 46: CO₂/N₂ separation factor and CO₂ permeance of membranes synthesized with TMHD, TMPD, and 1-MIM.

The only difference between TMHD and TMPD is the length of the alkyl chain in between the two amine groups, which is respectively six and three. This makes TMPD more water soluble, and a slightly weaker nucleophile¹⁷¹. As the selectivity of the TMPD membranes is low, a defect-free selective layer is unlikely to have formed. Nevertheless, polymerization occurred, as can be confirmed via ART-FTIR measurements. For the TMPD membrane, the oxirane band of PEGDE at $\sim 910\text{ cm}^{-1}$ disappears (Appendix, Figure 67, highlighted in purple) while a clear ether band (C-O-C stretching at 1097 cm^{-1})^{172, 173} remains, suggesting TMPD was able to initiate the reaction.

There can be several hypotheses explaining the bad performance of the TMPD membranes, with pore plugging being the most probable. Interfacially formed polymer chains could migrate into the aqueous phase inside the pores, since poly(ether) chains are highly water soluble¹⁷⁴. The pores are likely to be clogged in a non-continuous fashion, resulting in a discontinuous polyether phase and a low $\alpha_{\text{CO}_2/\text{N}_2}^*$ and $P_{\text{CO}_2/\text{N}_2}$.

This discontinuous phase of hydrophilic polyether chains would retain some water inside the pores even after drying. This is confirmed by FTIR measurements, broad water bands around 3350 cm^{-1} (stretching), and 1650 cm^{-1} (bending) are present (Appendix, Figure 67). These water bands are more pronounced in the TMHD and TMPD membranes than in the 1-MIM membranes. As these first two initiators have two reactive tertiary amine groups, the more pronounced presence of water peaks could also be due to more incorporation of hygroscopic quaternary ammonium groups¹⁷⁵. In none of the FTIR spectra, characteristic initiator absorption bands can be distinguished. This might be because bands from other chemical bonds are more intensely present at about the same wavenumber as the initiator bands.

3.2.3.1 TMHD

TMHD can effectively be used as an initiator to synthesize GS membranes. It is clear that a 2S-type membrane is required, as the 1S membrane has a separation factor which is equal to the separation factor of a PDMS layer (~ 10)¹⁷⁶. However, there are several reasons to believe a polymerization reaction is occurring during the 1S step. The decrease in permeance, compared to the PDMS coated support, for example, can prove this might be happening, as the CO_2 permeance of a thin PDMS layer would be orders of magnitude higher (~ 3000 barrer)¹⁷⁶. The infrared spectra indicate polymerization as well. After washing the membranes in toluene, the oxirane peak at $\sim 910\text{ cm}^{-1}$ disappears, while maintaining ether bands (Appendix, Figure 68). Looking at the 2S membranes, there does not seem to be any significant difference in separation factor between the different synthesis conditions (initiator concentration, 1S or 2S membrane type, or duration of reaction steps, Figure 47). This indicates that the tested

polymerization conditions do not favor the formation of a more defect-free selective layer, as the separation factor is expected to be higher in that case¹⁷⁷.

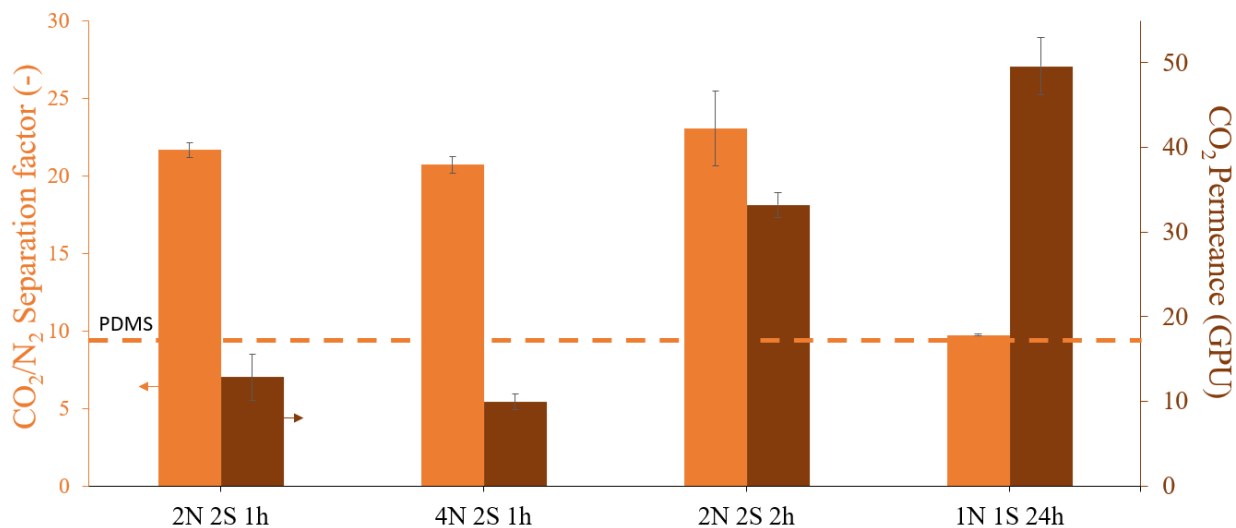


Figure 47: CO₂/N₂ separation factor and CO₂ permeance of membranes synthesized with TMHD. The selectivity of a pure PDMS layer is visualized with the orange dotted line.

3.2.3.2 1-Methylimidazole (1-MIM)

The performance of the 1N 2S 1h, 2N 2S 1h, and 2N 2S 2h membranes demonstrate that both a higher concentration and longer reaction time result in a higher separation factor and lower permeance (Figure 48). The reaction time plays a more pronounced role in the 1-MIM system (62% increase in selectivity between 2N 2S 1&2h membranes) compared to the TMHD system (6% increase in selectivity between 2N 2S 1&2h membranes). This is possibly the result of 1-MIM being an overall weaker nucleophile. This is further substantiated by comparing the performance of the 1N 1S 1&24h membranes: the permeance drops by 98% when the reaction step is 24 h compared to 1 h, however the separation factors only increase minimally. Here the pore plugging theory applies again, where a discontinuous polyether phase results in both low $\alpha_{\text{CO}_2/\text{N}_2}^*$ and $P_{\text{CO}_2/\text{N}_2}$.

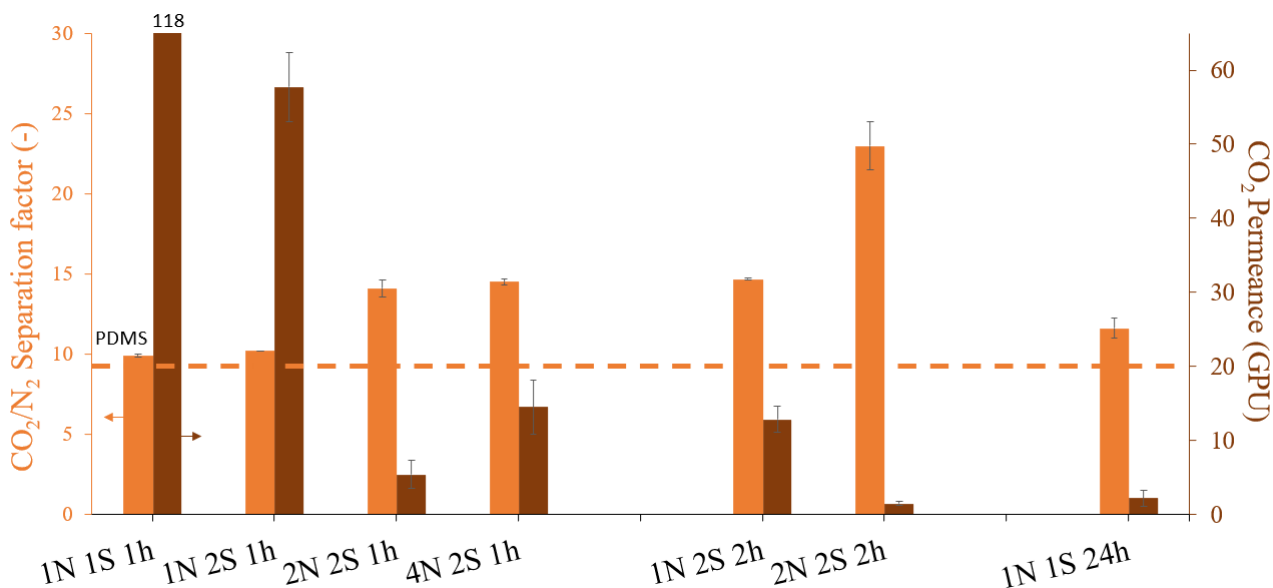


Figure 48: CO₂/N₂ separation factor and CO₂ permeance of membranes synthesized with 1-MIM. The selectivity of a pure PDMS layer is visualized with the orange dotted line.

Contrarily to the effect of varying synthesis conditions using imidazoles for the RO membranes (decrease in selectivity, increase in permeance when going from a 1S to a 2S membrane), GS membranes made using 1-MIM as an initiator show an increase in selectivity going from a 1S to a 2S membrane. This might indicate re-initiation and densification could be happening for the GS membranes during the 2S step. A possible explanation can be found in the synthesis. In the 1S step, the support pores are filled with the aqueous PEGDE solution after impregnation, on which the organic solution containing the initiator is added. However, in the 2S step, PEGDE is applied as a solution in the organic phase. Polymerization might happen more quickly when PEGDE is present in this organic phase, as the termination by water would happen more slowly and less diffusion of the newly formed oligomers away from the selective layer into the water phase would occur.

3.2.4 MBDA and 1-MBI

Finally, initiators containing aromatic rings were used. These molecules are insoluble in water, making them ideal candidates to obtain a more defined reaction zone at the interface and hence a thinner and denser layer. However, both membranes showed selectivities similar to PDMS (Figure 49), even though permeance of both membranes is lower than what would be expected if no reaction happened (thin PDMS layer permeance ~3000 barrer)¹⁷⁶.

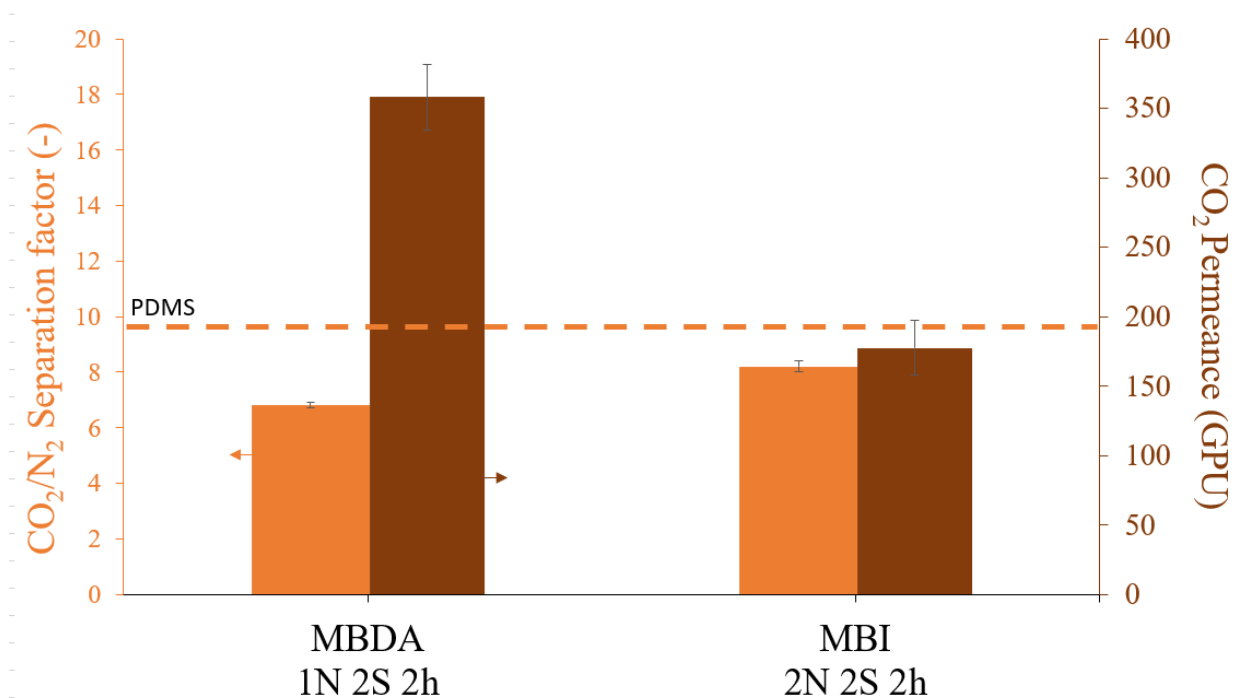


Figure 49: CO₂/N₂ separation factor and CO₂ permeance of membranes synthesized with MBDA and MBI. The selectivity of a pure PDMS layer is visualized with the orange dotted line.

The FTIR intensity of the ether band is low compared to the band around 1240 cm⁻¹ (support band: C-O stretching of PVAc), whereas for the TMHD membrane the ether band is multiple times the intensity of this support band (Figure 69). As the ether band has low intensity, the epoxide band is expected to have an even lower intensity, hence these bands might disappear in the noise of the spectrum. Another explanation for the absence of epoxide bands could be that polymerization is happening at a small extent which is not enough to result in selective membranes. Again, lower initiator reactivity might lay at the base of this observation^{80, 178}. The low affinity to water of these type of initiators might also play a role in their low reactivity, as water catalyzes the initiation and propagation reactions¹⁷⁹. The availability of the initiators at the toluene-water interface might be too low, and in addition, toluene rather than water will coordinate with these initiators. It might thus be hard to obtain the catalytic effect of water needed during the initiation reaction to make it happen at sufficient speed^{179, 180}.

PART 4: GENERAL CONCLUSIONS AND PERSPECTIVES

RO system

As the current state-of-the-art PA TFC membranes used in RO applications still have limited chemical stability, the recently introduced chemically robust epoxide-based TFC membranes show great potential in applications that involve aggressive feed streams or cleaning procedures. These membranes are synthesized by a newly introduced IIP method, where a tertiary amine initiator will perform the ROP reaction of the four-functional epoxide monomer EPON. 1S- and 2S membranes can be synthesized, where the latter contains an extra densification and re-initiation step essential to form a salt selective membrane, yielding NaCl rejections of ~80% when the reference initiator TMHD is used. However, the current four hour synthesis time and the black-box approach to prepare these membranes limits their scale-up. In this work, the synthesis mechanism was investigated in more detail, with as goal to reduce the overall synthesis time. This was done by investigating the effect of different initiators on the reaction mechanisms, the membrane performance and physicochemical properties. TMHD has been used as the initiator in previous research and was therefore used as a reference to compare the newly investigated initiators with.

Besides TMHD, five other initiators (imidazole (IM), 1-methylimidazole (1-MIM) , 2-methyl imidazole (2-MIM), 1,4-diazabicyclo[2.2.2]octane (DABCO), and tris(2-dimethylaminoethyl) amine (Me6Tren)) were studied in the ROP reaction of EPON for the synthesis of epoxide-based TFC membranes for RO applications. The initiator nucleophilicity believed to play an important role in the ROP of EPON and is expected to increase with the order $IM \approx 1-MIM < 2-MIM < DABCO \approx Me6Tren < TMHD$ based on their pK_b values. The pK_b of the second N in DABCO is 11, suggesting this initiator can be seen as a monofunctional tertiary amine, which is not able to form crosslinks. Contrary to IM and 2-MIM, 1-MIM is not able to form crosslinks either due to the methyl group on the 1-(N) nitrogen. This happens through a proton transfer mechanism, resulting in a maximal charge incorporation of only one charge per imidazole-type initiator. TMHD and Me6Tren are bi- and trifunctional, respectively, resulting in a maximum of two or three incorporated charges per initiation step with the additional ability to form crosslinks.

Remarkably, indications of polymerizations are only observed for the imidazole-type initiators (SEM pictures, XPS-, and filtration data) and not for the DABCO and Me6Tren membranes. The 1S IM- and 1-MIM-initiated TFC membranes have significantly higher salt rejections (58%)

than the baseline (NI) membrane (41%), and 1S TMHD reference membrane (36%) when made on a PAN PX support. This indicates a selective layer can be obtained using a short total reaction time which is not the case for TMHD. Hence, a salt selective 1S membrane has been obtained for the first time, using IM and 2-MIM initiators. However, the 2S TFC membranes for IM and 1-MIM, 2-MIM, DABCO and Me6Tren are nonselective. The limited crosslinking ability and the restricted charge incorporation (imidazoles), or insignificant occurrence of IIP (DABCO and Me6Tren) result in little densification during the 2S step, which likely causes the nonselectivity¹⁵⁷. Nonselective membranes are also obtained when the 1S IM- and 1-MIM-initiated TFC membranes are resynthesized on in-house cast supports, yielding salt rejections lower than 10%. This influence of the support on the selective layer synthesis is assigned to the presence of PVAc which is only present in PAN PX. PVAc improves the support hydrophilicity compared to in-house cast supports, offers the opportunity to produce alcohols (which will accelerate polymerization) by saponification reactions, and might induce specific interactions with epoxide groups. Additionally, defects in the toplayer will more strongly affect the performance of the TFC membrane on the self-made supports as they have a larger surface porosity than PAN PX.

Compared to the other initiators, only the 2S TMHD-initiated TFC membranes on in-house cast supports are selective. Hence, it can be concluded that TMHD is the best initiator for IIP in this system, likely due to its high nucleophilicity. DABCO and Me6Tren, which theoretically are mono- and trifunctional initiators, respectively, are relatively strong nucleophiles but do not yield selective membranes. This suggests the preference in this EPON system towards a bifunctional initiator. In addition, the distance between the epoxide groups due to the bulky aromatic core of the four-functional EPON epoxide monomer might require longer crosslinkers than those tested. TMPD, which contains a three-carbon alkyl chain, did not yield selective membranes in a previous study, therefore pointing towards an ideal length of TMHD as a crosslinker, as it contains a six-carbon alkyl chain. With this in mind, longer initiators would also be worthwhile to investigate in the future.

Additional information was gathered about the initiation and densification mechanism of TMHD by varying the reaction times. Filtrations and characterization of the membranes suggests that the re-initiation and densification step is the most important step to achieve salt selectivity. The TMHD reaction rate was deduced to be faster in the densification step by using XPS-, zeta potential- and filtration data, which also elucidated the way TMHD is incorporated in the polymer network as a function of reaction time. Top-view SEM pictures show that the toplayer

forms with increasing reaction times, in agreement with the filtration and other physicochemical characterization data.

GS system

As ether oxygens have strong interactions with CO₂, the possibility to extend the applications of these epoxide-based TFC membranes from liquid separations to GS was investigated. To improve the content of ether oxygens in the selective layer, PEGDE was used as an epoxide monomer in this system. In order to understand the system better, multiple initiators were tested similarly to what was done for the RO membranes.

The potential of TMHD, TMPD, 1-MIM, MBDA and 1-MBI as initiators in the ROP reaction of PEGDE was studied by synthesizing GS membranes with different synthesis conditions (varying reaction time, initiator concentration, 1S and 2S membrane type). The synthesis procedure for the GS membranes was different than for RO membranes, as an attempt was made to create a thinner and denser selective layer by dissolving the monomer and initiator in their preferred phase, hence creating a more defined interfacial reaction zone. This synthesis method does not seem to yield favorable results, as generally, a low separation factor and permeance is observed. This is likely due to pore plugging, a problem that could not be alleviated by the use of initiators with different properties. The tested water-soluble initiators result in selective membranes, while water-insoluble initiators do not. This is possibly because water molecules near the initiation site are necessary for the polymerization to happen at a sufficiently high rate.

Take aways and future work

The take aways from this work can be applied to improve the membrane synthesis efficiency. When TMHD is used as an initiator, total synthesis time could be reduced by shortening the first steps in the 2S procedure, but maintaining a longer final densification and charge incorporation step. When TMHD or imidazoles are used as initiators, synthesizing the membranes at elevated temperatures, which is often done in epoxide curing processes, could accelerate reactions and thus shorten synthesis times¹¹². Other methods to increase reaction rates could be the addition of catalysts like alcohols, which are already used in epoxide curing¹⁰¹. The alcohol can be added as such, or it could be present as a functional group on a bifunctional tertiary amine initiator. Since DABCO and Me6Tren do not show promising signs of polymerization, further investigations should best focus on long, bifunctional, highly nucleophilic initiators, optionally containing hydroxyl groups.

Some claims made in this work could be further substantiated by doing additional characterization, such as experimental determination of partitioning coefficients, PALS analysis on the TMHD 1S membrane to verify the hypothesized gradient in density of the top layer, and measuring cut-off curves of the membranes to see how the synthesis parameters affect the rejection of a range of solutes of different molecular weights and hence target different membrane applications. Furthermore, additional characterization of the films made in support-free polymerization might provide information about their properties, and titration of amine groups in TMHD 2S membranes could reveal whether the amine groups are present as quaternary ammonium groups or as dangling amines. Additional interesting experiments which could be done are changing the biphasic system to move away from toluene from a scale-up perspective, investigate post-functionalization to increase membrane performance, and using different markers than dyes to prevent, *e.g.*, dye adsorption.

REFERENCES

- ¹ University of Wollongong (2019). *Global problems*. Retrieved October 18, 2022, from <https://www.futurelearn.com/info/blog>
- ² U.S. Geological Survey. (2019). *How Much Water is There on Earth?* Retrieved December 31, 2022, from <https://www.usgs.gov/special-topics/water-science-school/science/how-much-water-there-earth>
- ³ Abengoa (2015). *A short history of desalination*. Retrieved October 18, 2022, from <http://www.theenergyofchange.com/short-history-of-desalination>
- ⁴ Victoria State Government (2019). *Desalination history*. Retrieved October 18, 2022, from <https://www.water.vic.gov.au/water-grid-and-markets/desalination/desalination-background/desalination-history>
- ⁵ Do Thi, H. T., Pasztor, T., Fozer, D., Manenti, F., & Toth, A. J. (2021). Comparison of Desalination Technologies Using Renewable Energy Sources with Life Cycle, PESTLE, and Multi-Criteria Decision Analyses. *Water*, 13(21), 21. <https://doi.org/10.3390/w13213023>
- ⁶ Mulder, M. Basic principles of membrane technology. (Kluwer Academic, 1996).
- ⁷ Younas, M. and Rezakazemi, M. (2022). Introduction to Membrane Technology. *Membrane Contactor Technology: Water Treatment, Food Processing, Gas Separation, and Carbon Capture, First Edition*, 16.
- ⁸ Burganos, V. N. (1999). Membranes and Membrane Processes. *MRS Bulletin*, 24(3), 19–22. <https://doi.org/10.1557/S0883769400051861>
- ⁹ Hunger, K., Schmeling, N., Jeazet, H. B. T., Janiak, C., Staudt, C. and Kleinermanns, K. (2012). Investigation of Cross-Linked and Additive Containing Polymer Materials for Membranes with Improved Performance in Pervaporation and Gas Separation. *Membranes*, 727-763.
- ¹⁰ Toh, Y. H. S. (2008). *MOLECULAR SEPARATIONS WITH ORGANIC SOLVENT NANOFILTRATION*. 232.
- ¹¹ Fernández-Barquín, A., Casado-Coterillo, C., & Irabien, Á. (2017). Separation of CO₂-N₂ gas mixtures: Membrane combination and temperature influence. *Separation and Purification Technology*, 188, 197–205. <https://doi.org/10.1016/j.seppur.2017.07.029>
- ¹² Khan, A. L., Basu, S., Cano-Odena, A., & Vankelecom, I. F. J. (2010). Novel high throughput equipment for membrane-based gas separations. *Journal of Membrane Science*, 354(1–2), 32–39. <https://doi.org/10.1016/j.memsci.2010.02.069>

-
- ¹³ Jansen, J. C. (2016). Ideal Gas Selectivity. In E. Drioli & L. Giorno (Eds.), *Encyclopedia of Membranes* (pp. 1–1). Springer. https://doi.org/10.1007/978-3-642-40872-4_301-1
- ¹⁴ He, Z., & Wang, K. (2018). The ‘ideal selectivity’ vs ‘true selectivity’ for permeation of gas mixture in nanoporous membranes. *IOP Conference Series: Materials Science and Engineering*, 323, 012002. <https://doi.org/10.1088/1757-899X/323/1/012002>
- ¹⁵ Malakhov, A.O.; Volkov, V.V. (2021). Mixed-Gas Selectivity Based on Pure Gas Permeation Measurements: An Approximate Model. *Membranes* 2021, 11, 833. <https://doi.org/10.3390/membranes11110833>
- ¹⁶ Matteucci, S., Yampolskii, Y., Freeman, B. D., & Pinnau, I. (2006). Transport of Gases and Vapors in Glassy and Rubbery Polymers. In Y. Yampolskii, I. Pinnau, & B. Freeman (Eds.), *Materials Science of Membranes for Gas and Vapor Separation* (pp. 1–47). John Wiley & Sons, Ltd. <https://doi.org/10.1002/047002903X.ch1>
- ¹⁷ Singh, R. (2005). Chapter 1—Introduction to membrane technology. In R. Singh (Ed.), *Hybrid Membrane Systems for Water Purification* (pp. 1–56). Elsevier Science. <https://doi.org/10.1016/B978-185617442-8/50002-6>
- ¹⁸ Drioli E, Giorno L (eds) (2010). *Comprehensive membrane science and engineering*. Elsevier Ltd. Oxford, UK ISBN: 978-0-08-093250-7
- ¹⁹ Strathmann H, Giorno L, Drioli E (2006). *An introduction to membrane science and technology*. CNR – Servizio Pubblicazioni e Informazioni Scientifiche, Rome, Italy
- ²⁰ Drioli, E., Quist-Jensen, C. A., & Giorno, L. (2016). Molecular Weight Cut-off. In E. Drioli & L. Giorno (Eds.), *Encyclopedia of Membranes* (pp. 1326–1327). Springer. https://doi.org/10.1007/978-3-662-44324-8_2216
- ²¹ Lee, A., W. Elam, J., & B. Darling, S. (2016). Membrane materials for water purification: Design, development, and application. *Environmental Science: Water Research & Technology*, 2(1), 17–42. <https://doi.org/10.1039/C5EW00159E>
- ²² Baker, R.W. (2004). *Membrane technology and applications* (2nd edition). John Wiley & Sons.
- ²³ Purkait, M.K. and Singh, R. (2018). *Membrane technology in separation science*. Taylor & Francis Group.
- ²⁴ *Fundamentals of Membrane Transport Phenomena*. (2017). In T. Uragami, *Science and Technology of Separation Membranes* (pp. 147–180). John Wiley & Sons, Ltd. <https://doi.org/10.1002/9781118932551.ch6>
- ²⁵ Ismail, A. F., Kusworo, T. D., Mustafa, A., & Hasbullah, H. (2005). *Understanding the Solution-Diffusion Mechanism in Gas Separation Membrane for Engineering Students*. Proceedings of the 2005 Regional Conference on Engineering Education.
- ²⁶ Wijmans, J.G. & Baker, R.W. (1995). The solution-diffusion model: a review. *Journal of Membrane Science*, 107, 1-21. [https://doi.org/10.1016/0376-7388\(95\)00102-1](https://doi.org/10.1016/0376-7388(95)00102-1).

-
- ²⁷ Hendrix, K., & Vankelecom, I. F. J. (2013). Solvent-Resistant Nanofiltration Membranes. In *Encyclopedia of Membrane Science and Technology* (pp. 1–33). John Wiley & Sons, Ltd. <https://doi.org/10.1002/9781118522318.emst120>
- ²⁸ Wijmans, J. G. H., & Baker, R. W. (2006). The Solution-Diffusion Model: A Unified Approach to Membrane Permeation. *Materials Science of Membranes for Gas and Vapor Separation*, 159–189.
- ²⁹ Lin, H., & Freeman, B. D. (2005). Materials selection guidelines for membranes that remove CO₂ from gas mixtures. *Journal of Molecular Structure*, 739(1–3), 57–74. <https://doi.org/10.1016/j.molstruc.2004.07.045>
- ³⁰ Abdullah, N., Rahman, M.A., Othman, M.H.D., Jafaar, J. and Ismail, A.F. (2018). Chapter 2 - Membranes and Membrane Processes: Fundamentals. . In A. Basile, S. Mozia, & R. Molinari (Eds.), *Current Trends and Future Developments on (Bio-) Membranes* (pp. 45–70). Elsevier. <https://doi.org/10.1016/B978-0-12-813549-5.00001-3>
- ³¹ Cherif, H., & Belhadj, J. (2018). Chapter 15—Environmental Life Cycle Analysis of Water Desalination Processes. In V. G. Gude (Ed.), *Sustainable Desalination Handbook* (pp. 527–559). Butterworth-Heinemann. <https://doi.org/10.1016/B978-0-12-809240-8.00015-0>
- ³² Lonsdale, H. K. (1982). The growth of membrane technology. *Journal of Membrane Science*, 10(2), 81–181. [https://doi.org/10.1016/S0376-7388\(00\)81408-8](https://doi.org/10.1016/S0376-7388(00)81408-8)
- ³³ Vankelecom, I. F. J. (2016). Membrane Technology.
- ³⁴ Ismail, A.F. an Matsuura, T., (2022). *Membrane separation processes*. Amsterdam, Netherlands: Elsevier
- ³⁵ Ritt, C. L., Stassin, T., Davenport, D. M., DuChanois, R. M., Nulens, I., Yang, Z., Ben-Zvi, A., Segev-Mark, N., Elimelech, M., Tang, C. Y., Ramon, G. Z., Vankelecom, I. F. J., & Verbeke, R. (2022). The open membrane database: Synthesis–structure–performance relationships of reverse osmosis membranes. *Journal of Membrane Science*, 641, 119927. <https://doi.org/10.1016/j.memsci.2021.119927>
- ³⁶ Nagy, E. (2019). Chapter 21—Pressure-Retarded Osmosis (PRO) Process. In E. Nagy (Ed.), *Basic Equations of Mass Transport Through a Membrane Layer (Second Edition)* (pp. 505–531). Elsevier. <https://doi.org/10.1016/B978-0-12-813722-2.00021-2>
- ³⁷ World sea temperatures (2022). *Mediterranean temperature*. Retrieved May 26, 2022, from <https://www.seatemperature.org/mediterranean-sea>
- ³⁸ NASA Earth Observatory (2012). *A Measure of Salt*. [Text article]. <https://earthobservatory.nasa.gov/images/78250/a-measure-of-salt>
- ³⁹ Wang, L., Cao, T., Dykstra, J. E., Porada, S., Biesheuvel, P. M., & Elimelech, M. (2021). Salt and Water Transport in Reverse Osmosis Membranes: Beyond the Solution-Diffusion Model. *Environmental Science & Technology*, 55(24), 16665–16675. <https://doi.org/10.1021/acs.est.1c05649>

-
- ⁴⁰ Atkins, P. W., & De Paula, J. (2006). *Atkins' Physical chemistry*. W.H. Freeman.
- ⁴¹ Espanani, R., Miller, A., Busick, A., Hendry, D., & Jacoby, W. (2016). Separation of N₂/CO₂ mixture using a continuous high-pressure density-driven separator. *Journal of CO₂ Utilization*, 14, 67–75. <https://doi.org/10.1016/j.jcou.2016.02.012>
- ⁴² Fernández-Barquín, A., Casado-Coterillo, C., & Irabien, Á. (2017). Separation of CO₂-N₂ gas mixtures: Membrane combination and temperature influence. *Separation and Purification Technology*, 188, 197–205. <https://doi.org/10.1016/j.seppur.2017.07.029>
- ⁴³ Caldwell, S. J., Al-Duri, B., Sun, N., Sun, C., Snape, C. E., Li, K., & Wood, J. (2015). Carbon Dioxide Separation from Nitrogen/Hydrogen Mixtures over Activated Carbon Beads: Adsorption Isotherms and Breakthrough Studies. *Energy & Fuels*, 29(6), 3796–3807. <https://doi.org/10.1021/acs.energyfuels.5b00164>
- ⁴⁴ Janusz-Cygan, A., Jaschik, J., Wojdyła, A., & Tańczyk, M. (2020). The Separative Performance of Modules with Polymeric Membranes for a Hybrid Adsorptive/Membrane Process of CO₂ Capture from Flue Gas. *Membranes*, 10(11), 309. <https://doi.org/10.3390/membranes10110309>
- ⁴⁵ Pal, P. (2015). Chapter 5—Arsenic Removal by Membrane Distillation. In P. Pal (Ed.), *Groundwater Arsenic Remediation* (pp. 179–270). Butterworth-Heinemann. <https://doi.org/10.1016/B978-0-12-801281-9.00005-9>
- ⁴⁶ Leam, J. J., Bilad, M. R., Wibisono, Y., Hakim Wirzal, M. D., & Ahmed, I. (2020). Chapter 7—Membrane Technology for Microalgae Harvesting. In A. Yousuf (Ed.), *Microalgae Cultivation for Biofuels Production* (pp. 97–110). Academic Press. <https://doi.org/10.1016/B978-0-12-817536-1.00007-2>
- ⁴⁷ Du, X., Shi, Y., Jegatheesan, V., & Haq, I. U. (2020). A Review on the Mechanism, Impacts and Control Methods of Membrane Fouling in MBR System. *Membranes*, 10(2), 24. <https://doi.org/10.3390/membranes10020024>
- ⁴⁸ Arar, O., Ipek, I., & Sarp, S. (2019). Chapter 11—Synthesis of nanomaterial-incorporated pressure retarded osmosis membrane for energy generation. In W.-J. Lau, A. F. Ismail, A. Isloor, & A. Al-Ahmed (Eds.), *Advanced Nanomaterials for Membrane Synthesis and its Applications* (pp. 253–270). Elsevier. <https://doi.org/10.1016/B978-0-12-814503-6.00011-2>
- ⁴⁹ Membrane solutions. (n.d.) *Four types of Membrane Fouling—Membrane Solutions*. Retrieved August 13, 2022, from https://www.membrane-solutions.com/News_1224.htm
- ⁵⁰ Luis, P. (2018). Chapter 1—Introduction. In P. Luis (Ed.), *Fundamental Modelling of Membrane Systems* (pp. 1–23). Elsevier. <https://doi.org/10.1016/B978-0-12-813483-2.00001-0>
- ⁵¹ Nicolaisen, B. (2020, June). *Membranes: Fouling & Cleaning*. Water & Wastes Digest. <https://www.wwdmag.com/water-filtration/article/10917681/membranes-fouling-cleaning>

-
- ⁵² ScienceDirect Topics. (n.d.). *Membrane Fouling—An overview*. Retrieved August 13, 2022, from <https://www.sciencedirect.com/topics/engineering/membrane-fouling>
- ⁵³ Xu, R., Wang, B., & Cai, Y. (2022). Preparation and structures of PEBA gas separation membrane modified by fumed silica for oil vapor separation. *Scientific Reports*, 12(1), 1. <https://doi.org/10.1038/s41598-022-05064-7>
- ⁵⁴ Alsayed, A. F. M., & Ashraf, M. A. (2021). 2—Modified nanofiltration membrane treatment of saline water. In P. Samui, H. Bonakdari, & R. Deo (Eds.), *Water Engineering Modeling and Mathematic Tools* (pp. 25–44). Elsevier. <https://doi.org/10.1016/B978-0-12-820644-7.00005-0>
- ⁵⁵ Qun, S. M. (2021). *Interfacial Polymerization Techniques for TFC/TFN*. Retrieved August 14, 2022, from <https://encyclopedia.pub/entry/7795>
- ⁵⁶ Peng, L. E., Yang, Z., Long, L., Zhou, S., Guo, H., & Tang, C. Y. (2022). A critical review on porous substrates of TFC polyamide membranes: Mechanisms, membrane performances, and future perspectives. *Journal of Membrane Science*, 641, 119871. <https://doi.org/10.1016/j.memsci.2021.119871>
- ⁵⁷ Lau, W.-J., Lai, G.-S., Li, J., Gray, S., Hu, Y., Misdan, N., Goh, P.-S., Matsuura, T., Azelee, I. W., & Ismail, A. F. (2019). Development of microporous substrates of polyamide thin film composite membranes for pressure-driven and osmotically-driven membrane processes: A review. *Journal of Industrial and Engineering Chemistry*, 77, 25–59. <https://doi.org/10.1016/j.jiec.2019.05.010>
- ⁵⁸ Al Mayyahi, A. (2018). Important Approaches to Enhance Reverse Osmosis (RO) Thin Film Composite (TFC) Membranes Performance. *Membranes*, 8(3), 68. <https://doi.org/10.3390/membranes8030068>
- ⁵⁹ Purkait, M. K., Sinha, M. K., Mondal, P., & Singh, R. (2018). Chapter 1—Introduction to Membranes. In M. K. Purkait, M. K. Sinha, P. Mondal, & R. Singh (Eds.), *Interface Science and Technology* (Vol. 25, pp. 1–37). Elsevier. <https://doi.org/10.1016/B978-0-12-813961-5.00001-2>
- ⁶⁰ Holda, A. K., & Vankelecom, I. F. J. (2015). Understanding and guiding the phase inversion process for synthesis of solvent resistant nanofiltration membranes. *Journal of Applied Polymer Science*, 132(27). <https://doi.org/10.1002/app.42130>
- ⁶¹ Garcia, J. U., Iwama, T., Chan, E. Y., Tree, D. R., Delaney, K. T., & Fredrickson, G. H. (2020). Mechanisms of Asymmetric Membrane Formation in Nonsolvent-Induced Phase Separation. *ACS Macro Letters*, 9(11), 1617–1624. <https://doi.org/10.1021/acsmacrolett.0c00609>

-
- ⁶² S., N., Ahamed, D., & Joseph, S. (2020). Thermodynamic analysis of phase diagram of H₂O-DMF-PCL system: Investigation on the influence of inorganic additives TiO₂/MMT. *Journal of Materials Science*, 55. <https://doi.org/10.1007/s10853-020-04386-z>
- ⁶³ Luo, T., Abdu, S., & Wessling, M. (2018). Selectivity of Ion Exchange Membranes: A Review. *Journal of Membrane Science*, 555. <https://doi.org/10.1016/j.memsci.2018.03.051>
- ⁶⁴ Bai, H., Zhou, Y., Zhang, L. (2015). Morphology and Mechanical Properties of a New Nanocrystalline Cellulose/Polysulfone Composite Membrane. *Adv. Polym. Technol.*, 34, 21471. <https://doi.org/10.1002/adv.21471>
- ⁶⁵ Guillen, G. R., Pan, Y., Li, M., & Hoek, E. M. V. (2011). Preparation and Characterization of Membranes Formed by Nonsolvent Induced Phase Separation: A Review. *Industrial & Engineering Chemistry Research*, 50(7), 3798–3817. <https://doi.org/10.1021/ie101928r>
- ⁶⁶ Xia, L., Vemuri, B., Saptoka, S., Shrestha, N., Chilkoor, G., Kilduff, J., & Gadhamshetty, V. (2019). Chapter 1.8—Antifouling Membranes for Bioelectrochemistry Applications. In S. V. Mohan, S. Varjani, & A. Pandey (Eds.), *Microbial Electrochemical Technology* (pp. 195–224). Elsevier. <https://doi.org/10.1016/B978-0-444-64052-9.00008-X>
- ⁶⁷ Purkait, M. K., Sinha, M. K., Mondal, P., & Singh, R. (2018). Chapter 1—Introduction to Membranes. In M. K. Purkait, M. K. Sinha, P. Mondal, & R. Singh (Eds.), *Interface Science and Technology* (Vol. 25, pp. 1–37). Elsevier. <https://doi.org/10.1016/B978-0-12-813961-5.00001-2>
- ⁶⁸ Zhang, F., Fan, J., & Wang, S. (2020). Interfacial Polymerization: From Chemistry to Functional Materials. *Angewandte Chemie International Edition*, 59(49), 21840–21856. <https://doi.org/10.1002/anie.201916473>
- ⁶⁹ Jaydevsinh, M. G. and Rikarani R. C. (2019). *Introduction to Nanostructured and Nano-enhanced Polymeric Membranes: Preparation, Function, and Application for Water Purification—ScienceDirect*. (n.d.). Retrieved May 4, 2022, from <https://www.sciencedirect.com/science/article/pii/B9780128139264000380>
- ⁷⁰ Li, L.-Q., Zhan, Z.-M., Huang, B.-Q., Xue, S.-M., Ji, C.-H., Wang, R.-Z., Tang, Y.-J., & Xu, Z.-L. (2020). RO membrane fabricated via a facile modified heat-treating strategy for high-flux desalination. *Journal of Membrane Science*, 614, 118498. <https://doi.org/10.1016/j.memsci.2020.118498>
- ⁷¹ Li, J., Wei, M., & Wang, Y. (2017). Substrate matters: The influences of substrate layers on the performances of thin-film composite reverse osmosis membranes. *Chinese Journal of Chemical Engineering*, 25(11), 1676–1684. <https://doi.org/10.1016/j.cjche.2017.05.006>
- ⁷² W.-C. Chao, Y.-H. Huang, W.-S. Hung, Q. An, C.-C. Hu, K.-R. Lee, J.-Y. Lai. (2012). Effect of the surface property of poly(tetrafluoroethylene) support on the mechanism of polyamide active layer formation by interfacial polymerization. *Soft Matter*, 8 (34) , pp. 8998-9004

-
- ⁷³ Pacheco, F.A.; Pinnau, I.; Reinhard, M.; Leckie, J.O. (2010). Characterization of isolated polyamide thin films of ro and nf membranes using novel tem techniques. *J. Membr. Sci.*, 358, 51–59
- ⁷⁴ Poliseti, V., Vyas, B., Singh, P., & Ray, P. (2014). Limiting thickness of polyamide–polysulfone thin-film-composite nanofiltration membrane. *Desalination*, 346, 19–29. <https://doi.org/10.1016/j.desal.2014.05.007>
- ⁷⁵ Guan, K., Sasaki, Y., Jia, Y., Gonzales, R. R., Zhang, P., Lin, Y., Li, Z., & Matsuyama, H. (2021). Interfacial polymerization of thin film selective membrane layers: Effect of polyketone substrates. *Journal of Membrane Science*, 640, 119801. <https://doi.org/10.1016/j.memsci.2021.119801>
- ⁷⁶ Elimelech, M., Xiaohua Zhu, Childress, A. E., & Seungkwan Hong. (1997). Role of membrane surface morphology in colloidal fouling of cellulose acetate and composite aromatic polyamide reverse osmosis membranes. *Journal of Membrane Science*, 127(1), 101–109. [https://doi.org/10.1016/S0376-7388\(96\)00351-1](https://doi.org/10.1016/S0376-7388(96)00351-1)
- ⁷⁷ Breite, D., Went, M., Prager, A., Kühnert, M., & Schulze, A. (2020). Reduction of Biofouling of a Microfiltration Membrane Using Amide Functionalities—Hydrophilization without Changes in Morphology. *Polymers*, 12, 1379. <https://doi.org/10.3390/polym12061379>
- ⁷⁸ Arts, W. (2018). Chemically Stable Poly(epoxyether) Thin-Film Composite Membranes. [Masterthesis, KULeuven].
- ⁷⁹ Verbeke, R.; Arts, W.; Dom, E.; Dickmann, M.; Egger, W.; Koeckelberghs, G.; Szymczyk, A.; Vankelecom, I. F. J. (2019). Transferring Bulk Chemistry to Interfacial Synthesis of TFC-Membranes to Create Chemically Robust Poly(Epoxyether) Films. *J. Memb. Sci.*
- ⁸⁰ Bruice, P. Y. (2016). *Organic Chemistry*. Eighth edition. Upper Saddle River, NJ: Pearson Education.
- ⁸¹ Burwell, R. L. (1954). The Cleavage of Ethers. *Chemical Reviews*, 54(4), 615–685. <https://doi.org/10.1021/cr60170a003>
- ⁸² Ouellette, R. J., & Rawn, J. D. (2014). 16—Ethers and Epoxides. In R. J. Ouellette & J. D. Rawn (Eds.), *Organic Chemistry* (pp. 535–565). Elsevier. <https://doi.org/10.1016/B978-0-12-800780-8.00016-4>
- ⁸³ Pure Aqua. Inc. (n.d.). *Membrane Cleaning Systems CIP*. Retrieved November 20, 2022, from <https://pureaqua.com/membrane-cleaning-systems-cip/>
- ⁸⁴ Brunelle, D. J. (2001). Macrocyclic Oligomers of Engineering Thermoplastics. In K. H. J. Buschow, R. W. Cahn, M. C. Flemings, B. Ilshner, E. J. Kramer, S. Mahajan, & P. Veysière (Eds.), *Encyclopedia of Materials: Science and Technology* (pp. 4712–4720). Elsevier. <https://doi.org/10.1016/B0-08-043152-6/00822-6>

-
- ⁸⁵ Pilli, R., & ASSIS, F. (2018). Organic Synthesis: New Vistas in the Brazilian Landscape. *Anais Da Academia Brasileira de Ciências*, 90, 895–941. <https://doi.org/10.1590/0001-3765201820170564>
- ⁸⁶ Dever, J. P., George, K. F., Hoffman, W. C., & Soo, H. (2000). Ethylene Oxide. In *Kirk-Othmer Encyclopedia of Chemical Technology*. John Wiley & Sons, Ltd. <https://doi.org/10.1002/0471238961.0520082504052205.a01>
- ⁸⁷ Blanckenberg, A., & Malgas-Enus, R. (2019). Olefin epoxidation with metal-based nanocatalysts. *Catalysis Reviews*, 61(1), 27–83. <https://doi.org/10.1080/01614940.2018.1492503>
- ⁸⁸ Oldring, P.K.T. (2003). Coatings, Colorants, and Paints. *Encyclopedia of Physical Science and Technology (Third Edition)*.
- ⁸⁹ Varinder, K. A., Badine, D.M. and Vijayalakshmi, A.M. (2006). Asymmetric synthesis of epoxides and aziridines from aldehydes and imines. In A. Yudin, A. K. (Red.) . *Aziridines and Epoxides in Organic Synthesis* (pp1-37). Toronto, Canada. John Wiley & Sons.
- ⁹⁰ Crandall, J. K., & Apparau, M. (2005). Base-Promoted Isomerizations of Epoxides. In *Organic Reactions* (pp. 345–443). John Wiley & Sons, Ltd. <https://doi.org/10.1002/0471264180.or029.03>
- ⁹¹ Gorzynski Smith, J. (1984). Synthetically Useful Reactions of Epoxides. *Synthesis*, 1984(08), 629–656. <https://doi.org/10.1055/s-1984-30921>
- ⁹² Cowie, J. M. G. & Arrighi, V. (2007). *Polymers: Chemistry and Physics of Modern Materials*. CRC Press.
- ⁹³ Brocas, A.-L., Mantzaridis, C., Tunc, D., & Carlotti, S. (2013). Polyether synthesis: From activated or metal-free anionic ring-opening polymerization of epoxides to functionalization. *Progress in Polymer Science*, 38(6), 845–873. <https://doi.org/10.1016/j.progpolymsci.2012.09.007>
- ⁹⁴ Hadjichristidis, N., & Hirao, A. (Eds.). (2015). *Anionic Polymerization: Principles, Practice, Strength, Consequences and Applications*. Springer Japan. <https://doi.org/10.1007/978-4-431-54186-8>
- ⁹⁵ Parker, R. E., & Isaacs, N. S. (1959). Mechanisms Of Epoxide Reactions. *Chemical Reviews*, 59(4), 737–799. <https://doi.org/10.1021/cr50028a006>
- ⁹⁶ Bonollo, S., Lanari, D., & Vaccaro, L. (2011). Ring-Opening of Epoxides in Water. *European Journal of Organic Chemistry*, 2011(14), 2587–2598. <https://doi.org/10.1002/ejoc.201001693>
- ⁹⁷ Ravve, A. (2012). Principles of polymer chemistry, third edition. Principles of Polymer Chemistry, Third Edition. doi:10.1007/978-1-4614-2212-9.
- ⁹⁸ Bastin, M., Raymenants, J., Thijs, M., Vananroye, A., Koeckelberghs, G., & Vankelecom, I. F. J. (2021). Epoxy-based solvent-tolerant nanofiltration membranes prepared via non-

solvent induced phase inversion as novel class of stable membranes. *Journal of Membrane Science*, 626, 119206. <https://doi.org/10.1016/j.memsci.2021.119206>

⁹⁹ *SN2 Mechanism—An overview | ScienceDirect Topics*. (n.d.). Retrieved April 26, 2022, from <https://www.sciencedirect.com/topics/chemistry/sn2-mechanism>

¹⁰⁰ Rozenberg, B. A. (1986). Kinetics, thermodynamics and mechanism of reactions of epoxy oligomers with amines. In K. Dušek (Ed.), *Epoxy Resins and Composites II* (Vol. 75, pp. 113–165). Springer-Verlag. <https://doi.org/10.1007/BFb0017916>

¹⁰¹ McCoy, J. D., Ancipink, W. B., Clarkson, C. M., Kropka, J. M., Celina, M. C., Giron, N. H., Hailesilassie, L., & Fredj, N. (2016). Cure mechanisms of diglycidyl ether of bisphenol A (DGEBA) epoxy with diethanolamine. *Polymer*, 105, 243–254. <https://doi.org/10.1016/j.polymer.2016.10.028>

¹⁰² Riccardi, C. C., & Williams, R. J. J. (1986). A kinetic scheme for an amine-epoxy reaction with simultaneous etherification. *Journal of Applied Polymer Science*, 32(2), 3445–3456. <https://doi.org/10.1002/app.1986.070320208>

¹⁰³ Ligon, S., Schwentenwein, M., Gorsche, C., Stampfl, J., & Liska, R. (2015). Toughening of photo-curable polymer networks: A review. *Polym. Chem.*, 7. <https://doi.org/10.1039/C5PY01631B>

¹⁰⁴ Laird, R. M. (1969). *The Mechanism of Epoxide Reactions. Part XI.I Reactions of Ethylene Oxide with Alcohols in the Presence of Sodium Alkoxides and of Tertiary Amines*. *Journal of the Chemical Society B: Physical Organic*, 0, 1062–1068. <https://doi.org/10.1039/J29690001062>

¹⁰⁵ Kushch, P. P., Komarov, B.A. and Rozenberg B.A. (1978). The role of proton donors in initiation of polymerization of epoxide compounds by tertiary amines. *Polymer science U.S.S.R.* 21. 1867-1875.

¹⁰⁶ Sorokin, M.F., Shode, L.G. and Shteinpress, A.B., (1969). Polymerization of phenyl glycidyl ether induced by tertiary amines in the absence of proton donating compounds. D. I. Mendeleyev Institute of Chemical Technology, Moscow.

¹⁰⁷ Sudo, A. (2013). Anionic Ring-Opening Polymerization. In S. Kobayashi & K. Müllen (Eds.), *Encyclopedia of Polymeric Nanomaterials* (pp. 1–11). Springer Berlin Heidelberg. https://doi.org/10.1007/978-3-642-36199-9_172-1

¹⁰⁸ Sorokin, M.F., Shode, L.G. and Shteinpress, A.B., (1970). Polymerization of phenyl glycidyl ether in the presence of tertiary amines and alcohols. D. I. Mendeleyev Institute of Chemical Technology, Moscow.

¹⁰⁹ Rodriguez, C. G., Ferrier, R. C., Helenic, A., & Lynd, N. A. (2017). Ring-Opening Polymerization of Epoxides: Facile Pathway to Functional Polyethers via a Versatile Organoaluminum Initiator. *Macromolecules*, 50(8), 3121–3130. <https://doi.org/10.1021/acs.macromol.7b00196>

-
- ¹¹⁰ Ricciardi, F., Joullié, M. M., Romanchick, W. A., & Griscavage, A. A. (1982). Mechanism of imidazole catalysis in the curing of epoxy resins. *Journal of Polymer Science: Polymer Letters Edition*, 20(2), 127–133. <https://doi.org/10.1002/pol.1982.130200209>
- ¹¹¹ Barton, J. M., & Shepherd, P. M. (1975). The Curing Reaction of an Epoxide Resin with 2-Ethyl-4-methylimidazole, a Calorimetric Study of the Kinetics of Formation of Epoxide-Imidazole Adducts. *Die Makromolekulare Chemie*, 176(4), 919–930. <https://doi.org/10.1002/macp.1975.021760408>
- ¹¹² Ellis, B. (1993). *Chemistry and Technology of Epoxy Resins*. Springer Netherlands. <https://doi.org/10.1007/978-94-011-2932-9>
- ¹¹³ Berger, J., & Lohse, F. (1985). Polymerization of p-cresyl glycidyl ether catalyzed by imidazoles I. The influence of the imidazole concentration, the reaction temperature, and the presence of isopropanol on the polymerization. *Journal of Applied Polymer Science*, 30(2), 531–546. <https://doi.org/10.1002/app.1985.070300207>
- ¹¹⁴ López-Barajas, F., Ramos-DeValle, L. F., Sánchez-Valdes, S., Ramírez-Vargas, E., Martínez-Colunga, G., Espinoza-Martínez, A. B., Flores-Gallardo, S., Mendez-Nonell, J., Morales-Cepeda, A. B., Lozano-Ramírez, T., & Beltrán-Ramírez, F. I. (2019). Curing kinetics of diglycidyl ether of Bisphenol-A epoxy system using a tertiary amine, through the study of its rheometric characteristics. *Polymer Testing*, 73, 346–351. <https://doi.org/10.1016/j.polymertesting.2018.11.043>
- ¹¹⁵ Lenntech (2013). *Chemical Pretreatment For RO and NF*. 111, 16.
- ¹¹⁶ Tolba, A. M., & Mohamed, R. A. (n.d.). *Performance and Characteristics of Reverse Osmosis Membranes*. Fourth International Water Technology Conference IWTC 99, Alexandria, Egypt.
- ¹¹⁷ Chevali, V., & Kandare, E. (2016). 13—Rigid biofoam composites as eco-efficient construction materials. In F. Pacheco-Torgal, V. Ivanov, N. Karak, & H. Jonkers (Eds.), *Biopolymers and Biotech Admixtures for Eco-Efficient Construction Materials* (pp. 275–304). Woodhead Publishing. <https://doi.org/10.1016/B978-0-08-100214-8.00013-0>
- ¹¹⁸ Ward, R. S., & Jones, R. L. (2011). 1.125—Polyurethanes and Silicone Polyurethane Copolymers. In P. Ducheyne (Ed.), *Comprehensive Biomaterials* (pp. 431–477). Elsevier. <https://doi.org/10.1016/B978-0-08-055294-1.00272-5>
- ¹¹⁹ Verbeke, R., Davenport, D. M., Stassin, T., Eyley, S., Dickmann, M., Cruz, A. J., Dara, P., Ritt, C. L., Bogaerts, C., Egger, W., Ameloot, R., Meersschaut, J., Thielemans, W., Koeckelberghs, G., Elimelech, M., & Vankelecom, I. F. J. (2021). Chlorine-Resistant Epoxide-Based Membranes for Sustainable Water Desalination. *Environmental Science & Technology Letters*, 8(9), 818–824. <https://doi.org/10.1021/acs.estlett.1c00515>
- ¹²⁰ James J. L., Dale W. S., (2011). *Chemistry, Formulation, and Properties of Adhesives. Adhesives Technology for Electronic Applications (Second Edition)*, 2011

¹²¹ Hexion Inc, (2001). Technical Data Sheet

¹²² Merck (n.d.). *Poly(ethylene glycol) diglycidyl ether*. Retrieved October 3, 2022, from <http://www.sigmaaldrich.com/>

¹²³ Mengyuan, H., Changlin, W., Tong, X., Ping, D., Xiaojun, Y., Huaying, S., Congying, L., Peng, G., & Zhufeng, C. (2022). Modification and preparation of four natural hydrogels and their application in biopharmaceutical delivery. *Polymer Bulletin*. <https://doi.org/10.1007/s00289-022-04412-x>

¹²⁴ Biosynth (n.d.). *Poly(ethylene glycol) diglycidyl ether, Mn~500*. Retrieved October 19, 2022, from <https://www.biosynth.com/p/FP180370/26403-72-5-polyethylene-glycol-diglycidyl-ethe>

¹²⁵ Lenaerts, N. (2022). Influence of support layer on chemically robust epoxide-based thin-film composite membranes. [Masterthesis, KULeuven]

¹²⁶ Nikolaeva, D., Azcune, I., Sheridan, E., Sandru, M., Genua, A., Tanczyk, M., Jaschik, M., Warmuzinski, K., Jansen, J. C., & Vankelecom, I. F. J. (2017). Poly(vinylbenzyl chloride)-based poly(ionic liquids) as membranes for CO₂ capture from flue gas. *Journal of Materials Chemistry A*, 5(37), 19808–19818. <https://doi.org/10.1039/C7TA05171A>

¹²⁷ Vanbruggenhout, S. (2021). Interfacial poly(epoxyether) chemistry as a novel platform for CO₂-selective thin-film composite membranes. [Masterthesis, KULeuven].

¹²⁸ Bull, C. (2022). Optimization of poly(β -alkanolamine) solvent tolerant nanofiltration membranes. [Masterthesis, KULeuven].

¹²⁹ Porometer. (n.d.). *Glossary*. Retrieved December 21, 2022, from <https://www.porometer.com/knowledge-center/glossary>

¹³⁰ Park, H. B., Kamcev, J., Robeson, L. M., Elimelech, M. & Freeman, B. D. (2017). Maximizing the right stuff: The trade-off between membrane permeability and selectivity. *Science* 356.

¹³¹ Mokobi, F. (2022). *Scanning Electron Microscope (SEM)- Definition, Principle, Parts, Images*. Microbe Notes. <https://microbenotes.com/scanning-electron-microscope-sem/>

¹³² U.S. Department of the interior. (2000). *Characterization of the Hydrophobicity of Polymeric Reverse Osmosis and Nanofiltration Membranes: Implications to Membrane Fouling*. Desalination and Water Purification Research and Development Program Report No. 57. <https://www.usbr.gov/research/dwpr/reportpdfs/report57.pdf>

¹³³ Nanoscience Instruments. (n.d.). Advancing and Receding Contact Angles. Retrieved December 13, 2022, from <https://www.nanoscience.com/techniques/tensiometry/advancing-and-receding-contact-angles/>

-
- ¹³⁴ ThermoFisher scientific. (n.d.). *X-Ray Photoelectron Spectroscopy*. Retrieved December 13, 2022, from <https://www.thermofisher.com/uk/en/home/materials-science/xps-technology.html>
- ¹³⁵ Van den Mooter, P.-R., Dedvukaj, L., & Vankelecom, I. F. J. (2021). Use of Ionic Liquids and Co-Solvents for Synthesis of Thin-Film Composite Membranes. *Membranes*, 11(4), 4. <https://doi.org/10.3390/membranes11040297>
- ¹³⁶ Freger, V. (2005). Kinetics of Film Formation by Interfacial Polycondensation. *Langmuir*, 21(5), 1884–1894. <https://doi.org/10.1021/la048085v>
- ¹³⁷ Falca, G., Musteata, V. E., Chisca, S., Hedhili, M. N., Ong, C., & Nunes, S. P. (2021). Naturally Extracted Hydrophobic Solvent and Self-Assembly in Interfacial Polymerization. *ACS Applied Materials & Interfaces*, 13(37), 44824–44832. <https://doi.org/10.1021/acsami.1c07584>
- ¹³⁸ Li, K., Zhu, J., Liu, D., Zhang, Y., & Van der Bruggen, B. (2021). Controllable and Rapid Synthesis of Conjugated Microporous Polymer Membranes via Interfacial Polymerization for Ultrafast Molecular Separation. *Chemistry of Materials*, 33(17), 7047–7056. <https://doi.org/10.1021/acs.chemmater.1c02143>
- ¹³⁹ Lonsdale, H. K., Riley, R. L., Lyons, C. R., & Carosella, D. P. (1971). Transport in Composite Reverse Osmosis Membranes. In M. Bier (Ed.), *Membrane Processes in Industry and Biomedicine: Proceedings of a Symposium held at the 160th National Meeting of the American Chemical Society, under the sponsorship of the Division of Industrial and Engineering Chemistry, Chicago, Illinois, September 16 and 17, 1970* (pp. 101–122). Springer US. https://doi.org/10.1007/978-1-4684-1911-5_6
- ¹⁴⁰ Singh, N., Chen, Z., Tomer, N., Wickramasinghe, S. R., Soice, N., & Husson, S. M. (2008). Modification of regenerated cellulose ultrafiltration membranes by surface-initiated atom transfer radical polymerization. *Journal of Membrane Science*, 311(1), 225–234. <https://doi.org/10.1016/j.memsci.2007.12.036>
- ¹⁴¹ Briggs, L. H., Colebrook, L. D., Fales, H. M., & Wildman, W. C. (1957). Infrared Absorption Spectra of Methyleneoxy and Aryl Ether Groups. *Analytical Chemistry*, 29(6), 904–911. <https://doi.org/10.1021/ac60126a014>
- ¹⁴² Colthup, N. B., Daly, L. H., & Wiberley, S. E. (1990). *Introduction to infrared and Raman spectroscopy* (3rd ed). Academic Press.
- ¹⁴³ Seynaeve, M. (2019). Epoxide chemistry for thin-film composite membranes. [Masterthesis, KULeuven].
- ¹⁴⁴ Hansen, C. M. (2007). *Hansen solubility parameters: A user's handbook* (2nd ed). CRC Press.

-
- ¹⁴⁵ Alqarni, M. H., Haq, N., Alam, P., Abdel-Kader, M. S., Foudah, A. I., & Shakeel, F. (2021). Solubility data, Hansen solubility parameters and thermodynamic behavior of pterostilbene in some pure solvents and different (PEG-400 + water) cosolvent compositions. *Journal of Molecular Liquids*, 331, 115700. <https://doi.org/10.1016/j.molliq.2021.115700>
- ¹⁴⁶ Liang, Y., Zhu, Y., Liu, C., Lee, K.-R., Hung, W.-S., Wang, Z., Li, Y., Elimelech, M., Jin, J., & Lin, S. (2020). Polyamide nanofiltration membrane with highly uniform sub-nanometre pores for sub-1 Å precision separation. *Nature Communications*, 11(1), 1. <https://doi.org/10.1038/s41467-020-15771-2>
- ¹⁴⁷ Syamani, F. (2020). Cellulose-based membrane for adsorption of dye in batik industry wastewater. *International Journal of Hydrology*, 4, 281–283. <https://doi.org/10.15406/ijh.2020.04.00255>
- ¹⁴⁸ Bogaerts, C. (2020). Epoxide-based polymers as a novel platform for chemically robust membranes. [masterthesis, KULeuven].
- ¹⁴⁹ Kishore Chand, A. A., Bajer, B., Schneider, E. S., Mantel, T., Ernst, M., Filiz, V., & Glass, S. (2022). Modification of Polyacrylonitrile Ultrafiltration Membranes to Enhance the Adsorption of Cations and Anions. *Membranes*, 12(6), 6. <https://doi.org/10.3390/membranes12060580>
- ¹⁵⁰ Domingo, L. R., & Pérez, P. (2011). The nucleophilicity N index in organic chemistry. *Organic & Biomolecular Chemistry*, 9(20), 7168. <https://doi.org/10.1039/c1ob05856h>
- ¹⁵¹ Santiso, E. E., George, A. M., Sliwiska-bartkowiak, M., Nardelli, M. B., & Gubbins, K. E. (2005). Effect of Confinement on Chemical Reactions. *Adsorption*, 11(S1), 349–354. <https://doi.org/10.1007/s10450-005-5949-9>
- ¹⁵² Machida, H., Yamada, H., Fujioka, Y., & Yamamoto, S. (2015). CO₂ Solubility Measurements and Modeling for Tertiary Diamines. *Journal of Chemical & Engineering Data*, 60(3), 814–820. <https://doi.org/10.1021/je500927h>
- ¹⁵³ PubChem. (n.d.). *PubChem*. Retrieved November 11, 2022, from <https://pubchem.ncbi.nlm.nih.gov/>
- ¹⁵⁴ *ChemicalBook—Chemical Search Engine*. (n.d.). Retrieved November 11, 2022, from https://www.chemicalbook.com/ProductIndex_EN.aspx
- ¹⁵⁵ *ChemSpider | Search and share chemistry*. (n.d.). Retrieved November 11, 2022, from <http://www.chemspider.com/>
- ¹⁵⁶ *Guidechem Chemical Network—China Chemical Manufacturers, suppliers, B2B Marketplace*. (n.d.). Retrieved November 11, 2022, from <https://www.guidechem.com/>

-
- ¹⁵⁷ Ham, Y., Kim, S., Shin, Y., Lee, D., Yang, M., Min, J., & Shin, J. (2010). A comparison of some imidazoles in the curing of epoxy resin. *Journal of Industrial and Engineering Chemistry - J IND ENG CHEM*, 16, 556–559. <https://doi.org/10.1016/j.jiec.2010.03.022>
- ¹⁵⁸ Gao, L., Wang, J., Shi, L., Huang, L., Wang, Y., Fan, X., Yu, T., Zhu, M., & Zou, Z. (2007). Hybrid mesoporous SC/SBA as a chemosensor for recognizing Cu²⁺. In D. Zhao, S. Qiu, Y. Tang, & C. Yu (Eds.), *Studies in Surface Science and Catalysis* (Vol. 165, pp. 861–864). Elsevier. [https://doi.org/10.1016/S0167-2991\(07\)80454-X](https://doi.org/10.1016/S0167-2991(07)80454-X)
- ¹⁵⁹ Merck KGaA. (n.d.). *IR Spectrum Table*. Retrieved December 23, 2022, from <https://www.sigmaaldrich.com/BE/en/technical-documents/technical-article/analytical-chemistry/photometry-and-reflectometry/ir-spectrum-table>
- ¹⁶⁰ Ramasamy, R. (2015). Vibrational spectroscopic studies of imidazole. *Armenian Journal of Physics*, 8(1), 51-55. <https://arar.sci.am/dlibra/publication/26144/edition/23397>
- ¹⁶¹ Ghosh, A. K., & Hoek, E. M. V. (2009). Impacts of support membrane structure and chemistry on polyamide–polysulfone interfacial composite membranes. *Journal of Membrane Science*, 336(1), 140–148. <https://doi.org/10.1016/j.memsci.2009.03.024>
- ¹⁶² Liu, F., Wang, L., Li, D., Liu, Q., & Deng, B. (2019). A review: The effect of the microporous support during interfacial polymerization on the morphology and performances of a thin film composite membrane for liquid purification. *RSC Advances*, 9, 35417–35428. <https://doi.org/10.1039/C9RA07114H>
- ¹⁶³ Liu, F., Wang, L., Li, D., Liu, Q., & Deng, B. (2019). A review: The effect of the microporous support during interfacial polymerization on the morphology and performances of a thin film composite membrane for liquid purification. *RSC Advances*, 9, 35417–35428. <https://doi.org/10.1039/C9RA07114H>
- ¹⁶⁴ Bugaenko, D. I., Karchava, A. V., & Yurovskaya, M. A. (2020). The versatility of DABCO: Synthetic applications of its basic, nucleophilic, and catalytic properties. *Chemistry of Heterocyclic Compounds*, 56(3), 265–278. <https://doi.org/10.1007/s10593-020-02655-y>
- ¹⁶⁵ Piradashvili, K., Alexandrino, E. M., Wurm, F. R., & Landfester, K. (2016). Reactions and Polymerizations at the Liquid–Liquid Interface. *Chemical Reviews*, 116(4), 2141–2169. <https://doi.org/10.1021/acs.chemrev.5b00567>
- ¹⁶⁶ Li, S., Shi, Y., Li, P., & Xu, J. (2019). Nucleophilic Organic Base DABCO-Mediated Chemospecific Meinwald Rearrangement of Terminal Epoxides into Methyl Ketones. *The Journal of Organic Chemistry*, 84. <https://doi.org/10.1021/acs.joc.8b03171>

-
- ¹⁶⁷ Oizerovich-Honig, R., Raim, V., & Srebnik, S. (2010). Simulation of Thin Film Membranes Formed by Interfacial Polymerization. *Langmuir*, 26(1), 299–306. <https://doi.org/10.1021/la9024684>
- ¹⁶⁸ PubChem. (n.d.). *1,4-Diazabicyclo[2.2.2]octane*. Retrieved December 26, 2022, from <https://pubchem.ncbi.nlm.nih.gov/compound/9237>
- ¹⁶⁹ Verbeke, R., Seynaeve, M., Bastin, M., Davenport, D. M., Eyley, S., Thielemans, W., Koeckelberghs, G., Elimelech, M., & Vankelecom, I. F. J. (2020). The significant role of support layer solvent annealing in interfacial polymerization: The case of epoxide-based membranes. *Journal of Membrane Science*, 612, 118438. <https://doi.org/10.1016/j.memsci.2020.118438>
- ¹⁷⁰ Van Havere, D. (2022). Interfacial synthesis of high-EO content TFC membranes for CO₂ separations. [Unpublished manuscript].
- ¹⁷¹ Tandon, R., Nigst, T. A. & Zipse, H. (2013). Inductive Effects through Alkyl Groups - How Long is Long Enough? *European Journal of Organic Chemistry* 2013.
- ¹⁷² González, M. G., Cabanelas, J. C., & Baselga, J. (2012). Applications of FTIR on Epoxy Resins—Identification, Monitoring the Curing Process, Phase Separation and Water Uptake. In *Infrared Spectroscopy—Materials Science, Engineering and Technology*. IntechOpen. <https://doi.org/10.5772/36323>
- ¹⁷³ Nandiyanto, A. B. D., Oktiani, R., & Ragadhita, R. (2019). How to Read and Interpret FTIR Spectroscopy of Organic Material. *Indonesian Journal of Science and Technology*, 4(1), 97. <https://doi.org/10.17509/ijost.v4i1.15806>
- ¹⁷⁴ Ensing, B., Tiwari, A., Tros, M., Hunger, J., Domingos, S. R., Pérez, C., Smits, G., Bonn, M., Bonn, D., & Woutersen, S. (2019). On the origin of the extremely different solubilities of polyethers in water. *Nature Communications*, 10(1), 1. <https://doi.org/10.1038/s41467-019-10783-z>
- ¹⁷⁵ Anastassopoulou, J. D. (1991). Mass and FT-IR Spectra of Quaternary Ammonium Surfactants. In E. Rizzarelli & T. Theophanides (Eds.), *Chemistry and Properties of Biomolecular Systems* (Vol. 8, pp. 1–9). Springer Netherlands. https://doi.org/10.1007/978-94-011-3620-4_1
- ¹⁷⁶ Selyanchyn, R., Ariyoshi, M., & Fujikawa, S. (2018). Thickness Effect on CO₂/N₂ Separation in Double Layer Pebax-1657®/PDMS Membranes. *Membranes*, 8, 121. <https://doi.org/10.3390/membranes8040121>
- ¹⁷⁷ Han, Y., & Ho, W. S. W. (2021). Polymeric membranes for CO₂ separation and capture. *Journal of Membrane Science*, 628, 119244. <https://doi.org/10.1016/j.memsci.2021.119244>

¹⁷⁸ Edwards, J. O., & Pearson, R. G. (1962). The Factors Determining Nucleophilic Reactivities. *Journal of the American Chemical Society*, *84*(1), 16–24.
<https://doi.org/10.1021/ja00860a005>

¹⁷⁹ Verbeke, R. (2022). 'On water' catalysis of phenyl glycidyl ether with tertiary amines. [unpublished manuscript].

¹⁸⁰ Kuznicki, T., Masliyah, J. H., & Bhattacharjee, S. (2009). Aggregation and Partitioning of Model Asphaltenes at Toluene–Water Interfaces: Molecular Dynamics Simulations. *Energy & Fuels*, *23*(10), 5027–5035. <https://doi.org/10.1021/ef9004576>

APPENDIX

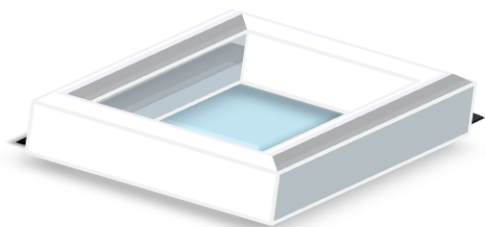
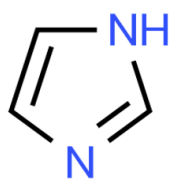
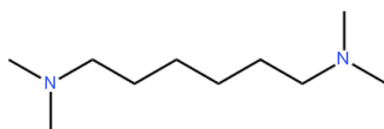


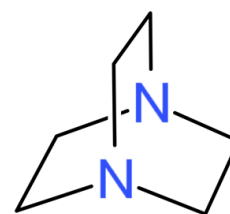
Figure 50: Design of the IIP set-up used for membrane synthesis¹²⁵.



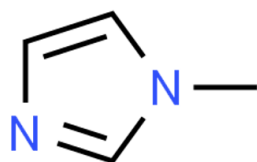
Imidazole (IM)



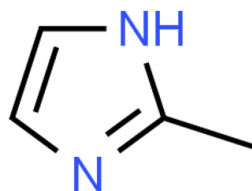
N,N,N',N'-Tetramethyl-1,6-hexanediamine (TMHD)



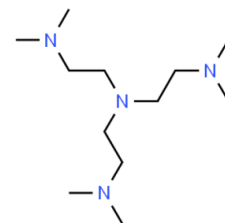
1,4-diazabicyclo[2.2.2]octane (DABCO)



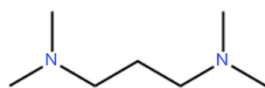
1-methylimidazole (1-MIM)



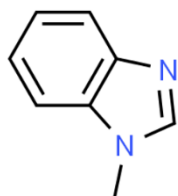
2-methylimidazole (2-MIM)



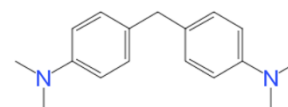
Tris[2-(dimethylamino)ethyl]amine (Me6Tren)



N,N,N',N'-Tetramethyl-1,6-propanediamine (TPMD)



1-methylbenzimidazole (MBI)



4,4'-methylenebis(N,N-dimethylaniline)

Figure 51: Overview of the chemical structures of all the used initiators.

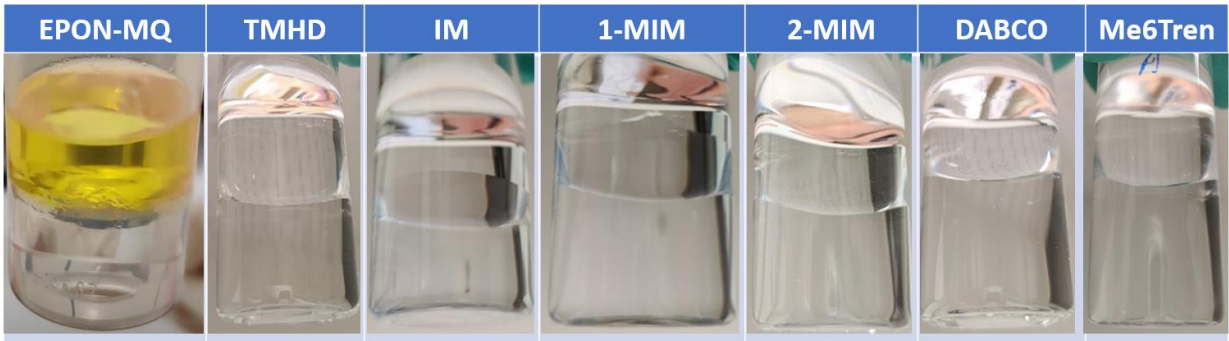


Figure 52: Reference vial tests for initiators used to synthesize RO membranes. Most left: EPON 5 w/v% EPON in toluene on top of pure MQ water. Other pictures: pure toluene on top of 1N aqueous initiator solution.

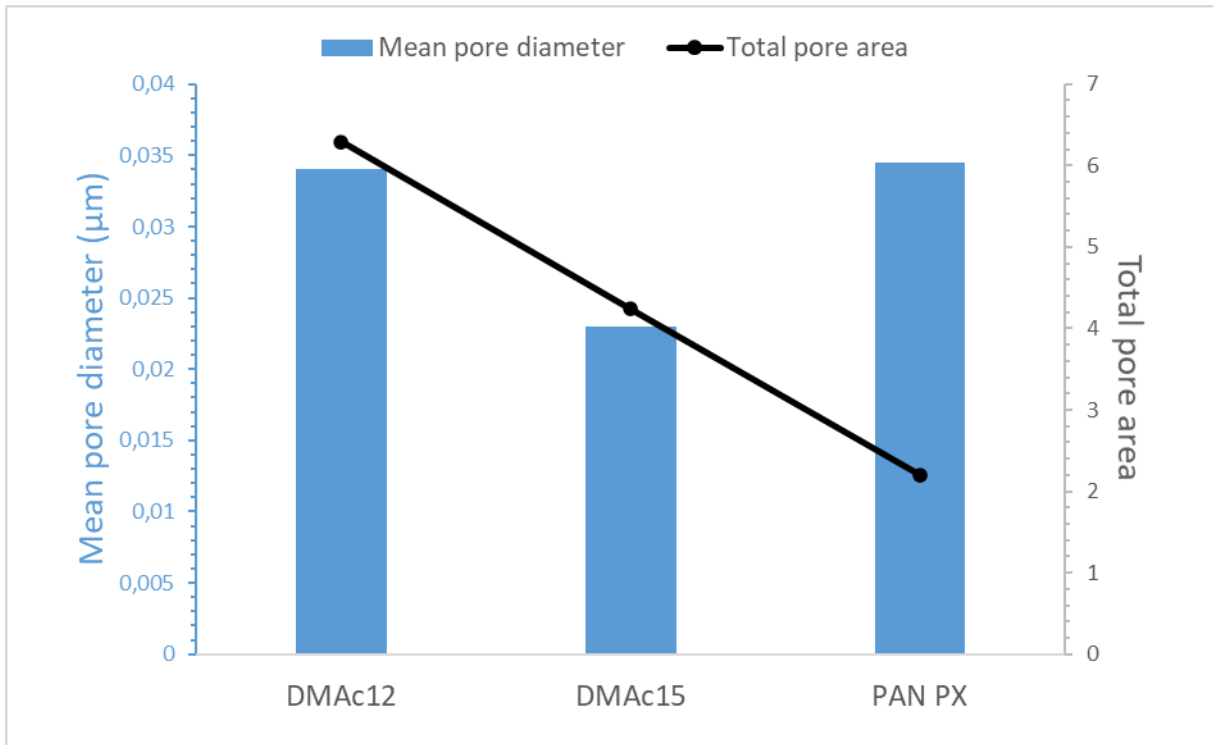


Figure 53: Mean pore diameter and total pore area of three support layers: DMAc12, 15 PAN PX. These values are obtained through gas liquid porometry.

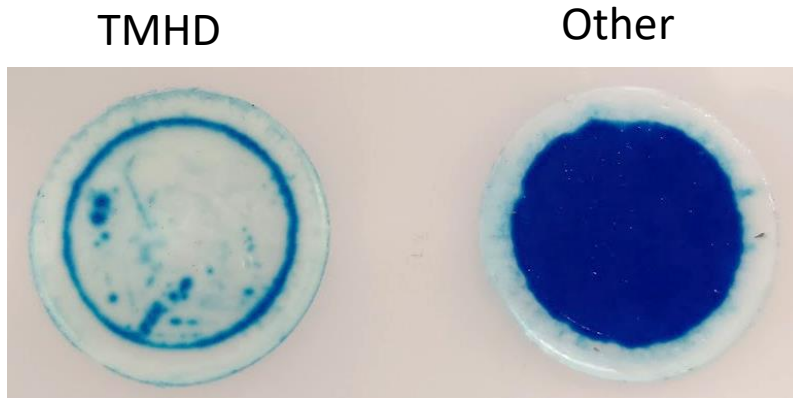


Figure 54: Membrane coupons after MB filtration. Left: TMHD-initiated TFC membranes, right: all other membranes.

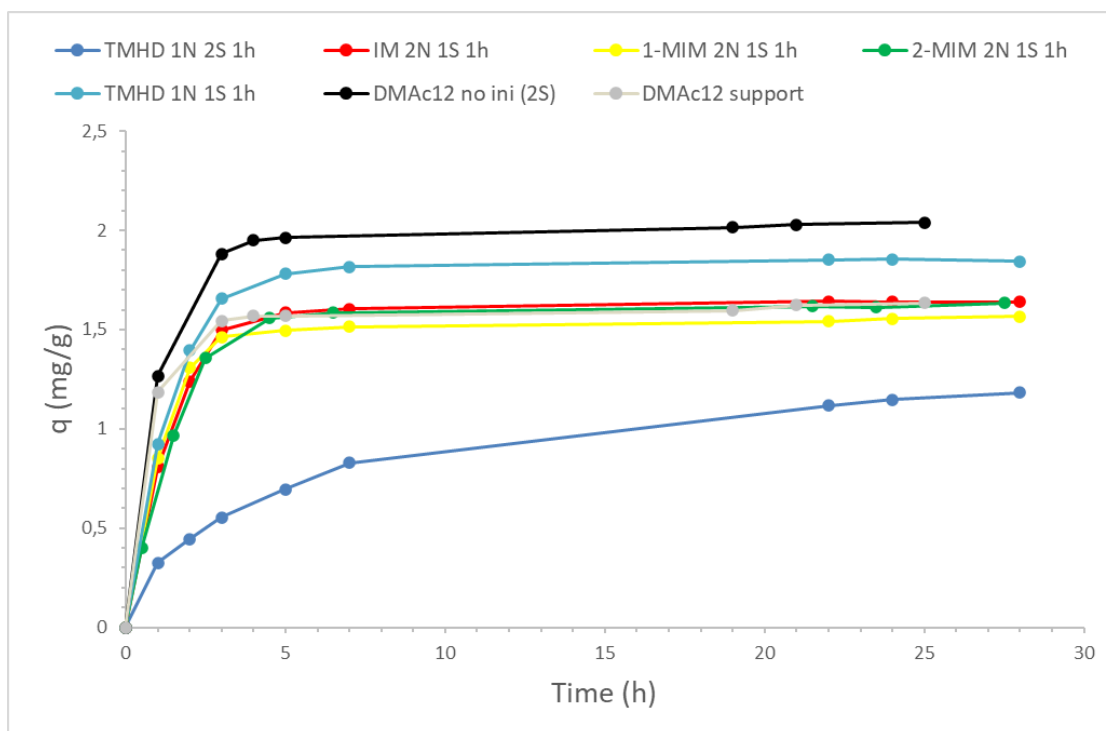


Figure 55: Adsorption capacity of multiple TFC membranes and DMAc12. Y axis: adsorption capacity in mg dye/g membrane. X axis: time.

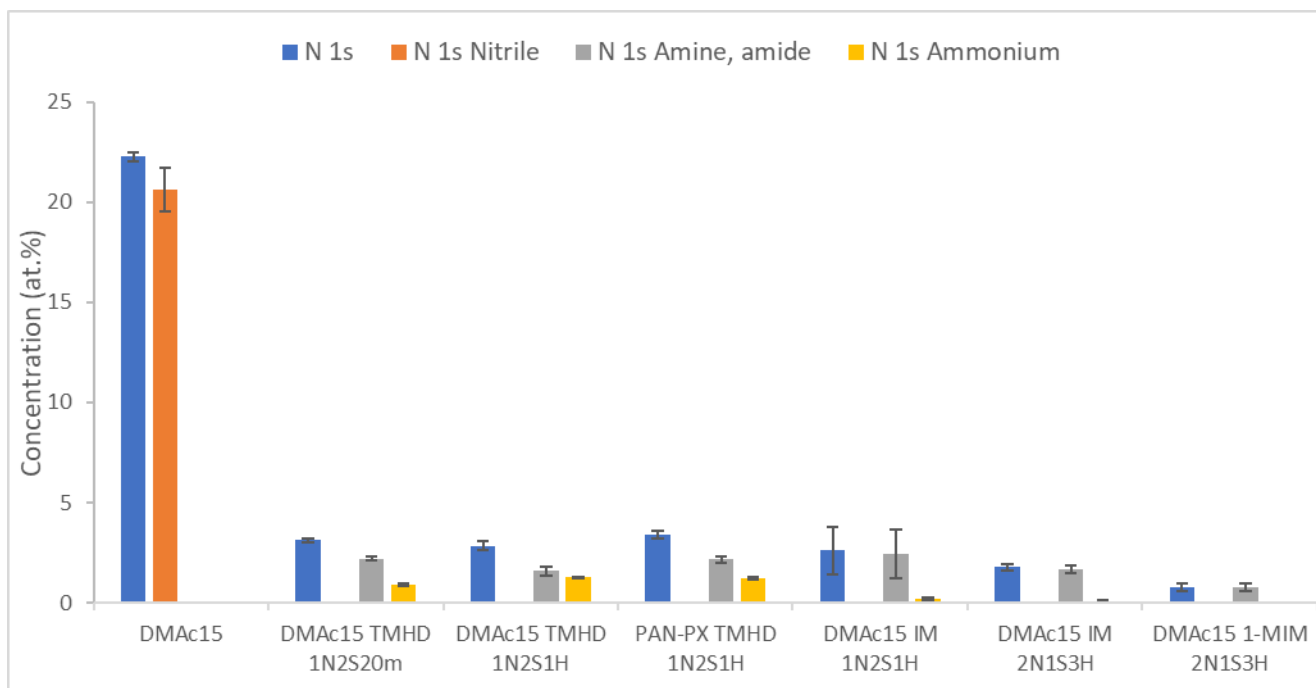


Figure 56: The occurrence of N in multiple TFC membranes and DMac15. These values are obtained through XPS-analysis. Y axis: atom percentage of a certain bond. No nitrile signals were detected for the TFC membranes.

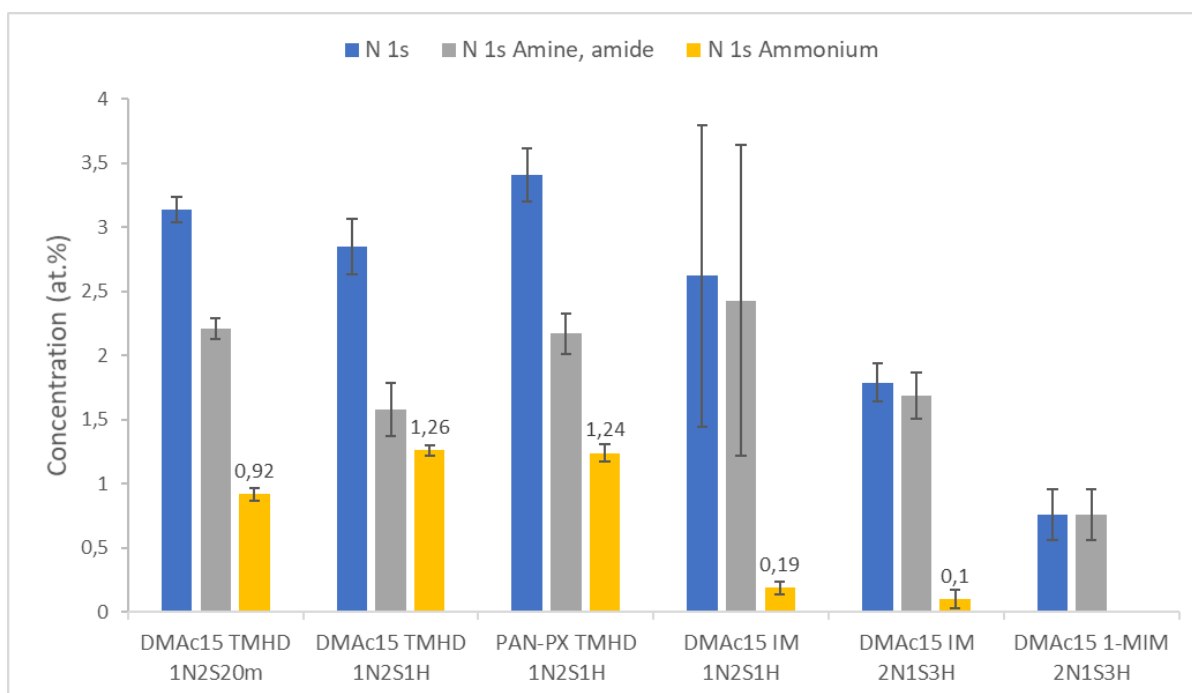


Figure 57: Zoomed-in view on lower concentrations for the occurrence of N in multiple TFC membranes and DMac15. Y axis: atom percentage of a certain bond.

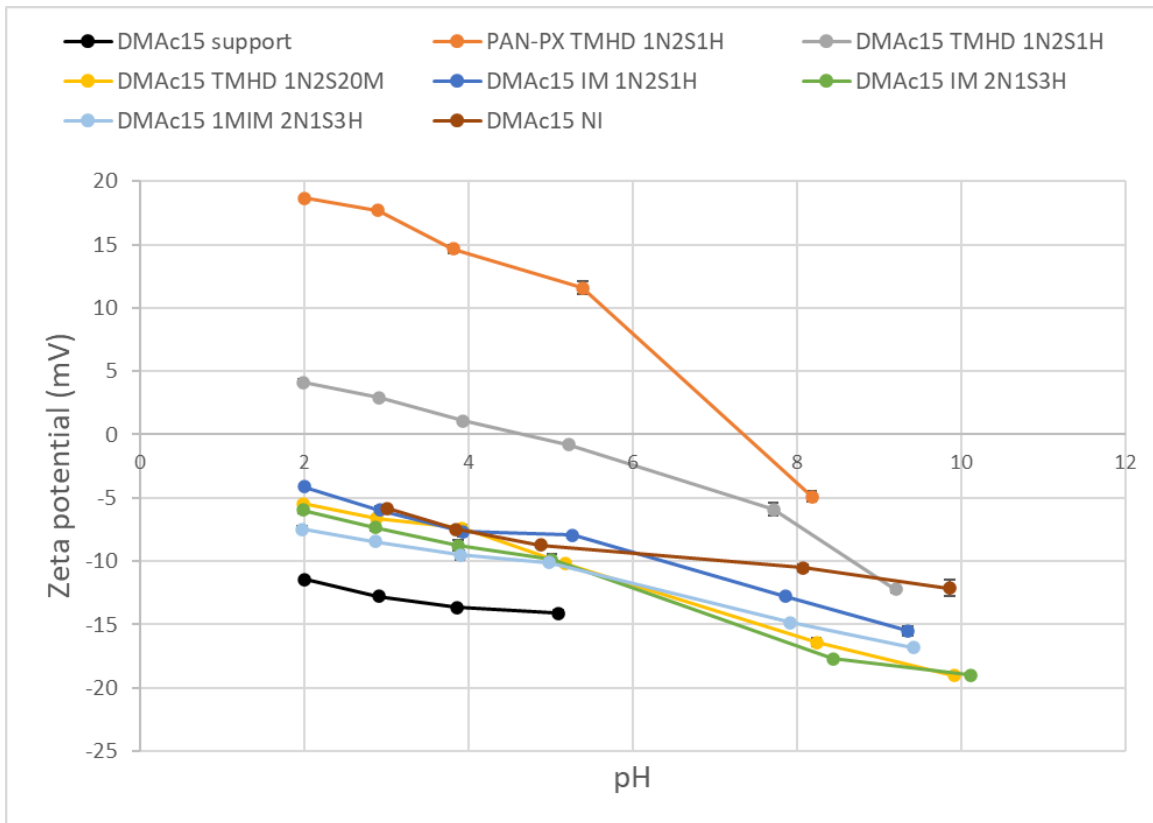


Figure 58: Zeta potential curve of multiple TFC and support membranes. Y-axis: Zeta potential (mV), X-axis: pH.

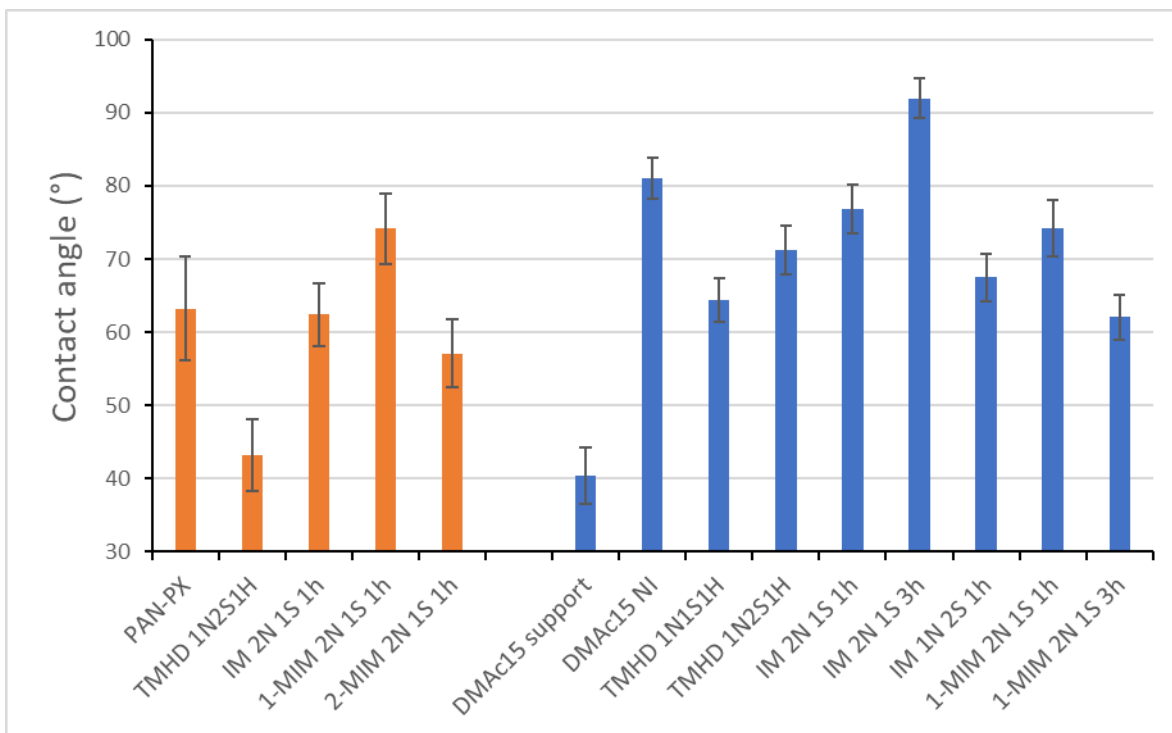


Figure 59: Static contact angle measurements for multiple TFC and support membranes. Red bars depict membranes with a PAN-PX support, blue bars depict membranes with a DMac15 support.

Table 4: Partial solubility parameter (PSP) of water with EPON and PAN, and the calculated R_a . Smaller R_a values indicate stronger interactions¹⁴⁵. PSP of PAN and EPON is calculated using the Hoftyzer and Van Krevelen (1976) method¹⁴⁴.

	δ_d	δ_p	δ_h	R_a
Water	15.5	16.0	42.3	-
EPON	23.5	1.6	8.1	40.4
PAN	19.9	14.1	8.0	35.5

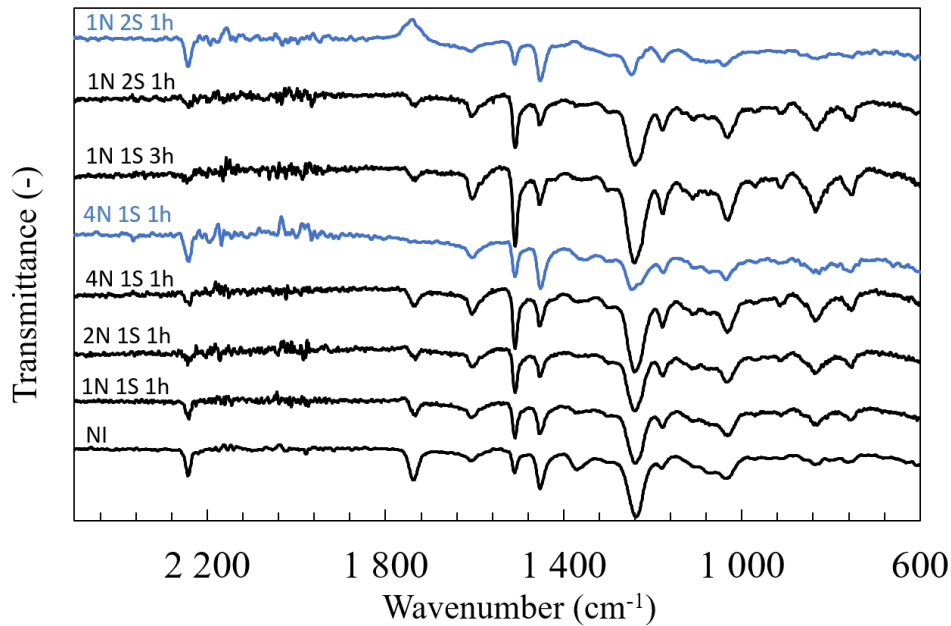


Figure 60: ATR-FTIR spectra of 2-MIM membranes on top of a PAN PX support (black lines), and DMAc12 support (blue lines). Spectra on DMAc12 were smoothed by taking the average transmittance of the surrounding six wavenumbers.

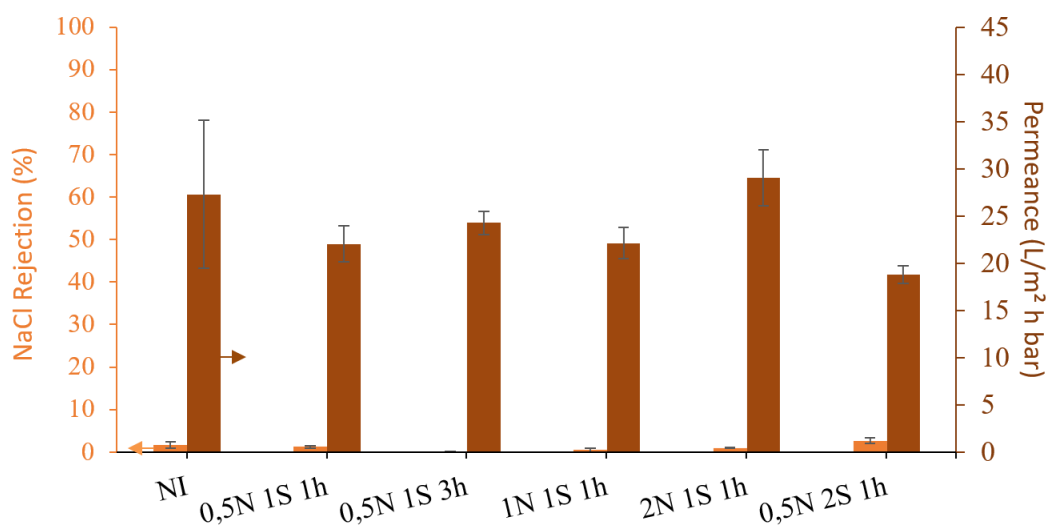


Figure 61: Performance of the DABCO membranes at different synthesis conditions: concentrations of 0.5N; 2N; type 1S and 2S; reaction times of 1 h and 3 h. Filtration conditions: 10 bar, 5 mM NaCl aqueous solution.

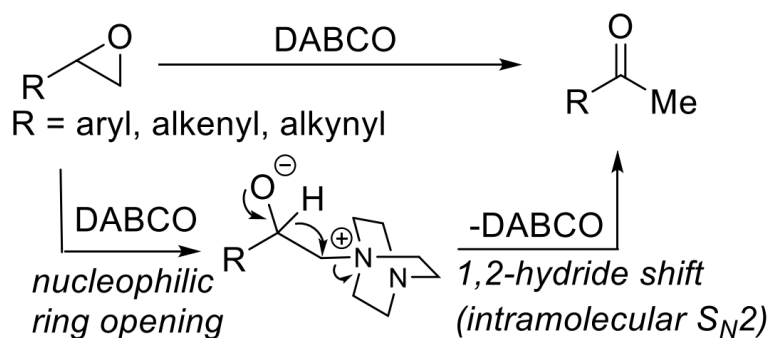


Figure 62: DABCO-mediated conversion of terminal epoxides to methyl ketones. From¹⁶⁶

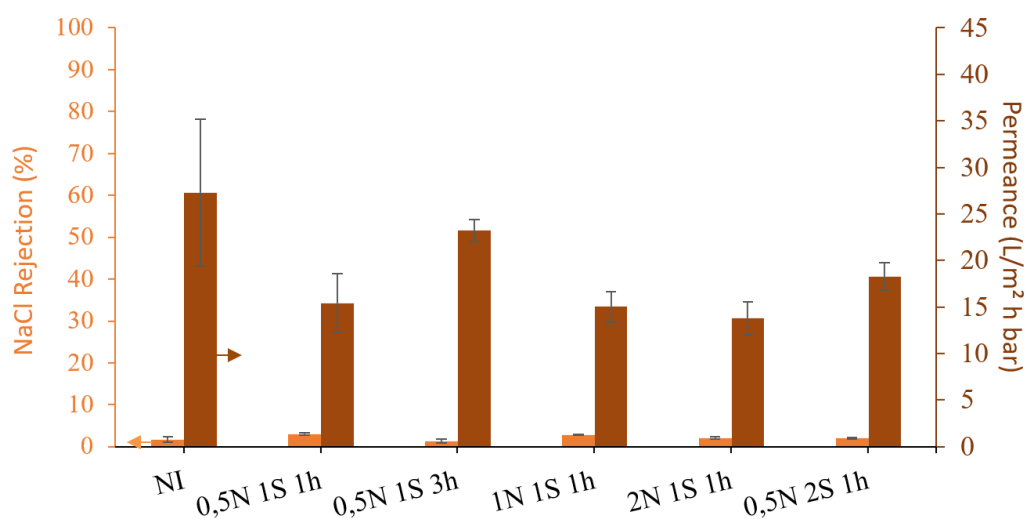


Figure 63: Performance of the Me6Tren membranes at different synthesis conditions: concentrations of 0.5N; 2N; type 1S and 2S; reaction times of 1 h and 3 h. Filtration conditions: 10 bar, 5 mM NaCl aqueous solution.

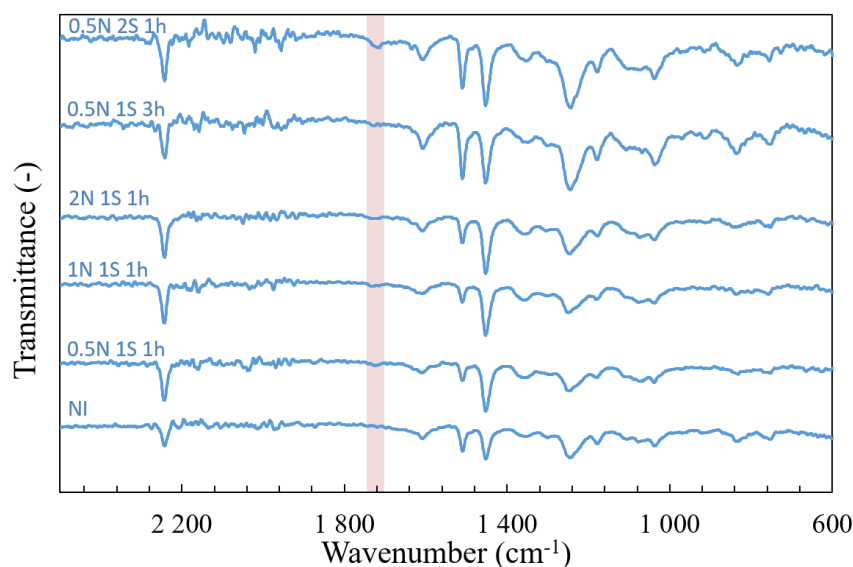


Figure 64: ATR-FTIR spectra of Me6Tren membranes on top of a DMac12 support. The spectra were smoothed by taking the average transmittance of the surrounding six wavenumbers. C=O band around 1715 cm⁻¹ highlighted in red.

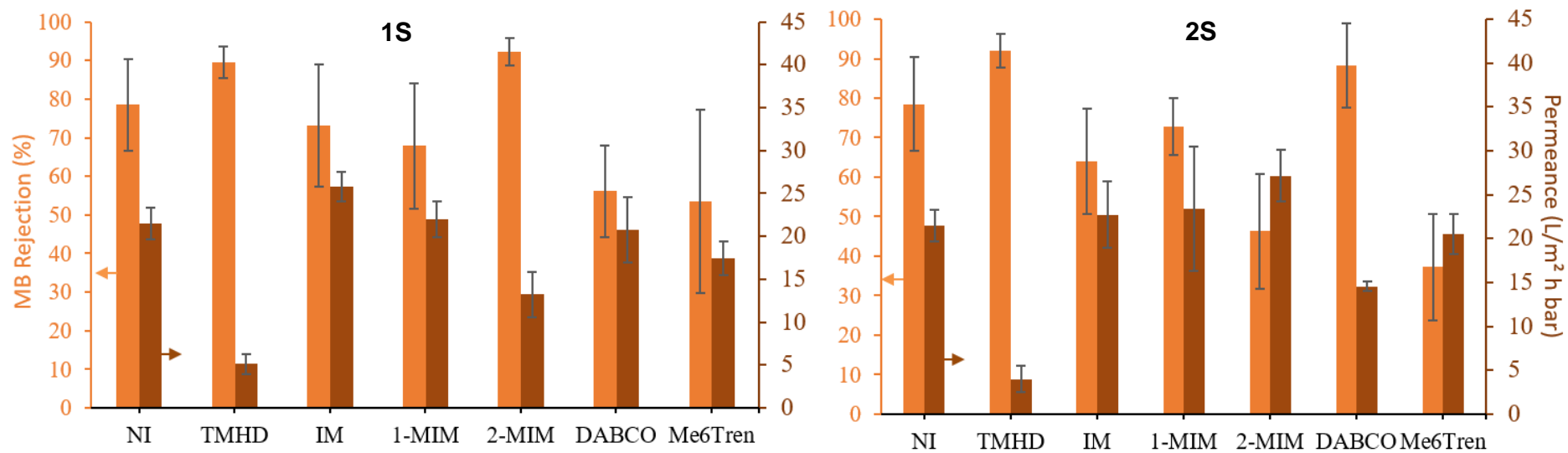


Figure 65: MB performance of 1S (left graph) and 2S (right graph) membranes synthesized on DMAc12 with different initiators. 1S membrane initiator conc: TMHD: 1N, IM: 4N, 1-MIM: 2N, 2-MIM: 4N, DABCO&Me6Tren: 2N. 2S membrane initiator conc: TMHD: 1N, IM: 1N, 1-MIM: 0.5N, 2-MIM: 1N, DABCO&Me6Tren: 0.5N. All reaction steps were of 1 h. Filtration conditions: 10 bar, 15 μ M methylene blue aqueous solution.

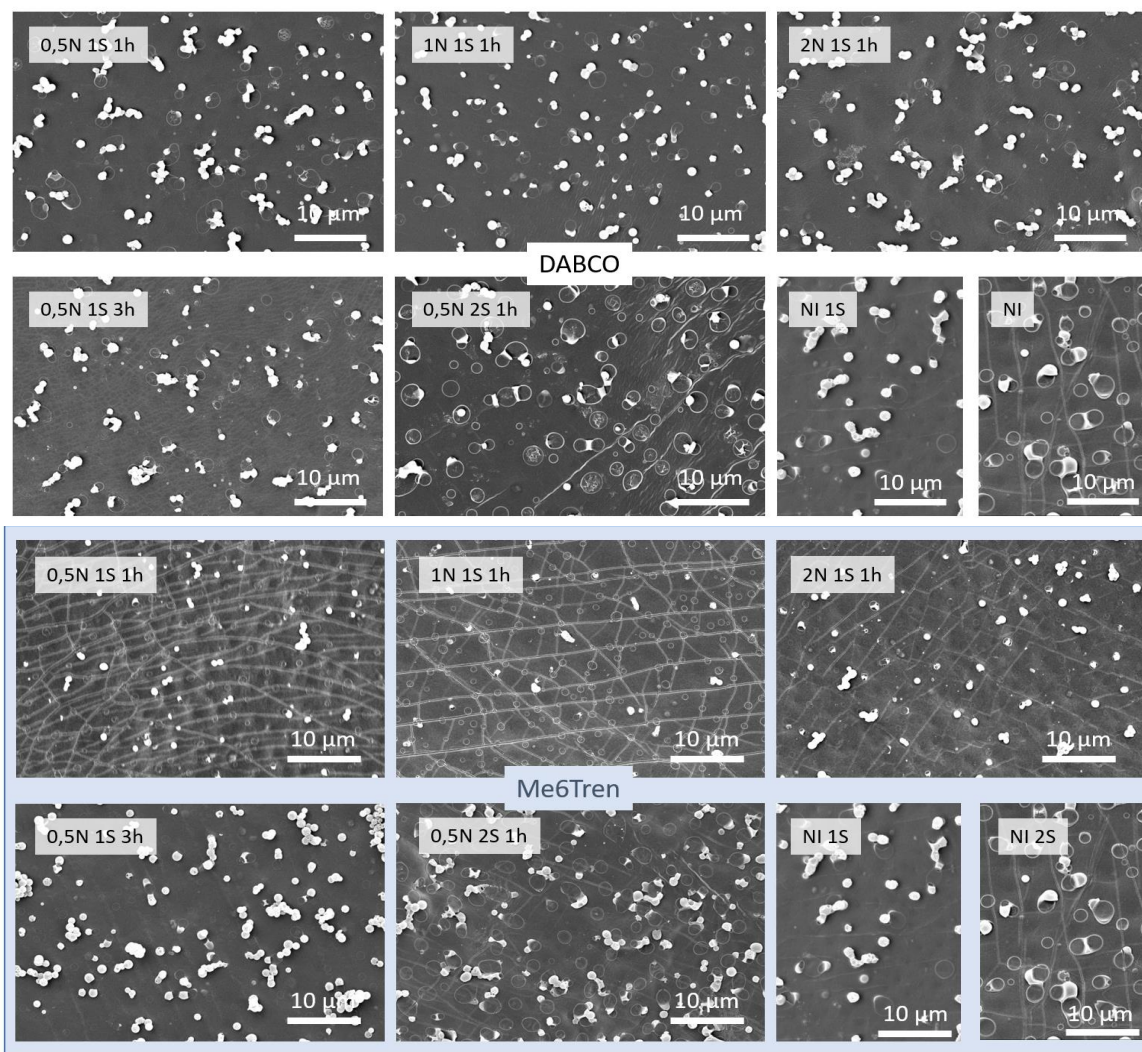







Figure 66: Top-view SEM images of DABCO (white background) and Me6Tren (blue background) synthesized with different conditions, all on top of DMAc12. 1S and 2S NI membranes are depicted at the bottom right corner.

Table 5: Vials experiments regarding the GS membrane synthesis. Upper phase: 1N initiator in toluene, lower phase: 5 w/v% PEGDE in MQ water. If there is no extra information at a specific time, this means nothing changed compared to what was visible before. Pictures were taken after 1 week.

	TMHD	TMPD	1-MIM	MBI	MBDA
Picture after 1 week					
Extra information	1h: Slight turbidity in TMHD-phase. More turbidity on interphase. Stayed the same for a whole week.	1h: toluene phase slightly white turbid 1 day: turbidity disappeared, white islands of relief are formed at interface	1 day: slight white shine on interphase is barely visible. 3 days: white shine on interphase 1 week: slight transparent relief on interphase	1 day: water phase got slightly turbid 3 days: white stripes on interface 1 week: clear white stripes on interface	1h: white islands of relief are formed at interface 1 day: white film is formed which sticks to the edges of the glass vial. BUT: For the same vial experiment but without PEGDE, a white film (non sticking) was formed.

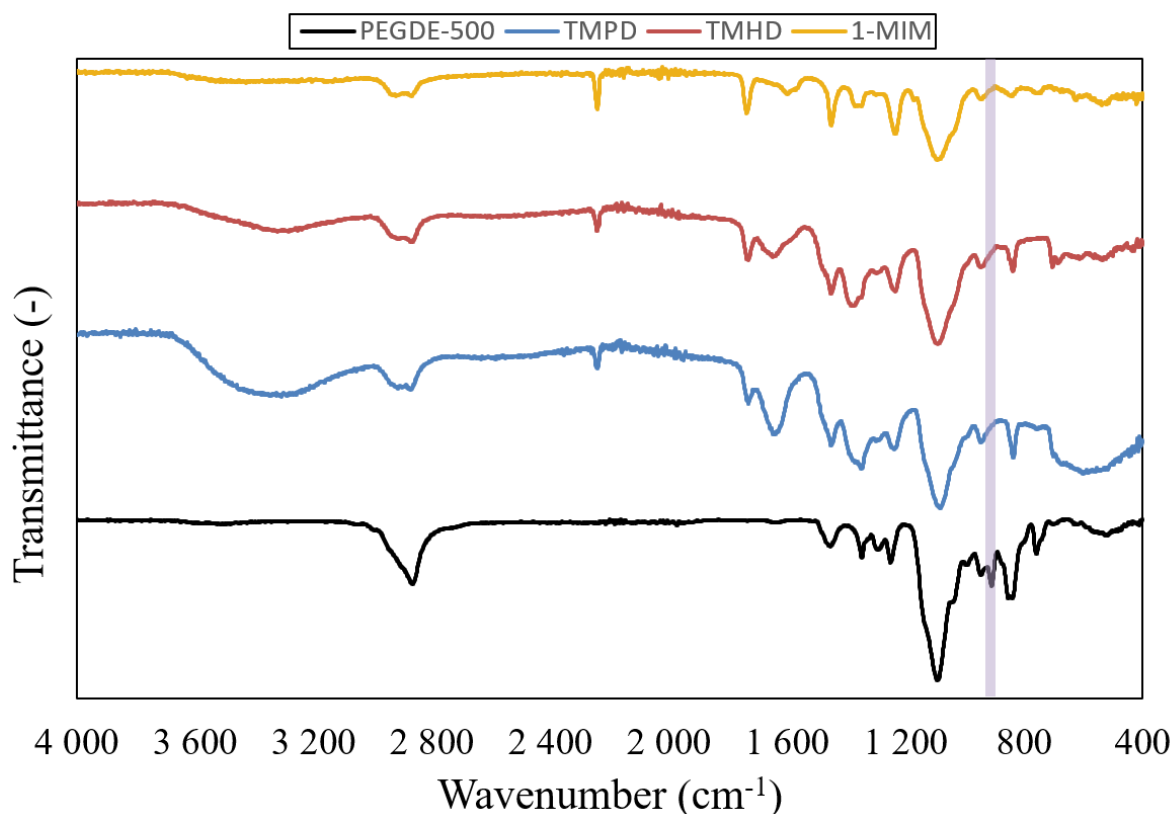


Figure 67: ATR-FTIR spectra of 2N 2S 1h membranes made with TMHD, TMPD, and 1-MIM. The epoxide signal is highlighted in purple.

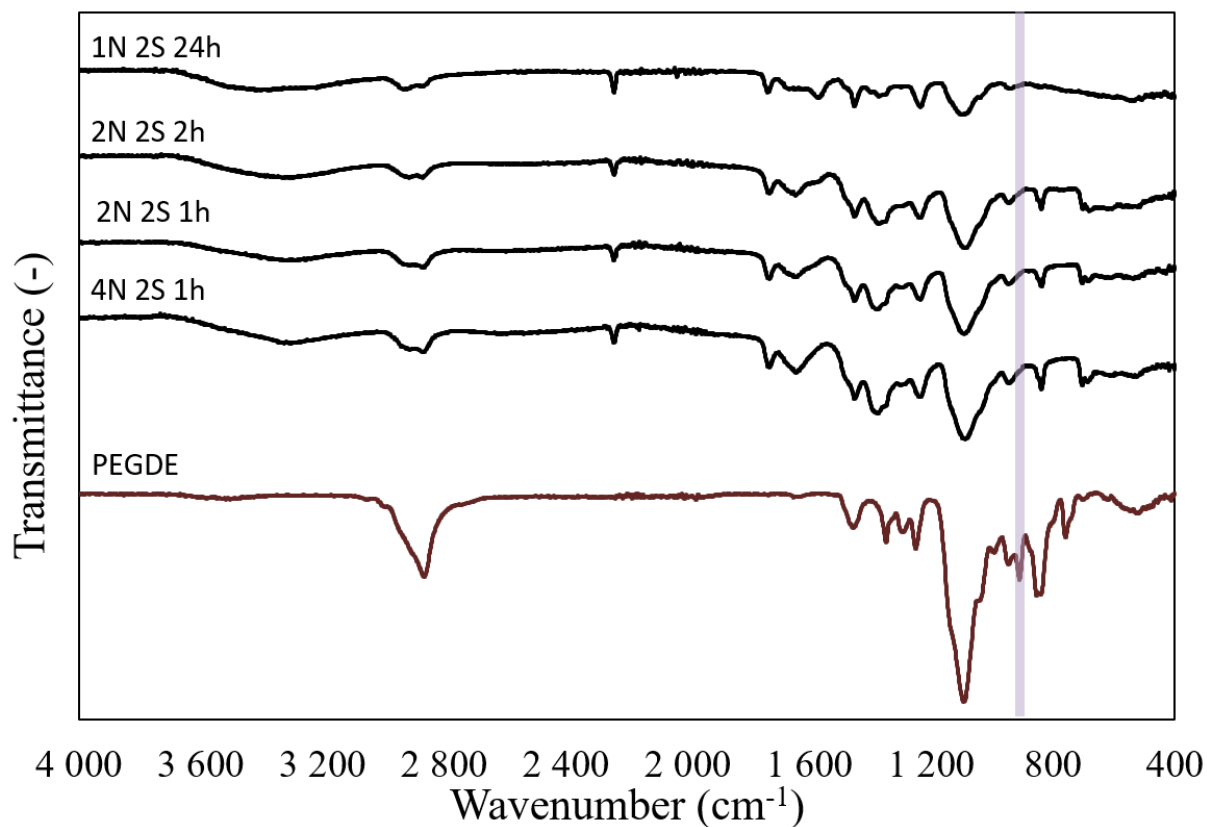


Figure 68: ATR-FTIR spectra of TMHD synthesized with different conditions. The epoxide signal is highlighted in purple.

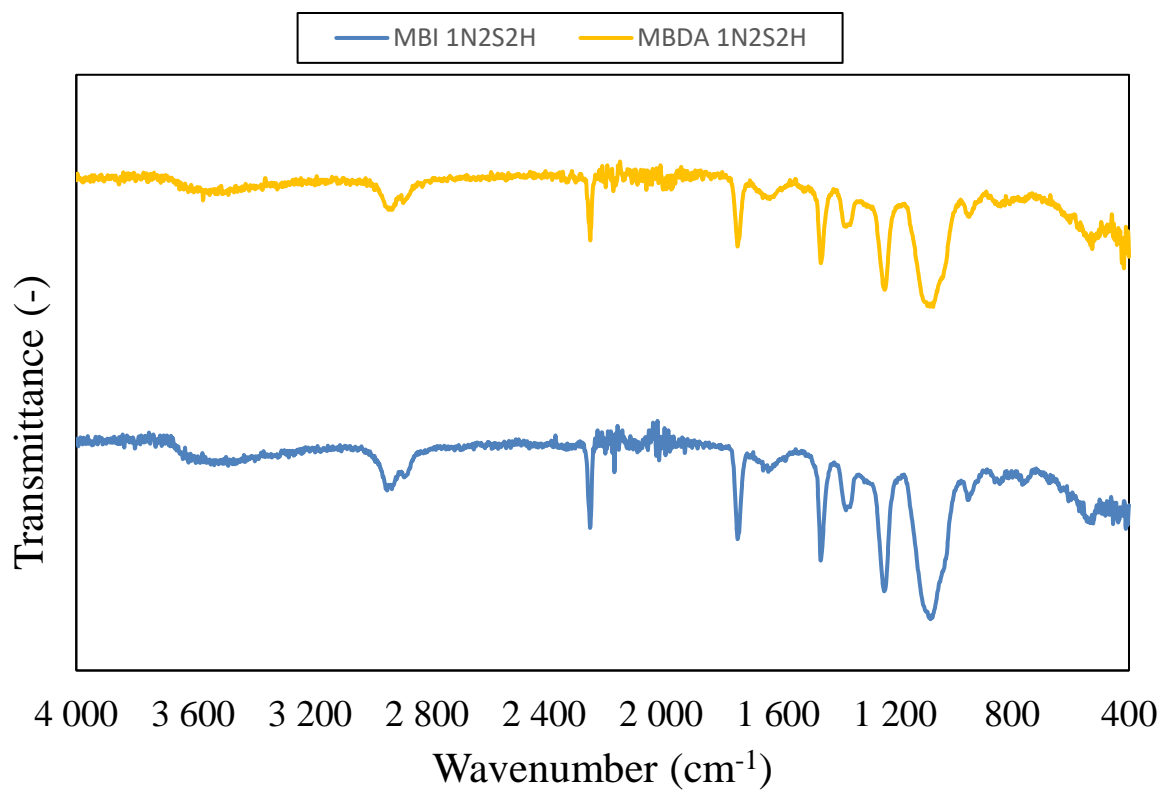


Figure 69: ATR-FTIR spectra of MBI and MBDA 1N 2S 1H membranes